Harnessing Functionalized Polysaccharides for Medical and Dental Applications

by

Nathan A. Jones

A dissertation submitted in partial fulfillment
of the requirements for the degree of
Doctor of Philosophy
(Macromolecular Science and Engineering)
in The University of Michigan
2017

Doctoral Committee:

Professor Joerg Lahann, Chair
Professor Mark M. Banaszak Holl
Dr. Steven Bloembergen, GreenMark Biomedical
Professor Emeritus Brian H. Clarkson
Professor Jinsang Kim

Nathan A. Jones

najone@umich.edu

ORCID iD: 0000-0002-5386-246X

In loving memory of Eric and Peggy, my grandparents.

ACKNOWLEDGEMENTS

This thesis would not have been possible without the support, assistance, and dedication of many people. I would like to first acknowledge my advisor Prof. Joerg Lahann, for guidance, insight, and support over the course of my degree at the University of Michigan. His assistance and guidance for this dissertation are only a small fraction of the contribution he has made as a mentor and advisor, which has strongly impacted me both personally and professionally and helped shape me into the scientist I am becoming. My situation coming to join the university was unusual – I had my own research project in mind – and this was both a challenge and a blessing: I had the flexibility to choose the advisor I most wanted to work with; however, I needed to persuade them of the value of my research and pursue additional funding mechanisms. If I were to start all over with the experience I have had, I would still eagerly choose Prof. Lahann as my advisor. I would also like to acknowledge my co-advisor, Dr. Pienta, formerly at the University of Michigan, but now at Johns Hopkins University. When deciding on my "dream team" of advisors, Dr. Pienta was at the top of the list, and I was humbled by his experience. I nervously emailed him my research ideas, and was delighted to receive a positive response, just minutes later. He has always been genuinely excited in the research I have been pursuing and that excitement is contagious, which provided needed motivation when experiments weren't giving expected results. I strongly considered Prof. Banaszak-Holl as my advisor, as he has been an incredible role model for me. He's a rock star, quite literally! His passion for life extends into his work, and I am thankful to include him on my advisory committee. I am further thankful for his role as the Director of the Macro Department and the positive changes he has been enacting to move the program to new levels. Prof. Clarkson has been a fortuitous blessing to my time here at Michigan. His guidance and support for the dental project has led to exciting results and wonderful opportunities to present my work around the world. Always happy to meet and discuss my work (over a pint, preferably!), my every interaction with him has been truly valued. Prof. Kim is another professor who is brimming with excitement for good science. He taught one of my favorite graduate level courses, Advanced

Functional Polymer Materials, which gave many examples of well-planned studies and has helped to shape my research strategy. Finally, to round off the members of my committee, I'd like to thank Dr. Steven Bloembergen. Having worked together for almost a decade now, Steven has been an incredible mentor, both professionally and personally. From taking a chance on me as a young co-op student many years ago, to providing opportunities to grow and test myself at EcoSynthetix, to supporting my decision to challenge myself in pursuing my PhD in the US, and now starting a new venture together, he has been resolutely steadfast in his support. His positive nature makes the hard work rewarding, and I am looking forward to our next steps working together to build GreenMark Biomedical. I would also like to thank our other collaborators, including the group of Dr. van Epps, and particularly his research technician Usha Kadiyala, who was a delight to work with and whose assistance was instrumental to the progress for the antibacterial project in Chapter 4. Additionally, Sywe-Ren Chang, Jason Sherbel, and Adam Jankovic from the UM Dental School were of great help on the dental project in Chapter 3, and Jelani Zarif (Johns Hopkins University) assisted kindly on the macrophage targeting project in Chapter 5.

I also want to thank the members of the Lahann Lab over the years, who have always been willing to lend a hand or a moment to discuss an idea or research question with me. PhD students Jonathan Gerzsburg, Ayse Muniz, Danny Quevedo, Dylan Neale, Jason Gregory, Seyed Reza Roghani, Hyesun Jun, Dr. Stacy Ramcharan, Dr. Jake Jordahl, Dr. Sahar Rahmani, Dr. Asish Misra, Dr. Thomas Eyster, Dr. Xiaopei Deng, and Dr. Jaewon Yoon, and Post-Docs Dr. Kathleen McEnnis, Dr. Stephie Christau, Dr. Luis Solorio, and Dr. Hakan Durmaz have been supportive colleagues who have answered any questions I have had when I stopped at their office door, and friends always happy to share a smile while working late hours in lab. I'd like to thank particularly the contributions of Dr. Kenneth Cheng, for his assistance with XPS measurements, Nahal Habibi, for her help with macrophage cell experiments, Ramya Kumar, for the preparation of sugar-coated surfaces, Dr. Domenic Kratzer, for his help optimizing several chemistries including the preparation of sugar-monomers, and Dr. Brad Plummer for his assistance with cell culture experiments. Additionally I'd like to acknowledge the assistance I received from undergraduate students over the years: Benjamin Serratos, Will Troske, Matthew Bodner, Mikaela Cesario, and Olivia Kemppainen. Their efforts were critical to the progress of my research and it was a joy to act as a mentor and watch them grow as researchers and young

adults. Finally, I also wish to thank the support of staff members in the Bio-Interfaces Institute and the Department of Macromolecular Science and Engineering. Mrs. Lisa Moran and Mrs. Julie Gales have been a pleasure to interact with and have helped with the organization of countless meetings over the years. Adam Mael, and previously Nonna Hamilton, are and were top-notch graduate coordinators who endeavored and succeeded in making Macro feel familial and welcoming. Funding support is graciously acknowledged from the National Science and Engineering Research Council (NSERC) PGS Fellowship, Industrial awards from EcoSynthetix, Colgate, and 3M, and the Rackham International Student Fellowship.

More personally, I'd like to thank the blessings I have been afforded by God, best exemplified by the support of my friends and family who have equally contributed to my graduate student experience. My Macro classmates, Siuon, Yasmine, Danny, Jiwon, Apoorv, David, Dowon, and Michael were welcome friends and colleagues who shared in the challenges of our coursework and qualifying exams. My team mates at Extreme Chaos Football Club, Joga Bonito, and my small group from Huron Hills Church have been an outlet from the daily stress at work and significant factors in maintaining my sanity. I'd be remiss if I did not mention the love and support from my family without whom I could not have made it to writing this dissertation. My parents, Dr. Glenn and Eeva Jones have always supported my efforts and dreams, and have been a fount of encouragement and advice, with the occasional sprinkling of statistical know-how. They are, and have been, loving parents, friends, and mentors for me. I would also like to thank my girlfriend, Paige Lewandowksi (and of course Charlie!) for abiding my turbulent relationship with science, including late hours in the lab and stressful impending deadlines. She continues to support my dreams, and even became my "Seoul-mate" when she joined me for a presentation at a conference in South Korea. My siblings, Sharaya and Kai, have always been loving and supportive, and I have no doubts they will achieve great things themselves as they pursue their own graduate degrees. Lastly, my grandparents, Mummo, Eric, and Peggy were heroes of their generation who left their homes as immigrants to Canada to provide a better future for the next generations. While saddened that they can't attend my defense, this dissertation is dedicated to the memory of Eric and Peggy, who are looking down from heaven with pride glowing in their hearts.

TABLE OF CONTENTS

LIST OF FIGURES

LIST OF TABLES

ABSTRACT

Polysaccharides are an important class of biomolecules with many different biological functions and unique properties, thus it is unsurprising that polysaccharides are heavily researched as materials solutions in medicine and dentistry. This dissertation explores the potential of harnessing inherent and well-understood biological properties of polysaccharides, using chemical and materials modification techniques to create clinically useful systems for medical and dental challenges. Engineered polysaccharides systems were prepared and characterized, including starch nanoparticles with control of particle size, charge, loading, and attachment of functional molecules, and glycocalyx-mimetic polymer brushes. These systems were applied as a diagnostic aid for dental caries, as an anti-bacterial treatment, and in targeting tumor-associated macrophages.

In the first application, fluorescent cationic (+5.8±1.2 mV) starch nanoparticles (size 101±56 nm) were prepared to target and adhere to early caries lesions to facilitate optical detection, test lesion activity, and monitor the impact of remineralization treatments *in vitro*. In the second application, similarly designed starch nanoparticles (size 440±58 nm) were loaded with antibacterial copper nanoparticles (6-7nm size, ~0.35% loading) to create a system which targets bacteria electrostatically and by their enzymatic metabolic processes. This system showed high antibacterial efficacy (3-log and 7-log bacterial reductions for S. aureus and B. subtilis, respectively, for copper nanoparticle dose of 17 µg/ml). The final application demonstrated high positive predictive value (>0.8 for M2 over M1) for cellular binding of glycocalyx-mimetic mannose-coatings with M2-polarized tumor-associated macrophages, with potential applications in cancer diagnostics and therapeutics. These examples highlight the utility of modified polysaccharides in the design of clinically useful systems in medicine and dentistry.

CHAPTER 1

Introduction

1.1 Background on Polysaccharides and Sugars

Carbohydrates refer to the class of biological molecules including sugars and polysaccharides. They are thus named because the structural formula is typically $C_n(H_2O)_n$, where n is a natural number, and consequently can be described as a hydrated carbon. A variety of sugars, including glucose, sucrose, mannose, fructose, and galactose play important biological roles and possess similar chemical structures, as demonstrated in **Figure 1-1**. Polymers built upon these monosaccharides are called polysaccharides, with some common biological examples shown in **Figure 1-2**, highlighting both the chemical similarities and variability that can be created using these molecules, similar to synthetic macromolecules. Polymer characteristics such as degree of polymerization (DP) and molecular weight (MW), branching, copolymerization with other saccharides and other biological molecules, and secondary interactions with other biomolecules impart incredible flexibility into the molecular properties and biological function of polysaccharides.

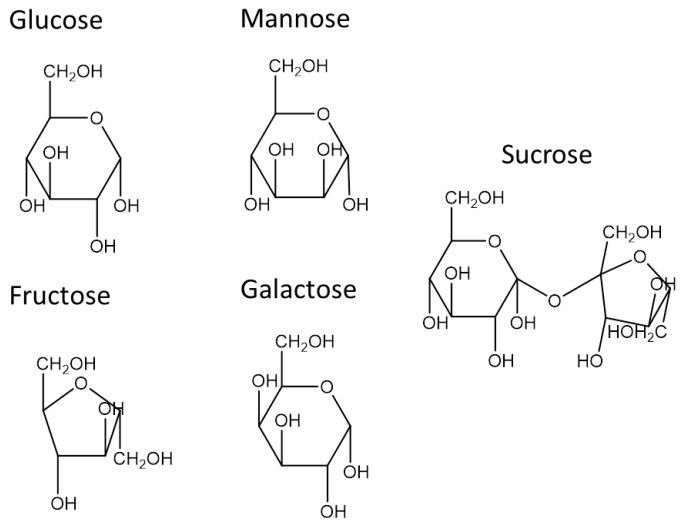

Figure 1-1: Chemical structures of simple sugars. Slight changes in stereochemistry effect large impact in their biological function.

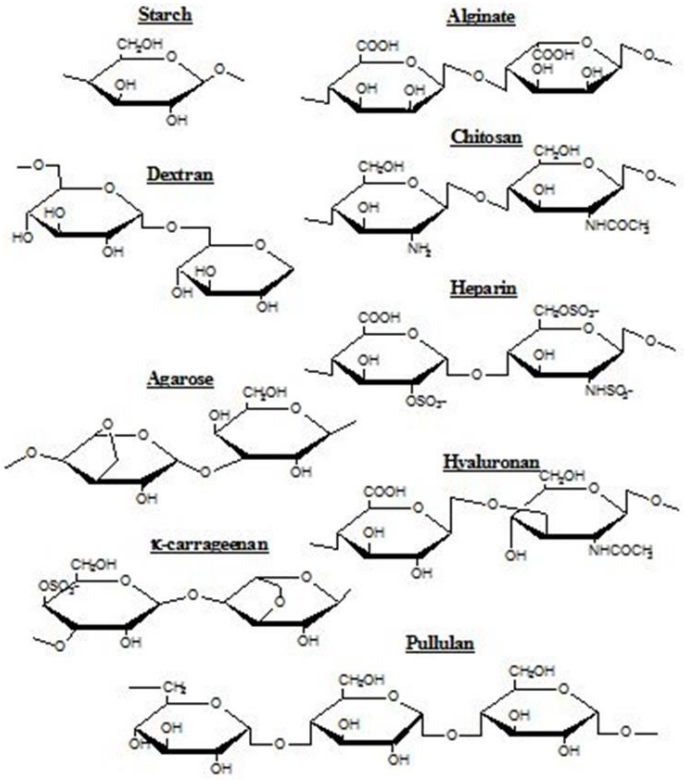

Figure 1-2: Chemical structures of various polysaccharides, highlighting the flexibility in chemical structures and functionalities, while maintaining similar chemical framework.[1]

1.2 Biological Roles of Polysaccharides

Carbohydrates serve several key roles in biology, including as metabolites, as structural support materials, and in biological interfaces as the glycocalyx. Glucose is the predominant monosaccharide and biologically functions primarily as an easily accessible energy currency via glycolysis and/or the Kreb's Cycle. Both amylose starch and cellulose are relatively simple polysaccharides that are chemically polymers of glucose with linkages at the 1-4 carbon atoms, demonstrated in **Figure 1-3**.

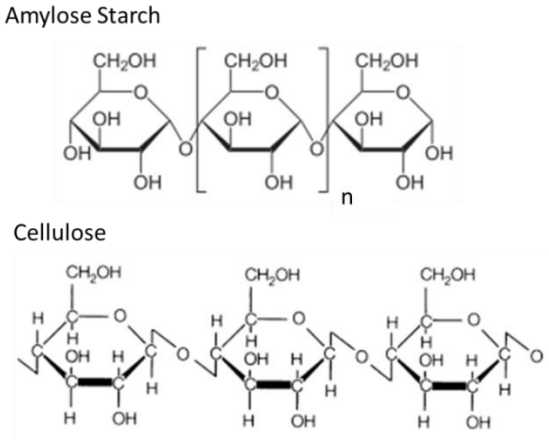

Figure 1-3: Difference in stereochemistry of amylose starch and cellulose.

Because glucose is a chiral molecule, the orientation of the monomers can play a key role in function. The key difference between starch and cellulose is that the linkage in starch is an alpha 1-4 link, with every glucose monomer aligned, while cellulose is a beta 1-4 link, with the orientation of glucose monomers alternating. This simple difference gives rise to very different properties, crystallinity, and biological function: starch is primarily used by plants to store glucose molecules as an energy reserve, as the

glucose is more readily accessible by hydrolysis from starch rather than cellulose, which makes it a choice food source; while cellulose serves a structural function, and cannot be easily digested. While starch can be water-soluble, cellulose has limited solubility, high rigidity, and high tensile strength, lending itself well for use in clothing (cotton), construction materials (wood), and paper applications. Another polysaccharide, chitosan, serves as a functional structural molecule – it forms the basis of crustacean and insect shells, but also has non-fouling and anti-bacterial properties.[2] By understanding the natural properties of polysaccharides, new applications can be discovered in medicine and industry.

Sugar molecules have also been adopted by biological systems for functional interfaces. The glycocalyx, literally meaning "sugar coat", is a glycoprotein coating which surrounds the cell membrane of bacteria and epithelial cells, as shown by the schematic in **Figure 1-4**.

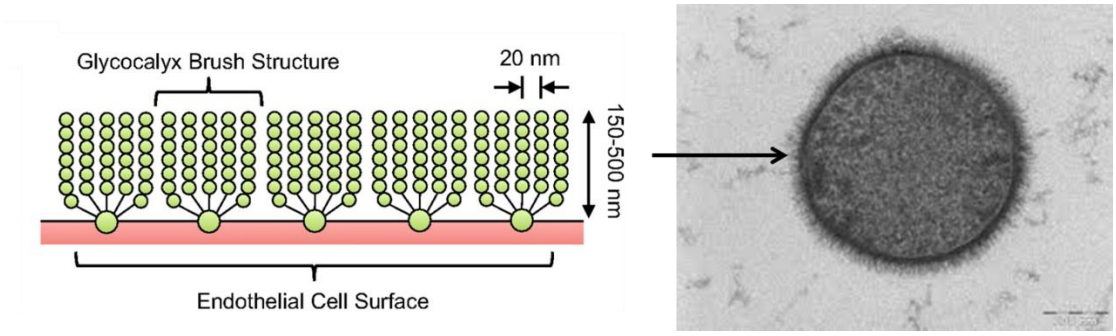

Figure 1-4: The glycocalyx on the surface of cells.[3,4]

These complex molecules contain carbohydrate, protein, and lipid molecules, and can extend from nanometers to microns in thickness.[5] On a cellular scale, the

carbohydrate portion of the glycocalyx plays an important biological role in cell-cell recognition, cellular communication, and intercellular adhesion.[6] The glycocalyx cushions the cellular plasma membrane to protect from chemical injury, and also enables the immune system to recognize and selectively attack foreign organisms, including cancer cells. Furthermore, this sugar brush sheaths the inner lumen of blood vessels, acting as a shield from the shear forces from direct blood flow, while simultaneously acting as a vascular permeability barrier. This helps to prevent coagulation and non-specific adhesion from immune cells, such as leukocytes, which regulates the immune response.[7] The glycocalyx and its properties are an interesting biological inspiration to the design of materials that will interface with biological systems and some early work has identified these properties can be mimicked using synthetic analogues.[8,9]

Understanding the roles of polysaccharides in biological settings can provide insight into desirable properties that can be manipulated towards the intelligent design of engineered materials for clinical applications. In particular, noting the roles of polysaccharides as key metabolites and in multifunctional biological interfaces can assist in designing systems that harness these properties towards a clinical objective.

1.3 Use of Polysaccharides in Medical Applications

Because of their roles in biology, modifiability, and ease of availability, it is not surprising that polysaccharides have been used in a variety of medical applications. Polysaccharides are used successfully in drug delivery, tissue engineering, and food

applications, and several review articles and textbooks have been released on these topics.[10-12] An overview of these applications is outlined in **Figure 1-5**.

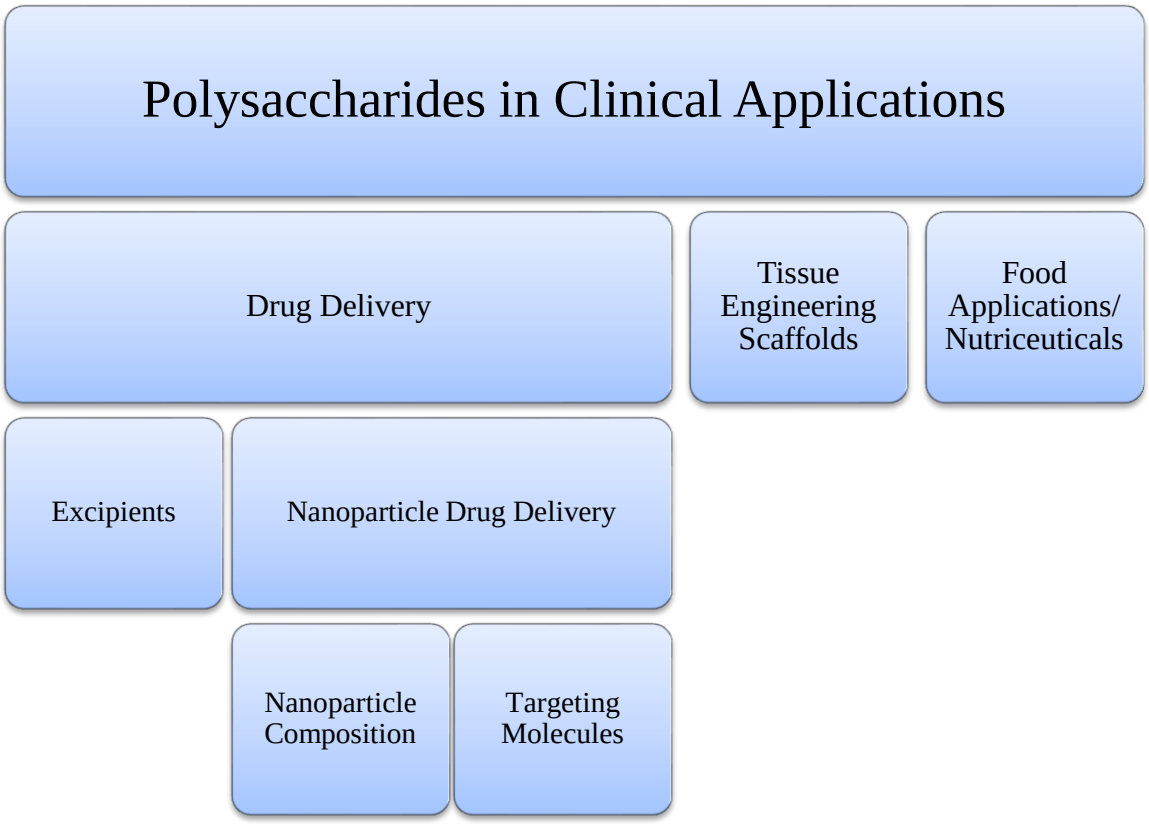

Figure 1-5: Overview of the clinical applications of polysaccharides.

1.3.1 Polysaccharides in Drug Delivery

There are several different uses for polysaccharides in drug delivery applications, including as excipients, in the composition of nano- and micro-particles, and as biological targeting molecules for active targeting of diseased cells.

Excipients

Excipients are materials used in addition to the active component to assist with the manufacture, administration, and pharmaceutical efficacy of a drug formulation.[13] For many pharmaceuticals, the appropriate dose of an active ingredient is too small for practical consumption, and excipients can act as a bulking agent or diluent to make dosing simpler and additionally improve long-term stability or the formulation. Furthermore, excipients can facilitate the manufacturing process, imparting improved powder flowability or non-stick properties, while also preventing denaturation or aggregation of the active ingredient. Excipients can enhance the therapeutic efficacy of the active ingredients by modifying the drug solubility and absorption, thereby impacting the pharmacokinetics and pharmacodynamics of the formulation. Of course, in the development of a drug formulation, it is required that all ingredients, as well as the products of their decomposition, be identified and proven to be safe for human use. Finally, development of novel excipients allows for patentability, and there can be significant value in the design and application of excipients, and combinations therein, within a formulation.

Polysaccharides have been used commercially as excipients in drug formulations by the pharmaceutical industry for decades, in large part due to their safety, ease of modification, and accessible supply.[13,14] Glucose and other sugars are useful as sweeteners for bitter tasting drugs. Saccharides such as sucrose and lactose, sugar alcohols like sorbitol, xylitol, and polysaccharides such as starch, cellulose, and various modifications therein can be used as binders to provide volume and mechanical resilience to pill formulations. Modified polysaccharides such as hydroxypropyl methylcellulose

can be formulated to act as coating, to prevent degradation of active ingredients due to water absorption, or mask bitter flavors. Other polysaccharides are used in enteric coatings for orally delivered formulations, which act to control the release and absorption of active ingredients within specific regions of the digestive tract. Finally, modified polysaccharides, including cross-linked carboymethylcellulose and modified starch sodium glycolate, can be used to control the disintegration of tablet formulations.[14]

Nanoparticle Drug Delivery

Nanoparticles have emerged as novel materials which are advantageous in the treatment and diagnosis of various diseases.[15-17] In particular, nanomaterials have shown relevant properties for the targeting and treatment of cancer including: longer circulation; modifiable surface properties; and controlled release. These result in reduced side effects and improved therapeutic efficacy.[18] Various systems have been developed and are currently used in clinical practice or in clinical trials.[19] Some of these systems use polysaccharides as the primary composition of the nanoparticulate drug delivery system or as specific targeting molecules for a particular indication.[11]

Nanoparticle Composition

Many different nanoparticle compositions have been developed and studied for drug delivery applications, including synthetic polymers, liposomes, inorganic materials, and biobased polymers, including proteins or polysaccharides.[15,17,18] Some examples of more successful polysaccharides in drug delivery include chitosan,[20] cyclodextrin,[21] and acetal detxtran,[22,23] with examples of these chemical structures shown in **Figure 1-5**.

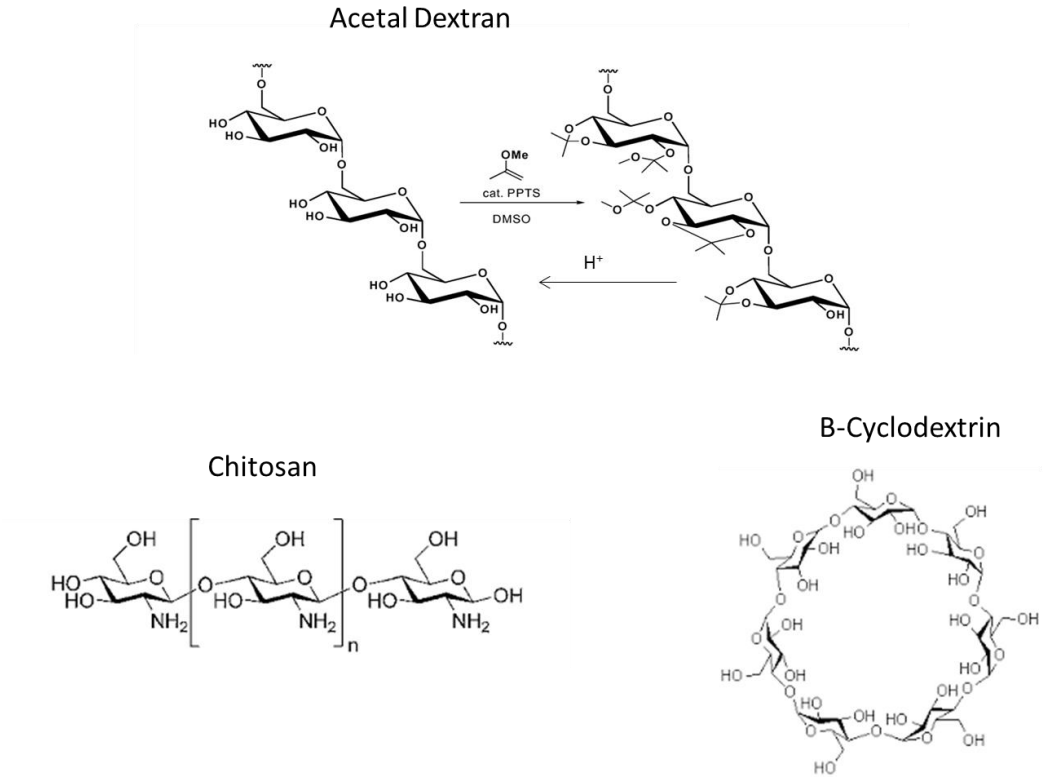

Figure 1-6: Chemical structures of polysaccharides used in drug delivery applications and the reaction to prepare and degrade acetal dextran.[20,21,24]

For each of these systems, success has been found when harnessing the innate biological properties of the polysaccharides within the design of the material. Chitosan is a polysaccharide which forms the structure of shells of insects and crustaceans, and has been successfully used to prepare modifiable nanoparticles capable of loading a variety of drugs for multiple different indications.[20,25] Some of the biological properties of chitosan which are beneficial in drug delivery applications include sensitivity and degradation at low pH,[26] useful for triggerable degradation in acidic media, hydrophobicity,[26,27] beneficial in the loading of hydrophobic drugs, and innate resistance to fouling by proteins,[20,28] useful in decreasing non-specific clearance of prepared nanomaterials by the

immune system. Cyclodextrins (CDs) are interesting polysaccharides which are ring-shaped oligomers of sugars, which have a unique structure with a hydrophobic core capable of loading hydrophobic drugs as host-guest complexes, and a hydrophilic modifiable exterior.[21] When loaded with a hydrophobic drug, CDs are capable of self-assembly into larger nanoparticles, and can thus take advantage of certain size-specific advantages.[29,30] Primarily lead by Mark Davis (CalTech), a formulation using CDs loaded with Camptothecin is currently in clinical trials,[31] and additional work has explored loading siRNA for gene knockdown therapy.[32] As a more recently developed polymer, acetal dextran, as prepared by the reaction scheme shown in **Figure 1-5,**[22] is a modification of dextran, a polysaccharide produced by bacteria that is similar to starch, but not digestible by humans. Dextrans are used clinically primarily as osmotic agents as highly hydrophilic non-degradable polymers.[33] Acetal-modified dextrans are hydrophobic at neutral pH, but revert to their original hydrophilic state upon exposure to an acidic environment. This pH-sensitive degradation facilitates targeted release of hydrophobic drugs within a tumor microenvironment,[22] areas of inflammation,[24] or within cellular endosomes.[23] One potential advantage using these polymers in drug delivery vehicles is their high osmotic potential which may facilitate endosomal escape, leading to improved therapeutic efficacy.[34] Due to their availability as plant-derived commodity resources, cellulose and starch have found some use in the preparation of drug-delivery vehicles, with more work focusing on cellulose.[35] Starch will be examined more closely later in this chapter. As emphasized in the examples of chitosan, cyclodextrins, and acetal dextran, specific advantages can be obtained by harnessing

particular biological properties of these molecules towards the development of clinically useful drug delivery platforms.

Targeting molecules

Saccharides are also used in drug delivery as targeting molecules, because of the ability of these biomolecules to interact specifically with proteins found naturally in biology. A significant targeting application has been with mannose, or the polymeric mannan, which bind specifically the mannose receptor (CD206). The mannose receptor is over-expressed on inflammatory macrophages, and consequently is an appealing target for inflammation in the context of cancer,[36] cardiovascular disease,[37] diabetes,[38] and other illnesses.[39] Mannose and/or mannan have been attached to a variety of nanoparticles and therapeutics for various applications, and specific applications will be examined more closely in Chapter 5.[40-42] Similarly, due to over-expression of glucose binding lectins, glucose has also been used as a targeting molecule for cancer[43] and also to facilitate permeability of drugs across the blood-brain-barrier, disguising the drug as a potential metabolite for resource-hungry cells.[44,45] Fucoidan is an interesting polysaccharide material which is derived from brown seaweed, with the structure shown in **Figure 1-6**. This polysaccharide has been shown to target and facilitate extravasation across inflamed vasculature, which can naturally target cancer or other indications, and can be activated synergistically by precisely targeted radiation treatment.[46-49] Additional research has suggested that coating nanoparticles or other surfaces with saccharide-based molecules acts similar to the cellular glycocalyx in creating a non-fouling hydrophilic water shield which prevents non-specific protein adsorption, thus improving the biocompatibility of

the substrate material.[50] In these examples, specific bio-interactions of the used sugars and polysaccharides are beneficial in their clinical utility. Understanding these interactions can guide the design of novel materials for clinical applications.

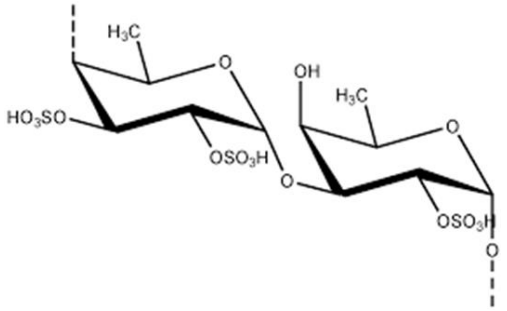

Figure 1-7: Chemical structure of fucoidan, a polysaccharide derived from seaweed. The sulfate functionalities facilitate specific binding to biological receptor molecules.[46]

1.3.2 Polysaccharides as Functional Foods and Nutriceuticals

Polysaccharides are a significant food source for humans and other animals because of their role in glycolysis and the Kreb's cycle, and even undigestible polysaccharides are beneficial to the digestive process, facilitating peristaltic transport of waste.[51] Beyond simple variations of glucose for their base nutritional value, some polysaccharides have been found to have additional health benefits when incorporated in food, and this has been used by humans for centuries.[52] Functional foods are foods enriched with functional components that offer medical and physiological benefits, while nutriceuticals are bioactive materials that can be derived from foods to be used specifically as medicines.[53] Many unusual polysaccharides are derived from marine sources such as seaweed or fungi, which result from adaptation to harsh environmental

conditions to use different metabolic pathways, store ions and vitamins, and protect against oxidative stress.[53-55] For example, carageenan, which is a polysaccharide derived from macroalgae, is often used to assist with gel formation and coatings in the meat and dairy industries, but has also been linked to anti-viral activity and anticoagulant properties.[56] Chitin and chitosan are used as gelling agents and edible protective films, but also function like dietary fiber and help reduce lipid absorption, while demonstrating bactericidal and fungicidal properties.[56] Fucoidan, discussed earlier, has shown benefits as a standalone nutraceutical in reducing oxidative stress.[48] Polysaccharides derived from mushrooms are used clinically in the treatment of certain cancers,[52,57] and further demonstrate immunomodulating, antimicrobial, hypocholesterolemic, hypoglycemic and health-promoting properties.[55] Similarly, intake of dietary fiber has been linked to improved outcomes in patients with coronary heart disease,[51] and intake of glycosaminoglycans has been studied as a treatment for arthritis[58] and inflammatory bowel disease.[59] These examples identify the potential to harness the specific properties of a wide range of polysaccharides to be used for medical benefit, even without additional engineering design.

1.4 Starch Nanoparticles (StNPs)

Starch is one of the most abundant biopolymers in the world, and is a critical part of the human diet. For use in many different food and industrial applications, starches from a variety of different feedstock have been used and chemically modified to obtain

useful properties. Nevertheless, preparing starch nanomaterials is challenging because starch polymers are crystalline in their native form and exist as granules on the order of tens of microns. To decrystallize the polymer, the starch is usually cooked at high temperatures, however upon cooling the polymer retrogrades and forms a gel.[60] To create a colloidal starch, chemical modifications are used to disrupt the crystallinity of the polymer, possibly by acidic or enzymatic hydrolysis,[61,62] or chemical cross-linking.[60,63] EcoSphere® starch nanoparticles (StNPs) are a commercially available starch-based nanoparticle with particle size ranging from 50-200 nanometers produced by a reactive extrusion process.[64] With the process of extrusion, high amounts of heat and mechanical force are applied to starch granules in the presence of aqueous solvent to disrupt the crystalline structure. Addition of cross-linking agents, such as dialdehydes, results in a dry agglomerate extrudate, which when dispersed into water or other appropriate solvent becomes a nanoparticle colloidal dispersion.[64-66] Other prepared starch nanoparticles can be made using emulsion,[67-69] nano-precipitation,[67,70,71] and electrospray[63] techniques, often incorporating cross-linkers such as citric acid,[62] hydrophobic grafted polymers,[69] sodium trimetaphosphate,[72] or dialdehydes.[73] Most of these materials are used in composites,[60-62,65,72,74] though some research has explored release applications in agriculture[75] and medicine.[67,69,73,76-79]

1.5 Starch Nanoparticles for Drug Delivery

While StNPs are used commercially as a replacement for synthetic latexes in the paper and composotie wood industries,[64,65] these nanoparticles are interesting as a novel drug delivery system. Initial research by EcoSynthetix and Duke University successfully encapsulated a number of toxic anti-cancer drugs, demonstrating sustained release performance.[80] Using StNPs it is possible to encapsulate fluorescent compounds, including the anticancer agent doxorubicin, using a phase inversion method. Doxorubicin was successfully loaded into StNPs, validating a phase separation method using lyophilization for loading small molecules. The release profile could be followed using a fluorescence technique and demonstrated a biphasic release profile. Similar studies were performed by Xiao *et al.* using starch particle prepared using emulsions to release doxorubicin with similar release kinetics.[73,79] Animal studies conducted in collaboration with Duke University Cancer Center demonstrated a 30% increase in survival for athymic mice with glioblastoma multiform tumors treated with doxorubicin-loaded StNPs relative to the appropriate controls. The key aspect of this initial success is thought to be due to the size of the starch nanoparticles and the ability of the drug-loaded particles to enter the cancer cells. Continued research at the University of Waterloo validated the functionalization and attachment of DNA aptamers to StNPs, as shown in **Figure 1-8(a)**, to impart the ability for specific targeting and uptake of the nanoparticles by cancer cells as demonstrated in the confocal microscopy images in **Figure 1-8(b)**.[80] This resulted in nearly doubling the cell-killing efficacy of loaded doxorubicin, as shown in the results of an LDH assay, in **Figure 1-9**. Similar concepts were shown by attaching folate to starch nanoparticles.[79] More recent research has identified the benefits of

hydrophobic modifications to starch nanoparticles to facilitate drug loading and also explore alternative routes of administration for drug delivery, including trans-nasally[77] and trans-dermally.[67,69] Finally, incorporating poly-L-lysine with starch has been explored for gene delivery *in vitro*.[78] These results begin to identify the potential of using StNPs as a modifiable platform for medical applications, and the continued work in this dissertation looks to build upon these principles by more specifically looking at the biological roles and interactions of starch and harnessing these to address clinical problems.

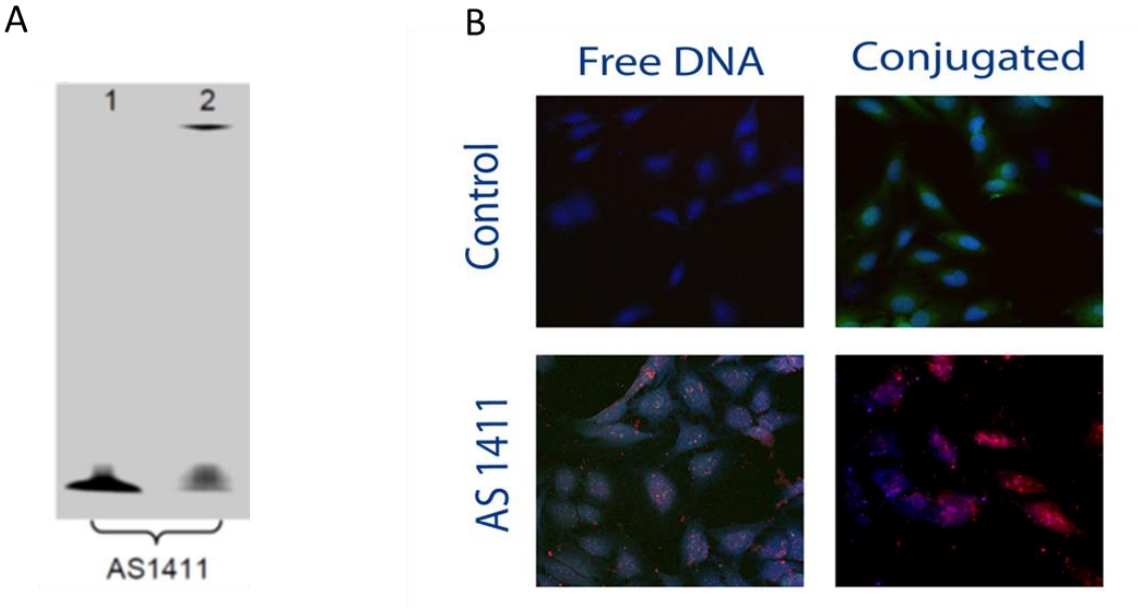

Figure 1-8: A) Validation of attachment of single-stranded DNA aptamer to starch particles by polyacrylamide gel electrophoresis. The stained unattached DNA moves freely to the bottom in channel 1, but the StNP-bound DNA (yield ~60%) in channel 2 remains trapped at the top. B) Confocal microscopy images showing nucleus stain (blue), actin stain (green), and fluorescent nanoparticles (red). Particles targeted with the AS1411 DNA aptamer showed specific uptake into HeLa cervical cancer cells, while untargeted particles (control) showed no uptake.[80]

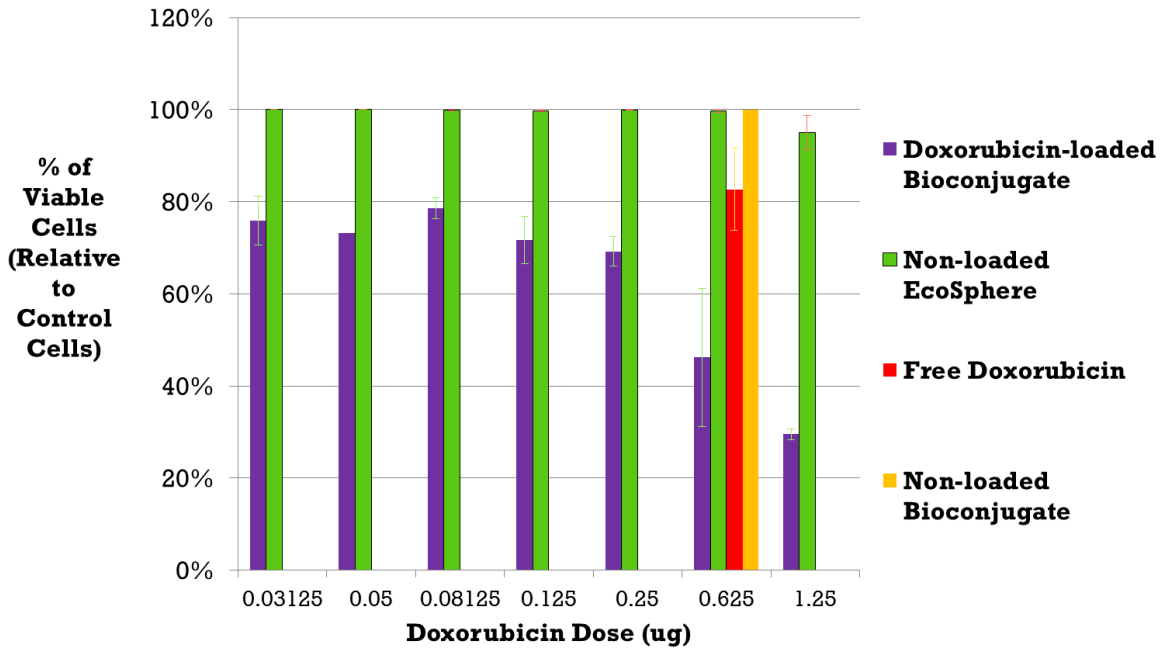

Figure 1-9: Results from an LDH toxicity assay on HeLa cells exposed to modified StNPs for 24 hours. Non-loaded StNPs (EcoSphere) showed no toxicity, however doxorubicin-loaded targeted particles doubled the efficacy of cell killing for the equivalent doxorubicin dose.[80]

1.6 Objectives of This Work

Polysaccharides are important biomolecules with a great range of properties and functions. These molecules play critical roles in biological systems as a biological energy currency, in the cellular glycocalyx affecting cellular surface properties and interactions, and structural functions in plants and animals. There is a large body of research exploring the use of polysaccharides in medicine, including in drug delivery, tissue engineering, and food applications, which has resulted in key clinical improvements, but there remains potential for further work in this field. The hypothesis of this thesis is that the unique properties of polysaccharides can be harnessed for specific medical and dental applications, and the following chapters will explore the preparation and modification of several polysaccharide nanomaterial systems for use in diagnosing

dental caries, providing targeted bactericidal delivery, and targeting cancer cells, towards three aims:

Aim 1: Polysaccharide are well-suited for various modifications and processing techniques that allow them to be prepared and functionalized for medical and dental applications. Building on the significant work already known, we can chemically modify polysaccharides to impart unique functionality, and process these as nanomaterials to engineer and design practical solutions for clinical challenges in medicine and dentistry.

Aim 2: The natural enzymatic degradation of polysaccharides can be harnessed to control the breakdown of nanoparticles for diagnostic and therapeutic applications. After modification of polysaccharides to create new functional nanomaterials, the inherent properties of the original material can still be maintained. The ability of these materials to interact with particular enzymes to be degraded allows for specific targeted degradation strategies in the design of a diagnostic for dental caries and an antibacterial therapeutic.

Aim 3: The specific bio-interactions of polysaccharides can facilitate targeting of eukaryotic or prokaryotic cells. Similar to the cell glycocalyx, engineered polysaccharide systems can interact with biological molecules and can have specific interactions with prokaryotic and mammalian cells. In particular, mannose brushes and cationic starches show high affinity for cancer cells and bacteria, respectively.

CHAPTER 2

Chemical Modification & Preparation of Polysaccharides

The material in this chapter has been partially adapted with minor modifications from the following articles:

(1) N.A. Jones, S. Chang, W.J. Troske, B.J. Clarkson, J. Lahann. "Nanoparticle-based targeting and detection of microcavities", *Advanced Healthcare Materials*, **2017**, 6(1), 160883.[81]

(2) N.A. Jones, U. Kadiyala, B. Serratos, S. van Epps, J. Lahann, "Amylase-Responsive Antibacterial Nanoparticles", *In preparation.*

(3) R. Kumar, N.A. Jones, N. Habibi, J. Zarif, K. Pienta, J. Lahann. "α-Mannose functionalized polymer brushes for the isolation of M2-polarized associated macrophages", *In preparation.*

2.1 Motivation and Background

Polysaccharides are a broad class of bio-based materials and have been used in many different industries and applications. Many of the properties of naturally occurring polysaccharides are desirable for medical and dental applications, including their hydrophilicity and water-solubility; biodegradability by natural biological processes; non-toxicity; and specific bio-interactions.[11] A wide variety of polysaccharide chemical

modifications have been well-studied because of the abundance of these materials, particularly starch and cellulose, with applications in medicine (pharmaceuticals and cosmetics), commodity industrial products (e.g. paper & board, fermentation for the production of amino acids, organic acids, enzymes and yeast, for surfactants, polyurethanes, resins, and in biodegradable plastics, in the construction industry for concrete admixtures, plasters and insulation, as well as in oil drilling, mineral and metal processing, etc.), and consumer products (e.g. textiles and widespread food applications including human and animal food products, beverages, etc.). However, additional niche properties may be desired for particular applications and modification of naturally occurring polysaccharides allows for control of particle size, charge, attachment of functional molecules such as fluorophores or biological targeting, and manipulation of drug-loading and release kinetics. In this chapter we explore the application and characterization of various chemical and material modifications of polysaccharides to prepare these materials for potential medical and dental applications.

2.2 Experimental Methods

2.2.1 Materials

Starch nanoparticles were provided by EcoSynthetix Inc. (Burlington, ON, Canada). Tetramethylpiperidinenitroxide (TEMPO), sodium bromide, sodium hypochlorite, glycidyltrimethylammonium chloride (ETA), fluoresceinamine isomer 1, 1-

ethyl-3-(-3-dimethylaminopropyl) carbodiimide hydrochloride (EDC), FITC-Dextran (10K mol. wt.), fluorescein sodium salt, poly(ethylene glycol) diglycidyl ether, and a Tox8 cell viability assay were used as purchased from Sigma Aldrich, USA. Isopropyl alcohol, sodium hydroxide, ethanol, N-hydroxysuccinimide (NHS) were purchased from Fisher Scientific.

2.2.2 Chemical Modification & Functionalization of Starch Nanoparticles

Cationization of Starch Nanoparticles

Starch nanoparticles were modified to be cationic according to a variation on the procedure shown in Huang *et al*.[67] Seven grams of starch nanoparticles were dispersed at 0.07 g/ml into 100 ml of 0.01 g/ml sodium hydroxide in deionized water. To this dispersion, 3 ml of isopropyl alcohol and 4.3 g (1:2 moles based on glycosidic repeat units of starch) of glycidyltrimethylammonium chloride (70% purity) were added, and allowed to mix for one hour. The mixture was then heated to 75 ^{o}C and left overnight, prior to precipitation in anhydrous ethanol and centrifugation, followed by lyophilization, yielding cationic starch nanoparticles (StNP-2)

TEMPO Oxidation of Starch Nanoparticles

Starch nanoparticles were oxidized according to a modification of the procedure described in Kato *et al*.[82] Briefly, a 100 ml 0.05 g/ml (5 g or 0.03 mol) dispersion of nanoparticles in deionized water was mixed with a 100 ml aqueous solution containing 0.048 g of TEMPO (0.3 mmol) and 0.635 g of sodium bromide (6.2 mmol). The mixture was cooled in an ice bath, and the pH value was adjusted above 10.0 by titrating with a

10% sodium hydroxide solution. Next, 20 g of an 11% sodium hypochlorite solution (1:2 molar ratio to starch nanoparticles) were slowly added to the mixture, while maintaining a pH value above 10.0. The reaction was continued overnight and the product was precipitated in ethanol and separated by centrifugation, followed by lyophilization to isolate the oxidized starch nanoparticles.

Preparation of Zwitterionic Starch Nanoparticles

Zwitterionic Starch Nanoparticles can be prepared by combining the cationization and TEMPO oxidation reactions on the same batch of nanoparticles. As the TEMPO oxidation is specific to the C6 hydroxyl of the starch structure, but the cationization reaction is able to modify any of the starch hydroxyls, these reactions are semi-orthogonal. The experimental protocol for preparation of zwitterionic nanoparticles involved running the TEMPO oxidation protocol on cationic starch nanoparticles, collected after the cationization reaction and purification.

Functionalization of Carboxylated Starch Nanoparticles via EDC/NHS Coupling

EDC/NHS coupling reactions are well-documented as a means of covalently linking molecules containing primary amines ($-NH_2$) to molecules containing carboxyls (-COOH) in non-harsh aqueous conditions. Both the oxidized starch nanoparticles and the zwitterionic starch nanoparticles contain carboxyl functionalities which allow for use of this chemistry to add additional functionality to the particles via any amine-modified functional molecule. For example, to create fluorescently-labelled starch nanoparticles, the following protocol was used, modified from Fischer.[83] Two grams of oxidized

nanoparticles were dispersed in a 20 ml solution of 0.1 M MES, 0.5 M NaCl buffer. A 10-fold molar excess of EDC was added (0.2 g) and allowed to mix for 20 minutes, followed by the addition of a 1.5-fold mass excess of NHS (0.3 g). A 20 ml solution of 0.1 M PBS, 0.15 M NaCl was added to raise the pH above 7. Fluoresceinamine was added at a 1:75 molar ratio (0.05 g) to the oxidized starch glycosidic units, and allowed to react for 2 hours. The particles were precipitated in ethanol, separated by centrifugation, and lyophilized, yielding fluorescein-labeled starch nanoparticles. Depending on the initial starch particles used (zwitterionic StNP-3, or anionic StNP-5), the final particles are fluorescent cationic starch nanoparticles (StNP-4) or fluorescent anionic starch nanoparticles (StNP-6).

2.2.3 Chemical Characterization of Modified Starch Nanoparticles

Fourier Transformed Infrared (FTIR) Spectroscopy

Fourier Transformed Infrared (FTIR) spectroscopy was performed using a Thermo Scientific Nicolet 6700 instrument. Samples were prepared by spin coating a 1% by mass dispersion of modified starch nanoparticles onto a gold-coated silicon wafer, followed by vacuum drying for 24 hours. 128 scans were collected for each sample.

Nuclear Magnetic Resonance (NMR) Spectroscopy

H' Nuclear Magnetic Resonance (NMR) analysis was performed using a Varian MR400 instrument. Samples were dispersed in D_2O at approximately 5% by mass solids

and resonance peak positions and integrations were compared to results from the literature.[82]

X-Ray Photoelectron Spectroscopy

X-ray Photoelectron Spectroscopy (XPS) was run on lyophilized dry starch nanoparticle powder samples using an Axis Ultra X-ray photoelectron spectrometer (Kratos Analyticals, UK), equipped with a monochromatized Al Kα X-ray source at a power of 150 kW.

2.2.4 Characterization of Modified Starch Nanoparticle Physical Properties

Starch nanoparticle samples StNP-1 - StNP-6 were dispersed in 0.01M phosphate buffered saline solution at $2.5x10^{-4}$ g/ml and analyzed by zeta potential and dynamic light scattering (DLS) analysis using a Malvern ZetaSizer, and Nanoparticle Tracking Analysis (NTA) using a NanoSight NS300. All samples had a pH of 7.4 and were measured at 25°C. The zeta potential measurements were conducted by inserting 1 ml of the dispersed nanoparticle formulations into a folded capillary cuvette and run using a standard protocol on the Malvern ZetaSizer, involving three repeat measurements to ensure repeatability. DLS measurements were performed by inserting 1 ml of the dispersed nanoparticle formulations into a polystyrene cuvette and running a standard protocol on the ZetaSizer. NTA size measurements were performed by injecting the sample into the flow chamber and completing three 30 second video measurements,

leading to a cumulative of thousands of individual particle size measurements for each sample condition.

2.2.5 Electrohydrodynamic (EHD) Jetting of Starch Nanoparticles

EHD jetting was performed on starch nanoparticles using the conditions detailed in **Table 2-1**, showing variations of the polymer solution concentration, modifications of starch nanoparticles, and addition of a secondary solvent to water to affect the viscosity and surface tension of the solution. Jetting distance was maintained at 10 inches from needle to collection plate, and voltage was optimized for each incident of jetting, but typically was in the range of 12-15 kV.

Table 2-1: Jetting conditions for starch nanoparticles

Trial	Starch Nanoparticle	StNP concentration (mass percent)	Solvents
A	Unmodified (StNP-1)	5%	80/20 Water/Ethanol
B	Unmodified (StNP-1)	10%	80/20 Water/Ethanol
C	Unmodified (StNP-1)	15%	80/20 Water/Ethanol
D	Cationic (StNP-2)	5%	80/20 Water/Ethanol
E	Anionic (StNP-5)	5%	80/20 Water/Ethanol

Scanning electron micrographs of jetted particles were collected using an Amray 1910 Field Emission Scanning Electron Microscope with a voltage of 5 kV and a beam current of 0.34 nA. From these images, particle size was measured using ImageJ image analysis software.

2.2.6 Cross-Linking of Jetted Starch Nanoparticles

To prevent fracture upon dispersion of EHD-jetted nanoparticles in water, a poly(ethylene glycol) diglycidyl ether (PEGDGE) cross-linker was added into the jetting solution. Initial cross-linking was validated macroscopically using a 10% by mass solution of unmodified, cationic, or anionic starch nanoparticles and adding diepoxide relative concentration of 10, 20 and 30% by mass relative to starch. Samples were left at 22 ^{o}C, 37 ^{o}C, or 45 ^{o}C, and monitored periodically for relative viscosity and qualitative gelation as evidence of cross-linking. Optimized cross-linking conditions from this experiment, as detailed in the discussion and **Figure 2-7** and **Figure 2-8**, were applied to EHD jetted particles resulting in no significant variation in particle size and morphology. Validation of the particle stability following curing was performed by examining SEM micrographs with particles exposed to water.

2.2.7 Evaluation of Modified Starch Nanoparticle Cellular Toxicity

Starch nanoparticle samples StNP-1 – StNP-6 were evaluated for cellular toxicity with a TOX8 (Resazurin based) assay on HeLa cells. The assay was performed according to manufacturer's instructions with appropriate controls. Cells were seeded in 96 well microtitre plates (1×10^4 cells/200 µl growth medium/well) followed by overnight incubation. Supernatants from the wells were aspirated out and fresh aliquots of growth medium (containing StNP in desired concentrations in the range of 0.1–10 mg/ml) were added. After 2 hour incubation time, supernatants were aspirated out and

the cell monolayers in the wells were washed with 200 µL PBS (0.1 M, pH 7.4). Subsequently, TOX8 reagent (20 µl) was added in each well, incubated for 3 h and fluorescence was recorded at a wavelength of 590 nm using an excitation wavelength of 560 nm using the plate reader, allowing for calculation of cell viability for each well. Each concentration was evaluated in triplicate to assess experimental variability.

2.2.8 Preparation of Mannose Brush Polymers

2'Acrylamidoethyl-α-d-mannopyranoside was prepared by Domenic Kratzer and Ramya Kumar of the Lahann Lab.[84] The chemical structure of this product and a schematic of the brush structure following surface-initiated atom transfer radical polymerization (SI-ATRP) is shown in **Figure 2-1**.

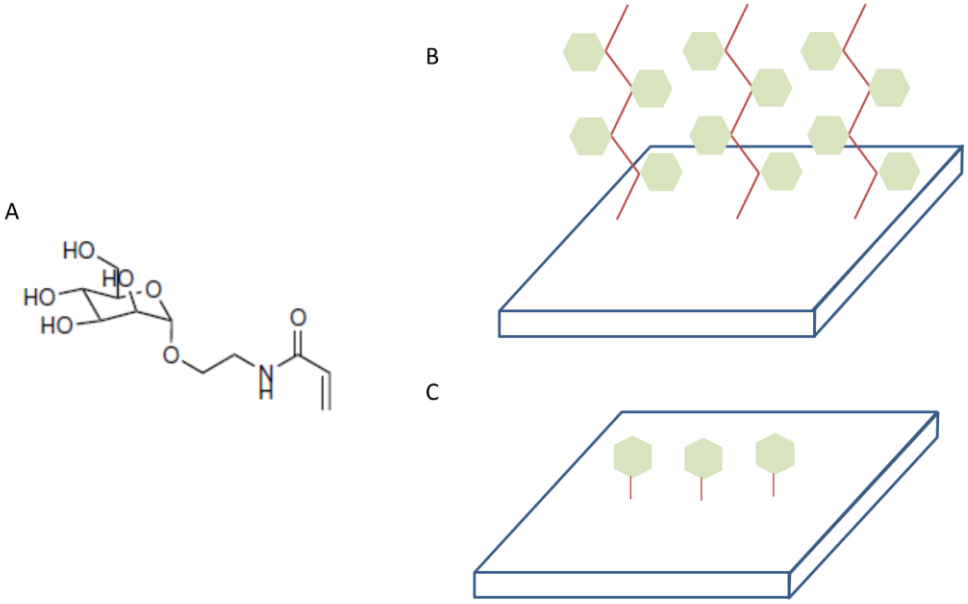

Figure 2-1: (A) 2'-acrylamidoethyl-α-d-mannopyranoside is a polymerizable acrylate with a mannose pendant molecule, capable of being used to prepared mannose brushes. (B) Schematic of sugar brush polymer coating prepared by SI-ATRP. (C) Schematic of sugar monolayer. Chemicals prepared by Ramya Kumar and Domenic Kratzer.[84]

2.3 Results and Discussion

Chemical Modification and Functionalization of Starch Nanoparticles

The chemical modification of starch nanoparticles followed the approach outlined in **Figure 2-2**. The cationic reaction was performed first to effectively modify free hydroxyl groups to make the starch cationic, followed by the TEMPO oxidation of remaining hydroxyl groups. Following the steps shown in Figure 1, cationic (StNP-2), anionic (StNP-5), and zwitterionic (StNP-3) particles were prepared.

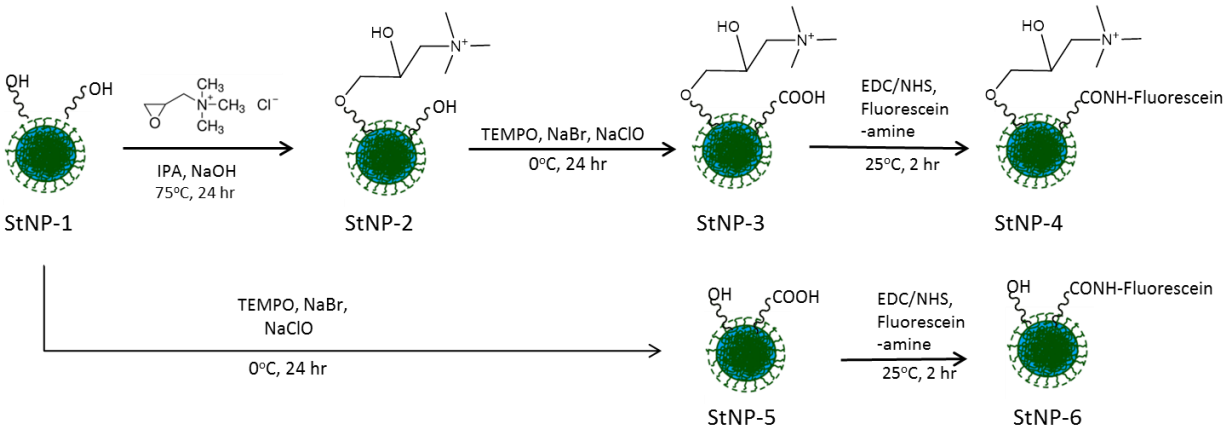

Figure 2-2: Chemical reaction scheme for preparation of starch nanoparticles. Unmodified particles (StNP-1) underwent cationization to prepare cationic particles (StNP-2). TEMPO oxidation on cationic particles (StNP-2) and unmodified particles (StNP-1) yielded zwitterionic particles (StNP-3) and anionic particles (StNP-5), respectively. EDC/NHS chemistry was performed on particles (StNP-3) and (StNP-5) with fluorescein amine to yield cationic fluorescent (StNP-4) and anionic fluorescent (StNP-6) StNP particles, respectively.[81]

FTIR Characterization of Modified Starch Nanoparticles

FTIR spectra of these particles are shown in **Figure 2-3**. All samples share characteristic bands of a starch backbone, including (C-O) stretching bands at 1154 cm^{-1}, 1121 cm^{-1}, and 1017 cm^{-1}, (CH) stretching bands at 2926 cm^{-1}, and a broad (OH) vibration band centered around 3414 cm^{-1}. There are increased bands at 2932 cm^{-1} (CH

alkane), 1450 cm^{-1} (CH alkane), and 1390 cm^{-1} (CH aldehyde) and the appearance of new bands at 2830 cm^{-1} (CH aldehyde), 1720 cm^{-1} (C=O aldehyde), and 1493 cm^{-1} (C-N). These results are consistent with previously reported data on similar reactions.[68,85,86] The IR spectrum of anionic StNPs indicates a sharp increase of the bands at 1710 cm^{-1} (C=O carboxyl) and 1422 cm^{-1} (-COOH). The zwitterionic StNPs show evidence of all of these bands, suggesting the presence of both carboxyl and cationic functional groups.

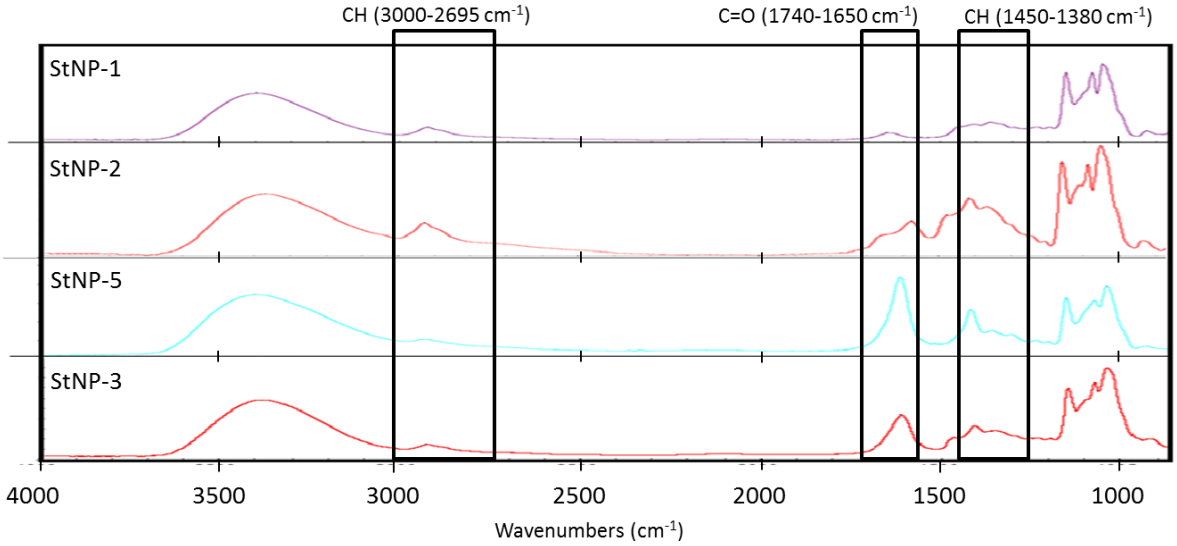

Figure 2-3: FTIR spectra for unmodified (StNP-1), cationic (StNP-2), anionic (StNP-5), and zwitterionic (StNP-3) starch nanoparticles. Regions of interest for C-H and C=O peaks are highlighted.[81]

X-ray Photoelectron Spectroscopy Analysis of Modified Starch Nanoparticles

XPS was performed to confirm the cationization of the starch nanoparticles, with results as shown in **Table 2-2**.

Table 2-2: X-ray Photoelectron Spectroscopy results for unmodified and modified starch nanoparticles, highlighting the efficiency of the cationization reaction by analysis of nitrogen content. Theoretically predicted values are shown in brackets.[81]

	StNP-1 (Unmodified)	StNP-5 (Anionic)	StNP-2 (Cationic)	StNP-3 (Zwitterionic)
O (532 eV)	36.4% (45.5%)	31.7% (50%)	31.4% (31.6%)	26.3% (38.7%)
C (285 eV)	63.3% (54.5%)	59.7% (50%)	65.7% (63.2%)	56.5% (58.1%)
N (401 eV)	0% (0%)	0% (0%)	1.5% (5.3%)	2.0% (3.2%)
Na (1071 eV)	0% (0%)	3.9% (0%)	0.4% (0%)	2.9% (0%)
Cl (198 eV)	0% (0%)	4.7% (0%)	0.3% (0%)	7.1% (0%)

The unmodified (1), anionic (5), cationic (2), and zwitterionic (3) starch nanoparticles were analyzed by XPS to determine the chemical composition, in particular examining the presence of Nitrogen which is unique to the cationic functional group, as is common in the literature for analysis of starch cationization.[67,68,74] Results shown indicate the measured atomic percentage of Oxygen, Carbon, Nitrogen, the theoretical expected maximum (in brackets) and the detectable most common impurities Sodium and Chlorine, resultant from the presence of these chemicals in both the oxidation and cationization reactions. It was noted that nitrogen was not detectable in the unmodified and anionic StNP samples, but was present in the cationic and zwitterionic StNP samples on the order of 1.5-2.0 atomic percent, which corresponds to a DS of approximately 0.28, consistent with similar studied reactions for highly cationic starch (ranging from 0.22-0.35).[85,86] Starch cationization is a commonly used reaction in industrial settings for food and textile applications,[85] and particularly in wet-end paper manufacturing due to desirable electrostatic interactions with anionic cellulose fibers and fillers. Thus, there is a wide body of work exploring nuances of reaction methodologies to control and optimize starch cationization reactions using batch[85] and continuous extrusion methods.[74] The DS could conceivably be stretched further using techniques in Pi-Xin *et al.*,[86] and

future studies can examine how the modification of particle charge impacts the ability of the particle to adhere to carious lesions.

TEMPO Oxidation of Starch Nanoparticles

To characterize the TEMPO oxidation reaction, ^{1}H NMR analysis was performed and shown in **Figure 2-4**.

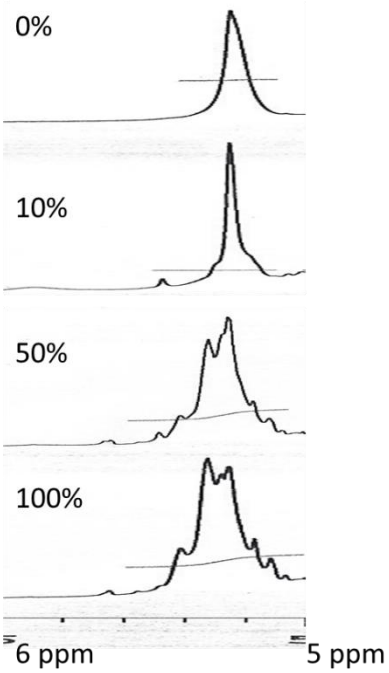

Figure 2-4: (^{1}H-NMR results for TEMPO oxidation reaction, showing the peak shift corresponding to conversion of the C6' hydroxyl to a C6' carboxyl (5.2→5.4ppm) with increasing amount of added sodium hydroxide (percentage on left)).[81]

Common methods for the oxidation of starch typically involve degradation of the ester backbone to create carboxylic acids.[82] These methods are destructive of the starch

chemical structure, and reduce molecular weight. In the modification of starch derived from granules, where the polymers have incredibly high molecular weight and are protected by the crystalline granule structure, these oxidation methods are acceptable, however in the controlled modification of starch nanoparticles, this is undesirable. Consequently, we explored the use of tetra-ethoxy-methyl-piperidine (TEMPO) as an oxidizing agent, using reaction schemes previously published by Kato *et al.*[82] This reaction offers several advantages over standard starch oxidation techniques. First, the oxidation is an additive chemical reaction compared to destructive. This allows for preservation of the molecular weight of the polymer, which is critical to the integrity and particle size of starch nanoparticles. Second, the oxidation is specific to the C‘6 hydroxyl of the starch, because of steric hindrance of the TEMPO oxidant. This controls the reaction to allow for stoichiometric substitution, and consequently more precise control of the number of functional carboxyls, depending on the reaction conditions, which is highly desired for the preparation of modified nanoparticles. Starch nanoparticles were modified by TEMPO oxidation, and ^{1}H-NMR results were measured for increasing amounts of added sodium hydroxide, shown as a percentage, with 100% corresponding to a 1:1 molar ratio of NaOH : starch glucose units. This allowed for a determination of the Degree of Substitution (DS) for the reaction by noting the peak shift of the C’6 hydroxyl to a C’6 carboxyl, from 5.2→5.4 ppm. Measuring the relative peak integrals determined that a maximum DS of approximately 55% was obtained. This reaction is limited from possibly reaching full conversion because of the cross-linking and branched nature of the starch, resulting in fewer chemically and sterically available C’6 hydroxyls. Furthermore, as discussed by Kato,[82] small levels of C’6 aldehyde or hemiacetal

intermediates can be formed, which explain the additional peaks visible in the ^{1}H-NMR spectra.

Characterization of Starch Nanoparticle Physical Properties

In addition to the chemical analysis, physical particle analysis was also performed on these samples, including particle size analysis by NTA and DLS, as well as zeta potential measurements (**Table 2-3**).

Table 2-3: Particle size and zeta potential results for modified StNPs. Size was measured by intensity-weighted dynamic light scattering and number-weighted nanoparticle tracking analysis.[81]

StNP Sample	Zeta Potential [mV]	DLS Size (Intensity-weighted) [nm]	NTA Size (Number-weighted) [nm]
StNP-1 (Unmodified)	-0.6 ± 1.0	53 ± 23	41 ± 28
StNP-5 (Anionic)	-30.5 ± 3.0	90 ± 76	24 ± 17
StNP-6 (Anionic Fluorescent)	-9.3 ± 2.3	36 ± 32	45 ± 33
StNP-2 (Cationic)	+22.7 ± 1.3	35 ± 33	20 ± 11
StNP-3 (Zwitterionic)	+8.2 ± 2.0	250 ± 110	101 ± 33
StNP-4 (Cationic Fluorescent)	+5.8 ± 1.2	209 ± 110	101 ± 56

Variation in particle size between NTA and DLS occurs, because NTA provides a number-weighted measurement, while DLS provides an intensity-weighted measurement of particle size. Consequently, DLS measurements of polydisperse or aggregated samples will report larger diameters than the NTA measurements of the same particles.[87] The NTA particle size distributions are shown in **Figure 2-5**.

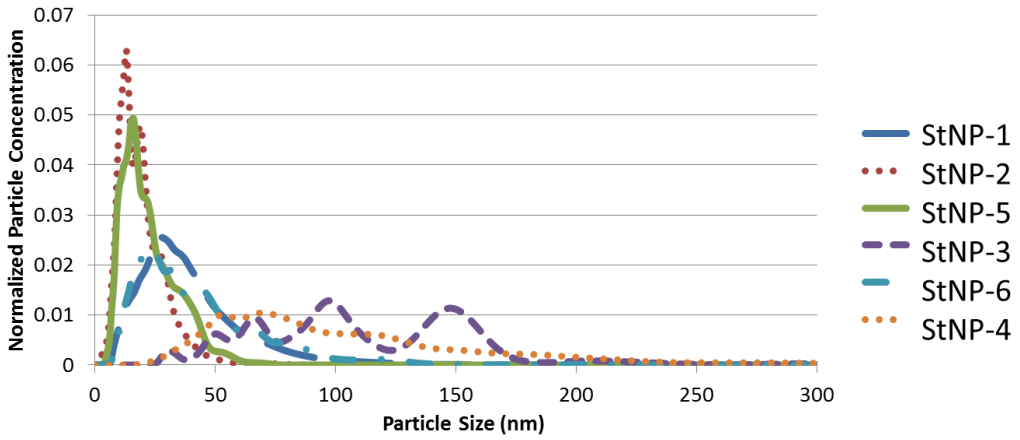

Figure 2-5: Particle size distribution of modified StNPs, measured by Nanoparticle Tracking Analysis. StNP-1: Unmodified; StNP-2: Cationic; StNP-5: Anionic; StNP-3: Zwitterionic; StNP-6: Anionic Fluorescent; StNP-4: Cationic Fluorescent.[81]

Initially, unmodified StNPs (StNP-1) showed a particle size of 41 nm and negligible charge. After TEMPO oxidation (StNP-5), particle charge decreased to -30.5 mV and average particle size decreased to 24 nm. The subsequent reaction with fluorescein via the EDC-NHS reaction reduced the particle charge from -30.5 to -9.3 mV to result in anionic fluorescent StNPs. In a separate preparation, after cationization (StNP-2), the average particle size decreased to 20 nm and the charge increased to +22.7 mV. For both anionically and cationically modified StNPs a decrease in particle charge was expected because of the addition of charged modalities on the particle surface, which inhibit aggregation, resulting in an overall decrease in average particle size. When both reactions were combined through TEMPO oxidation of the cationic StNPs zwitterionic particles were prepared, and the average particle size increased to 101 nm corresponding

with an increase in PDI and particles showed a moderate net cationic charge of +8.2 mV. This can be explained due to the interaction of alternately charged groups present on the surface of the particles resulting in aggregation, increasing the average particle size and the breadth of the size distribution. The subsequent reaction with fluorescein via the EDC-NHS reaction reduced the particle charge from +8.2 to +5.8 mV, and appeared to have no significant impact on particle size.

EHD Jetting of Starch Nanoparticles

The Lahann Lab has used electrohydrodynamic (EHD) jetting as a method to prepare polymeric fibers and particles of sizes ranging from nanometers to microns.[88-90] This method can be modified using co-jetting, allowing for the preparation of particles or fibers with two or more distinct compartments, which promises to be a robust technological platform for imaging and therapy in medical and dental applications.[89,91-93] With each jetting needle, precise control of the loading with a desired amount of an imaging modality or therapeutic can be encapsulated in a polymer matrix of choice. For each compartment, the degradation rate can thus be set independently of the other compartments.[24,92,94,95] This technology allows for control of particle and fiber properties, including formation of multi-compartmental particle geometries[89,96,97] which enable independent control of key parameters, such as chemical composition,[94,98] surface functionalization,[99,100] biological loading,[24,92,93,95,101,102] shape,[103-105] and size[24,89,90] for each hemisphere of the particle or fiber, and can produce a wide range of multifunctional therapeutic carriers.[24,90,92,95,102,106]

EHD jetting was performed using StNPs to control particle size, morphology, drug loading, and add additional functionalities to the particles. Initial tests using StNP dispersions in water were unsuccessful as the solution tended to drip resulting in minimal production of particles. Ethanol was substituted into the solutions up to 20% by volume to lower the surface tension, resulting in less dripping and more stable jetting which yielded nanoparticles. Examples of EHD StNP particles as jetted are shown in **Figure 2-6** for increasing StNP concentrations in the jetting solution.

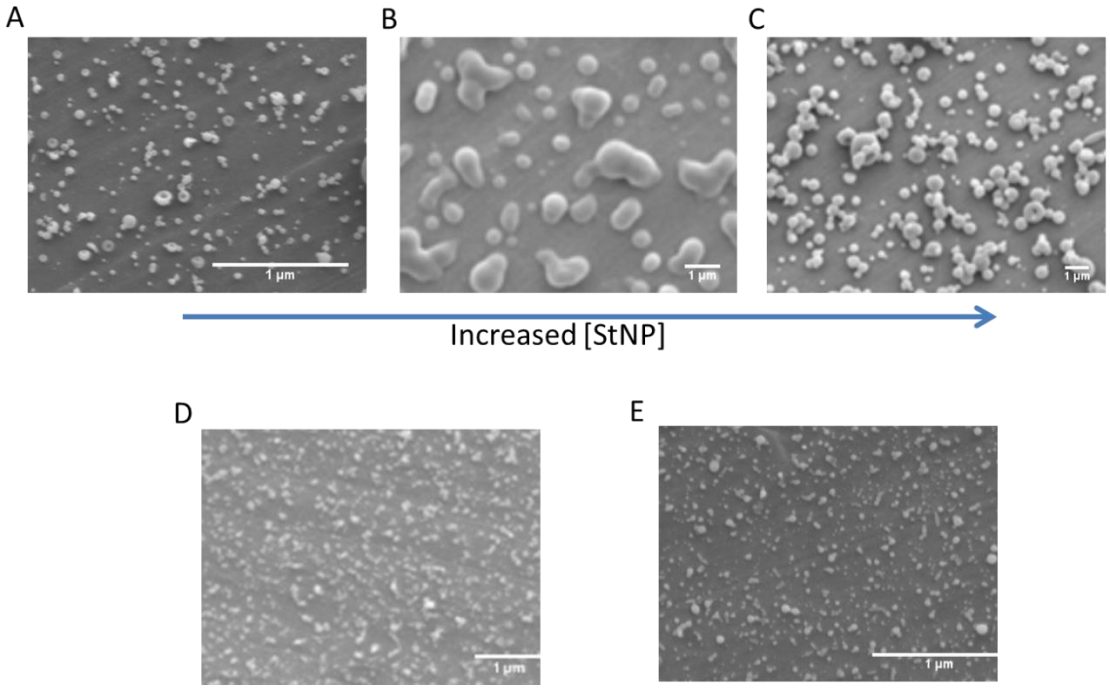

Jetting Recipe Description	Particle Size (nm)
A) 5% StNP	152 ± 54
B) 10% StNP	524 ± 203
C) 15% StNP	385 ± 153
D) 5% Anionic StNP	102 ± 35
E) 5% Cationic StNP	110 ± 45

Figure 2-6: Scanning Electron Micrographs of EHD jetted starch nanoparticles for conditions described in table, with particle size measurements.

Generally, increasing the StNP concentration in the jetting solution increased the average particle size, a result previously reported by the Lahann Lab for other polymer systems.[89] Furthermore, recipes formulated with charged StNPs were smaller than comparable recipes using uncharged StNPs, possibly because of increased droplet-droplet repulsive forces resulting in lower surface energy, similar to the effect of incorporating ionic surfactants in other studied recipes.[90] These studies identify the potential of using EHD jetting to prepare starch nanoparticles with control of the particle size and incorporation of modified starched.

Cross-Linking of Jetted Starch Nanoparticles

As the jetted StNPs are simply dried aggregates, dispersion in water results in immediate reversal of the jetting protocol and quick dispersion of the original StNPs. Therefore, a Poly(Ethylene Glycol) Diglycidyl Ether (PEGDGE) cross-linker was incorporated into the recipe to stabilize the jetted particles. This cross-linker is advantageous because it has low reactivity at room temperature and it can be activated by applying thermal energy. As a result, the jetting solutions are stable for the duration of the EHD jetting process, and the particles can be cross-linked by curing in an oven. Initial tests were performed to determine macroscopic gelation for various StNP samples, and temperatures, as a function of time. It was found that the cross-linker reacted best with the cationic StNPs, as compared to other modifications, and it is suspected that the quaternary ammonium has higher reactivity with the glycidyl ether than hydroxyls or carboxyls in unmodified or anionic StNPs. Reaction kinetics with the cationic StNPs for 10%, 20%, and 30% by mass relative cross-linker concentrations were probed by

qualitatively determining viscosity of the solution, and it was found that temperature elevation over the course of 72 hours with 30% incorporation of PEGDGE was sufficient to achieve full gelation, with results shown in **Figure 2-7**.

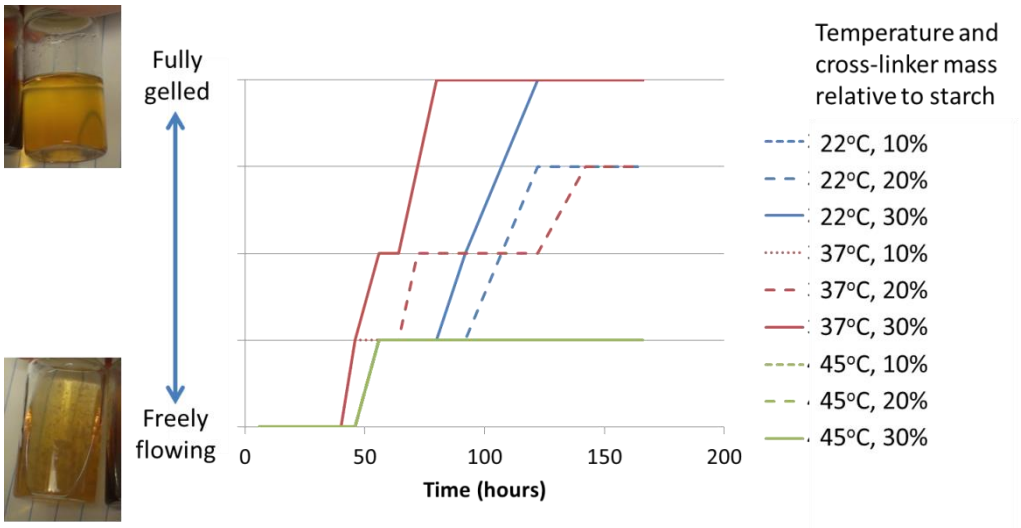

Figure 2-7: Qualitative analysis of cationic starch cross-linking kinetics by poly(ethylene glycol) diglycidyl ether for varying temperatures and relative cross-linker concentrations.

Using these optimized conditions, the PEGDGE cross-linker was added into the jetting recipes with minimal impact on the particle size and morphology. Successful curing was validated by examining the particle morphology with SEM after wetting and subsequent drying of the particles, shown in **Figure 2-8**.

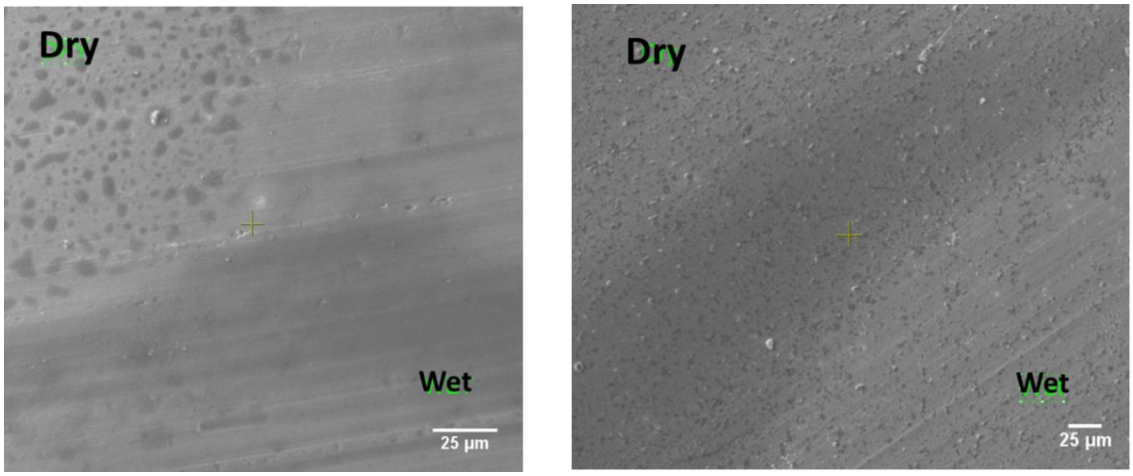

Figure 2-8: Scanning electron micrographs of jetted cationic starch particles before (left) and after (right) curing. The lower right diagonal was wetted, leaving the upper left diagonal dry to observe particle stability upon wetting.

For the uncured sample, the wetted region is devoid of particles, while the unwetted region showed evidence of volatile organic compounds with the appearance of dark carbon patches, likely the unreacted liquid PEGDGE. In contrast, the cured sample showed consistent particle morphology before and after wetting, and no evident release of volatile organic compounds.

Evaluation of Modified Starch Nanoparticle Cellular Toxicity

The results from the Tox8 cellular toxicity assay are shown in **Figure 2-9**. These results indicate that all the particles were nontoxic even at high concentrations of 0.01 g/ml.

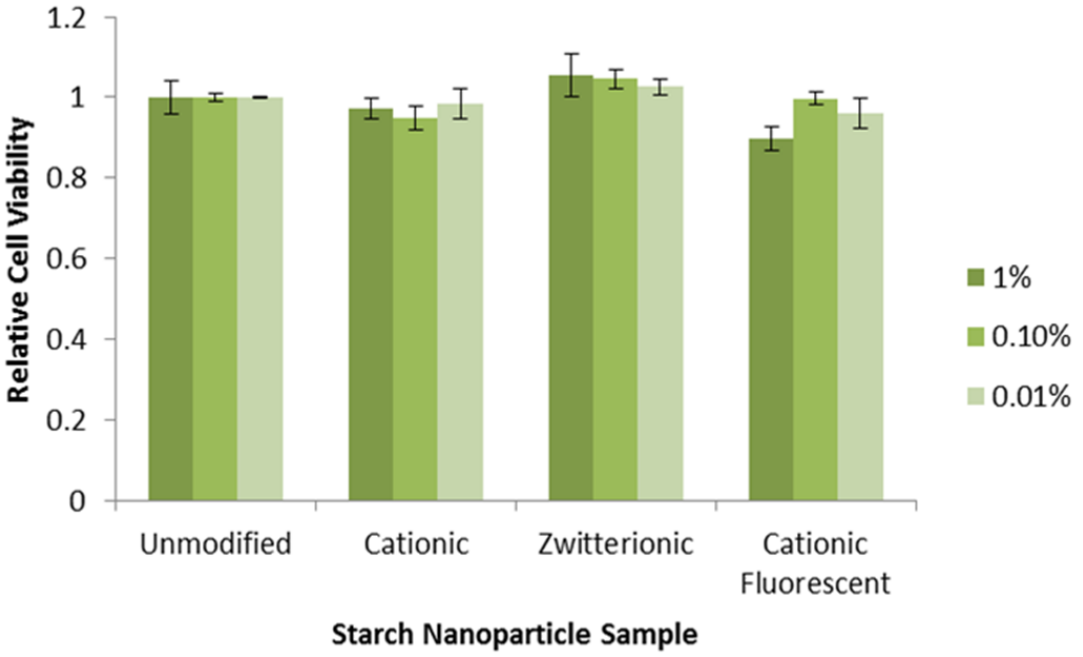

Figure 2-9: HeLa cell viability following 2 hour incubation with modified starch nanoparticles, as determined by Tox8 assay. Bradley Plummer (Lahann Lab) ran the toxicity assay. [81]

2.4 Summary

In this chapter several modifications and preparations of functional polysaccharide macromolecules are discussed. We examined how starch nanoparticles can be modified to control the charge, size, and incorporation of functional molecules. Furthermore, we evaluated the potential of using EHD jetting to prepare starch nanoparticles to further manipulate the materials properties. These novel molecules were characterized using a variety of techniques, including NMR, FTIR, XPS, NTA, DLS, and SEM, and the cellular toxicity was evaluated to be minimal for high concentrations of particles. Using this toolbox of modifications and chemistry, which only represents a small portion of the flexible chemistries and materials preparation techniques used to modify polysaccharides, we will explore specific applications of these functional polysaccharides in dentistry and medicine in the following chapters of this dissertation.

CHAPTER 3

Biopolymer Nanoparticle-Based Targeting and Detection of Dental Caries

The material in this chapter has been adapted with minor modifications from the following articles:

(1) N.A. Jones, S. Chang, W.J. Troske, B.J. Clarkson, J. Lahann. "Nanoparticle-based targeting and detection of microcavities", *Advanced Healthcare Materials*, **2017**, 6(1), 160883.[81]

(2) N.A. Jones, S. Chang, B. Serratos, W.J. Troske, B.J. Clarkson, J. Lahann. "Targeted Nanoparticles for Remineralization of Dental Caries", *In preparation.*

3.1 Motivation and Background

The use of nanoparticles for medical applications has garnered considerable interest, particularly for drug delivery, diagnostics, and imaging.[15,106,107] Oral health applications of nanoparticles have not yet received as much attention, but offer potential for technological advances that can immediately impact patient treatment and outcomes. Nearly everyone will develop caries at some point in their life.[108,109] Worldwide, dental caries is the most prevalent disease with approximately 36% of the world's population presenting with active caries. In the US, dental caries is the most common chronic disease and more than 90% of adults will have experenced dental caries in their permanent teeth. The average American adult has 3.3 decayed or missing teeth, and 25.5% of adults have

untreated dental caries. Adults and children of lower socioeconomic class have more untreated dental caries, because of lack of access to affordable treatment.[110]

Dental cavities form when bacteria in the dental biofilm on the surface of teeth ferment sugars and produce acids, which demineralize enamel and/or dentin. Generally inactive lesions require no treatment while active lesions do. Early active lesions permit conservative remineralization treatment, while cavitated lesions require dental restoration. An active lesion is one that is progressing and has a slightly decalcified (approximately 5% compared to normal enamel) microporous surface, overlying a subsurface lesion that may have a porosity as high as 30-40%.[111,112] In contrast, an inactive lesion is not progressing, because the porosity, particularly on the surface, has been reduced by mineral and/or protein deposition, thus facilitating conservative management. Smaller, early stage active carious lesions, also called "microcavities", incipient carious lesions, or white spot lesions, can be reversed by a process called remineralization, which uses the calcium and phosphorous in the saliva and is aided by the presence of fluoride in drinking water or toothpaste.[109] However, if decalcification continues, irreversible cavitation will occur, requiring a dental procedure to avoid further progression of the carious lesion. If left untreated, caries progression can lead to pain, tooth loss, alveolar bone resorption, and in rare cases, death.

The diagnosis of active dental caries is challenging, as presentation is highly variable.[108,113,114] Typically, diagnosis of caries is carried out optically and tactically with a dental mirror and explorer using techniques which have not changed in almost a century.[114,115] However, tactile detection of a carious lesion by applying pressure on a dental explorer on a demineralized lesion may lead to cavitation.[114] X-ray images of the

teeth can be taken to identify cavities, particularly for regions in between teeth (interproximal caries); however, this suffers from several limitations. X-ray images lack the resolution to identify early forming lesions, which can still be repaired by an improved oral hygiene regimen and a fluoride application.[116] There are several new alternative methods for caries diagnosis that have been developed to address these drawbacks, including fluorescence, optical, radiographic, and electrical conductance methods.[108,117] These methods require additional equipment, show minimal benefit over optical diagnosis, and incur greater cost to dentist and patient.[108,113,117] Most importantly these methods only diagnose a lesion in the enamel surface, but do not distinguish between active and inactive lesions, which is the most critical need in modern cariology.[113]

If active carious lesions can be diagnosed before irreversible cavitation occurs, the patient and dentist can be alerted to improve dental hygiene in specific regions of the mouth. In this study, we have indirectly shown that the carious lesions have a negative surface charge, and therefore cationic nanoparticles may be used for targeting lesions due to electrostatic interactions. To this end, we report a starch-based fluorescently-labeled cationic nanoparticle which selectively adsorbs onto active white spot enamel lesions *in vitro*. The use of food-grade starch as the base polymer makes the particles non-toxic and biodegradable upon exposure to salivary amylase. Fluorescein was chosen as a fluorophore for its understood safety profile and low toxicity in other diagnostic applications.[118] Using fluorescein, carious lesions can be identified using a standard dental composite curing light, commonly used in dental offices. With further research and following successful clinical studies, these particles could be used by patients as a

local application, mouth wash or rinse after cleaning the teeth, and then evaluated by a dentist or dental hygienist with illumination using a standard dental composite curing lamp to identify stained regions as active carious lesions.

In summary, our ultimate goal is to develop a new clinically valid methodology to diagnose early active carious lesions that also enables effective monitoring of conservative treatment. The work reported here establishes the proof-of-principle which demonstrates the potential of this technology. We have developed a nanoparticle technology which specifically targets active carious lesions. The nanoparticles are made from food grade corn starch. We have functionalized them so they specifically target the inside of dental caries. They are tagged with a safe fluorescent dye so the caries will illuminate and be easily seen using a standard dental curing lamp. This would allow dentists to differentiate whether a carious lesion is active or inactive, and could be used to monitor treatment results. The product envisioned is a mouth rinse or local application containing a low concentration of the nanoparticles in water. This would help detect early active carious lesions not visible on the tooth surface, because the extremely small nanoparticles are able to penetrate through surface pores into a very early active lesion. The starch-based nature of these particles allows for rapid degradation by amylase, an enzyme present in human saliva, so teeth will no longer fluoresce upon leaving the dentist's office. With earlier detection of caries and less invasive management, cavitation and expensive treatments will be prevented, resulting in a reduction in dental expenditures by patients, insurance companies and other payers.

3.2 Experimental Methods

3.2.1 Chemical Modification of Starch Nanoparticles

The chemical reaction scheme for modification of starch nanoparticles was presented in **Figure 2-2,** found in chapter 2, and used materials, the chemical reaction protocol, and chemical and physical characterization of the prepared nanoparticles is also included there.

3.2.2 Particle Degradation Assays

Starch particles were dispersed at 0.01 g/ml in deionized water. Half of the particle dispersions were set aside as an initial dispersion and diluted at a 1:1 ratio with DI-water. The remaining half of the particle dispersions were taken and diluted at a 1:1 ratio with saliva, and placed in an incubator at 37° C for 30 minutes. Saliva was collected (donated; human subject exempt) and used immediately to minimize potential denaturation of salivary enzymes. Both the initial and final dispersions were tested with iodine and Benedict's reagent.

Iodine Test

Twenty microliters of iodine solution were added to 2 ml of the initial and final dispersions, and examined for color using ImageJ software.[119]

Benedict's Reagent Test

Twenty microliters of Benedict's reagent were added to 2 ml of the initial and final dispersions and heated to 80°C for 30 minutes, and then evaluated with a UV-Vis spectrophotometer to measure absorbance at a wavelength of 735 nm.

3.2.3 Preparation of Artificial Carious Lesions in Extracted Human Teeth

Extracted teeth were obtained from the School of Dentistry, University of Michigan (human subject exempt) and stored in 0.01 g/ml sodium azide before use. The teeth were coated with an acid resistant varnish leaving a 1 mm^2 enamel window on the buccal surface of the crowns of the teeth. The teeth were then immersed in a pH 5.0 demineralization gel containing 0.1 M lactic acid, 4.1mM $CaCl_2$-$2H_2O$, 8 mM KH_2PO_4, and 1% w/v carboxymethylcellulose sodium at 37^o C for 8 days.[120] At the completion of demineralization, the teeth were rinsed with DI-water before subjection to caries activity testing. Residual varnish was removed by washing in acetone.

3.2.4 Scanning Probe Microscopy

Image Acquisition

SPM images were acquired on a PicoPlus^{TM}-SPM (Scanning Probe Microscopy) instrument from Agilent Technologies. The images were obtained in air with AC (tapping) mode using a multipurpose small scanner. Non-contact silicon tips were used (made by Nanosensors^{TM}) with aluminum coating on the detector side. The tip parameters are as follows: thickness: 4.1 ± 1 µm, length: 125.0 ± 10 µm, width: 27.0 ±

7.5 µm, resonance frequency: 345 kHz. Picoview® 1.4 USB software from Agilent Technologies was used for image collection, and SPIP® (Scanning Probe Image Processor) 4.5 software from Nanosensors was used to process collected images. Typically, a range of 1.0-2.0 line/s scanning speed was used, with a setpoint of +0.85 V of the cantilever oscillation amplitude in free air. To avoid the hydrodynamic effect of thin air gaps, the resonance was carefully measured at a small tip-sample distance (<300 µm).

Pore Size Analysis

SPM tapping mode images were collected for sound and demineralized enamel surfaces. Pore sizes were calculated using ImageJ analysis software, and compared statistically using a student's T-test.

Surface Potential Analysis

SPM surface potential images were collected by using the same image collection parameters, except substituting a Bruker SCM-PIT-V2 0.01-0.025 Ω/cm Antimony-doped Silicon tip with the following parameters: thickness: 2.8 µm ± 1 µm; length: 225 µm ± 10 µm; width: 35 µm ± 7.5 µm, resonance frequency: 75 kHz. Corresponding topology and relative surface potential measurements were collected for a variety of sound and demineralized surfaces.

3.2.5 Cavity Diagnostic Testing

For caries testing, 0.01 g/ml solutions of FITC-dextran, StNP-4, and StNP-6, and a 10^{-5} g/ml solution of fluorescein sodium salt were prepared. Teeth were exposed to 20 µl of sample for 3 minutes prior to rinsing in DI water. Rinsing proceeded for 10 seconds, and the teeth were examined and photographed, while illuminated with a dental curing light. Rinsing was then continued for an additional 10 seconds, followed by imaging, and this was repeated for up to 5 minutes to determine residence times for each sample used to optimize the exposure and rinsing procedure.

A 20 second rinse in DI water was sufficient to wash away all but the cationic fluorescent StNPs, which remained even up to 5 minutes. Fifteen teeth were divided into 3 groups of 5 samples for testing with each control (fluorescent FITC-Dextran, anionic fluorescent StNP, and fluorescein sodium salt). After a 3 minute exposure followed by 30 seconds of rinsing, imaging was performed under illumination by the dental curing light. The same teeth were then dosed with fluorescein-labeled cationic StNPs and imaged to demonstrate the ability of these particles to illuminate the carious lesions that could not be lit by the various controls.

3.2.6 Remineralized Lesions Activity Testing

Prior to remineralization, active lesions were illuminated with StNP-4 to obtain a baseline readout. These demineralized teeth were then remineralized by immersion in a remineralization solution containing 0.02 M cacodylic acid sodium salt, trihydrate, 1.5 mM $Ca(NO_3)_2$-$4H_2O$, 0.9 mM NaH_2PO_4-H_2O, 150 mM KCl, and 0.05 ppm NaF, with pH

value adjusted to 7.0.[121] Teeth were immersed at 37°C for 13 days. Images of remineralized teeth were taken for analysis prior to, and after exposure to cationic fluorescent StNPs.

3.2.7 Image Analysis

Digital images were taken with a Canon DS126061 DSLR camera with a Sigma 105 mm 1:2.8 DG Macro lens and analyzed using ImageJ image analysis software. This provided RGD images and ImageJ image analysis techniques were used to compare the brightness of the carious lesion relative to the background tooth. Green pixel images were then extracted using ImageJ software and analyzed by the same methods. Digital images were also taken with a Fluorchem M Imaging system, with auto-exposure, blue light illumination and a green 542 nm bandpass filter applied to validate the particle fluorescence in the carious lesions, and analyzed using the same methods with ImageJ image analysis software.

3.2.8 Two-Photon Microscopy

Treated teeth were examined using a Leica TCS SP8 Two-Photon Confocal Microscope equipped with FLIM & FCS capabilities using a 40X oil-immersion objective. Samples were immersed in oil and placed on a glass-bottomed petri dish. The illumination wavelength was set to 810 nm, and z-stack images were collected for a variety of tooth samples.

3.3 Results and Discussion

Degradation of Biopolymer Nanoparticles in Saliva

The degradation of starch particles in saliva was demonstrated using iodine and Benedict's reagent tests (**Figure 3-1**). A colorimetric method of analyzing the iodine solutions was used instead of direct absorbance measurements to avoid precipitation in the well plates.[119]

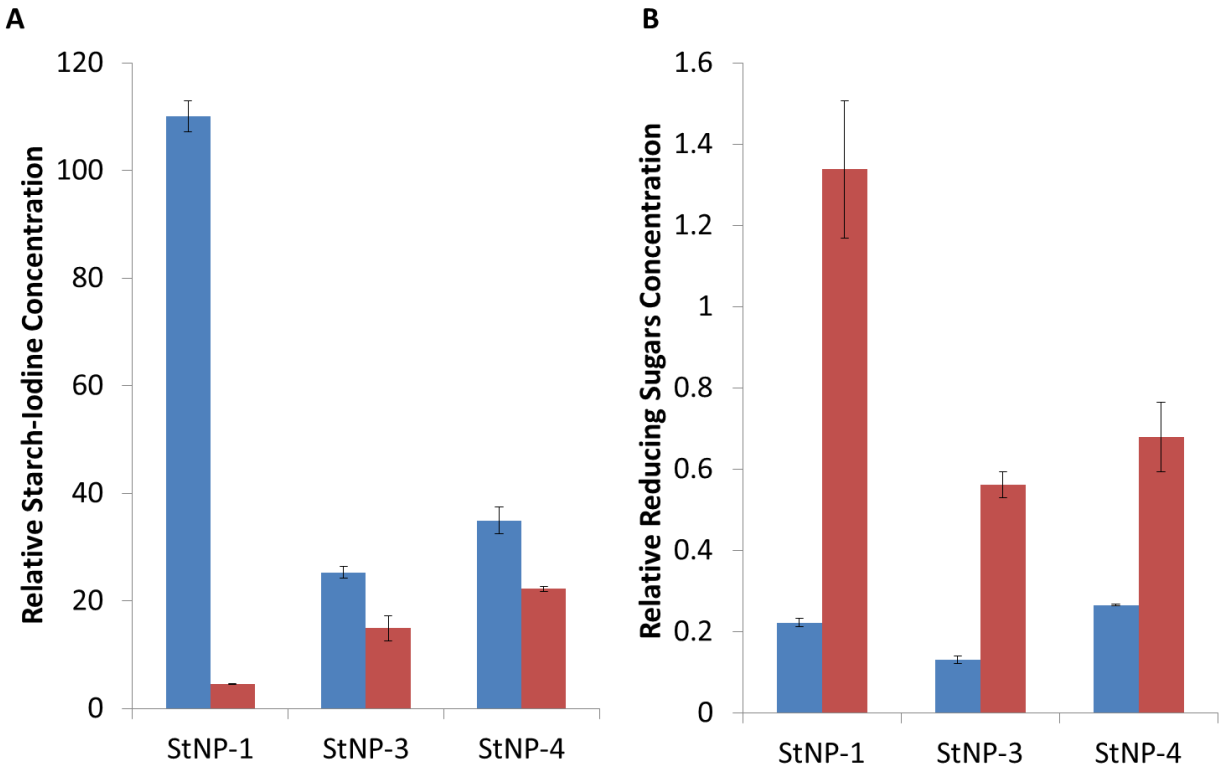

Figure 3-1: Starch degradation results for StNP-1 (unmodified), StNP-3 (zwitterionic), and StNP-4 (cationic fluorescent) starch nanoparticles, showing levels of starch-iodine complex in A) and reducing sugars content by Benedict's test in B). Both graphs show initial levels, in blue, and a final measurement, in red, after 30 minutes of exposure to salivary amylase in human saliva. A) The iodine concentration is a measure of red intensity, which decreases from initial to final states when exposed to saliva, indicating degradation of starch. The Benedict's reaction was measured by comparing absorption values at 575 nm and shows an increase in absorption after degradation by saliva, indicating the presence of reducing sugars. Results show that in the presence of saliva, starch and modified starch nanoparticles are degraded into simple sugars. ($p<0.005$ for all initial (blue) *vs.* final (red) comparisons).[81]

UV-Vis absorbance measurements were used to quantify the Benedict's test. For unmodified (StNP-1), zwitterionic (StNP-3), and cationic fluorescent (StNP-4) StNPs, the iodine test showed a decrease in starch staining after 30 minutes of exposure to saliva, while the Benedict's test showed an increase in the presence of reducing sugars. The initial starch-iodine concentration of StNP-1 is higher than the modified nanoparticles (StNP-3 and StNP-4) because the modifications to the starch chemistry inhibit the ability of the iodine to interact with the starch.[122] Similarly, with Benedict's test the modified starches yield fewer reducing sugars, because the starch modification prevents degraded sugars from reducing the Benedict's copper reagent. Nevertheless, these results indicate that starch particles are degraded into reducing sugars after a 30 minute exposure to saliva. Based on these data, we concluded that the starch particles can degrade in the patient's mouth within less than an hour after they have been used by the dentist for diagnosis.

Topological and Surface Potential Evaluation of Dental Caries by SPM

Teeth with and without active dental caries were evaluated using a Scanning Probe Microscope for topology and surface potential. Using ImageJ image analysis software, pore sizes were measured and statistically evaluated. A sample 3-D topographical map which shows the edge of a carious lesion bordering sound enamel is demonstrated in **Figure 3-2**.

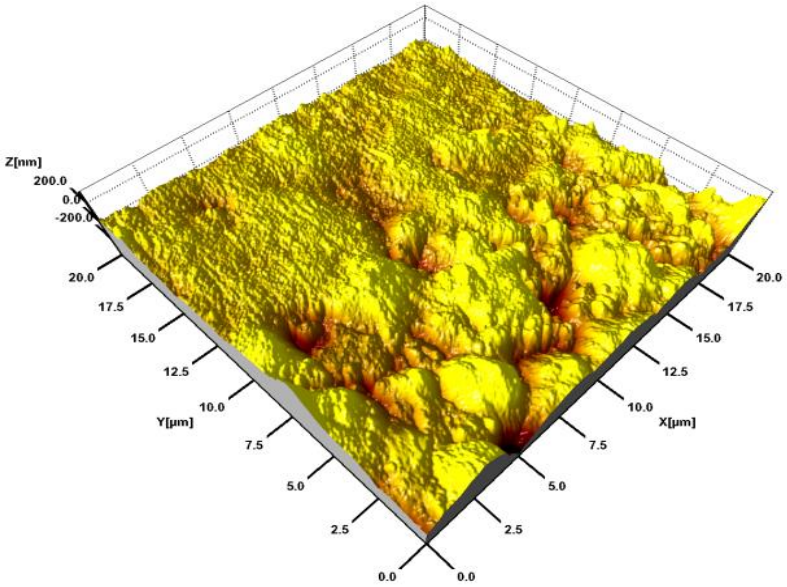

Figure 3-2: Three-dimensional model of the border between sound and carious enamel surfaces, determined by SPM. Border is orthogonal to the Y-axis at Y=10 µm. Porous carious enamel has lower depth regions which are displayed with reddish tint. Image collected by Jason Sherbel (UM Dental School).

Figure 3-3 shows the standard AFM topographical view for this surface, and the steps for the image analysis technique for determination of pore size.

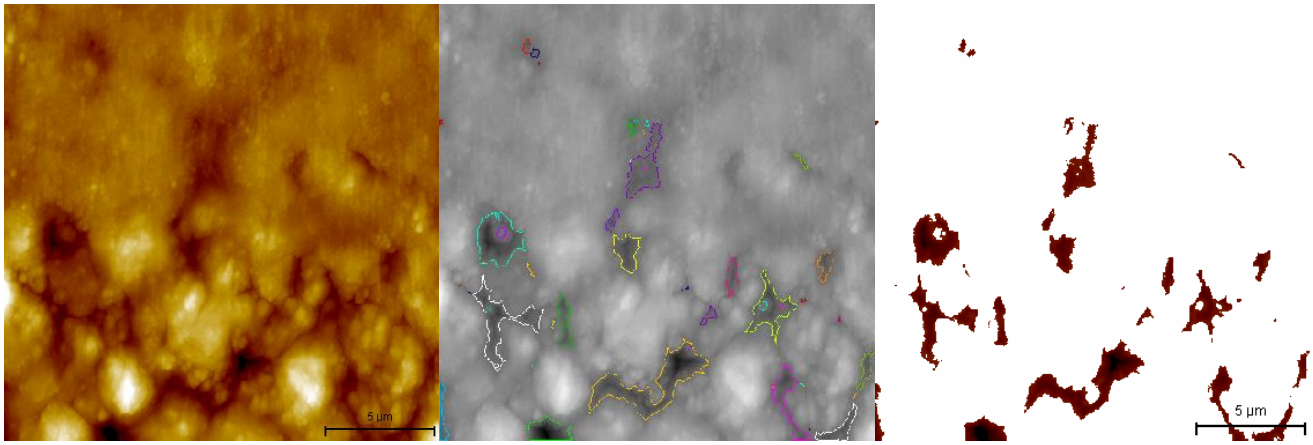

Figure 3-3: Image analysis process for determination of pore size using ImageJ image analysis software. Left image is a standard topographical view and center and right images show subsequent analysis steps. Images collected by Jason Sherbel (UM Dental School).

The average pore size for carious enamel was calculated to be 450 nm ± 600 nm. The large standard deviation is because of the presence of several very large pores several microns in size with the majority in the range of 300-400 nm. Conversely, sound enamel had fewer and significantly smaller pores, with an average pore size of 117 nm ± 103 nm ($p=0.0032$, unpaired student's t-test *vs.* carious enamel). Of note, the measured pore sizes are likely a slight underestimation of the true pore size, because of the conical shape of the AFM tip. This analysis identifies that nanoparticles below 300 nm are small enough to penetrate into carious lesions in enamel.

Evaluation of relative surface potential of carious lesions

Samples were evaluated with a charged tip to determine the relative surface potential of carious enamel. These measurements are only relative, as exact surface potentiometry requires an electrically conductive surface. Nevertheless, general observations can correlate the presence of pores with a lower surface potential, as demonstrated in Figure 3-4. When considered with published data on the surface charge of enamel, these results indicate that carious lesions are more negatively charged than sound enamel.[123,124]

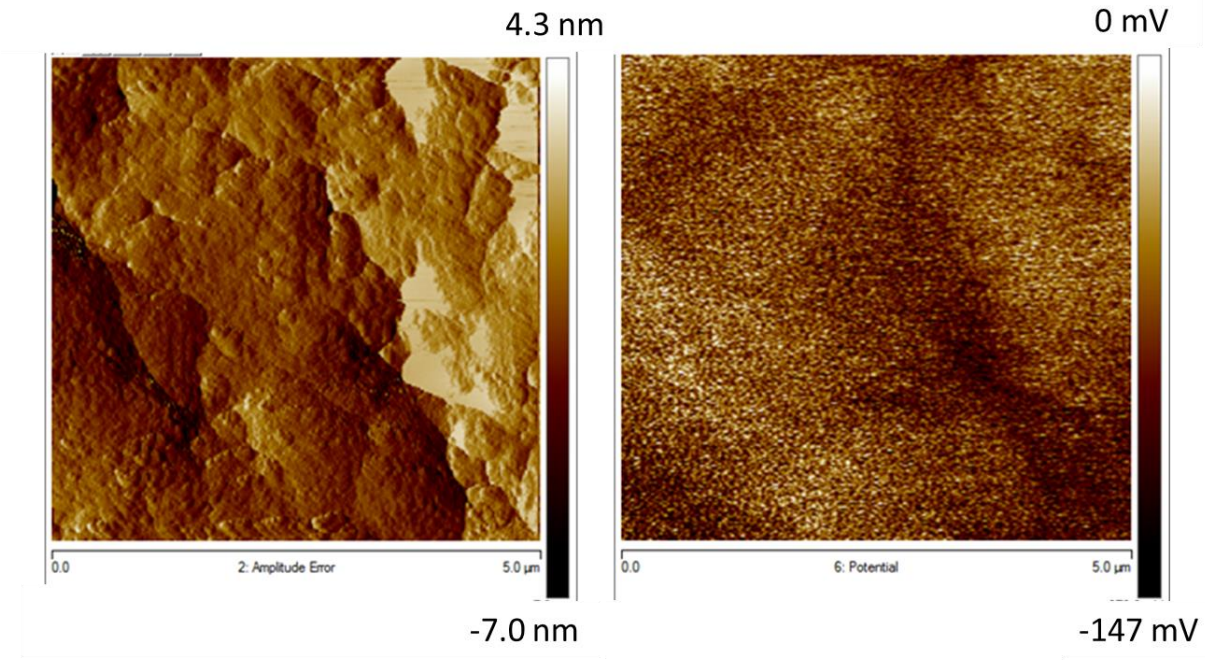

Figure 3-4: Evaluation of relative surface potential of carious enamel. The left image shows a topographical display of the surface roughness (height in nm), while the right image shows the corresponding relative surface potential map (relative surface potential in mV). Carious enamel regions show lower height and lower surface potential relative to sound enamel. Images collected by Adam Jankovic (UM Dental School).

Dental Activities Testing

Initial testing compared fluorescein sodium salt, fluorescent FITC-dextran, anionic fluorescent StNP, and cationic fluorescent StNP dispersions at selectively targeting carious lesions. Fluorescein sodium salt solution was evaluated at a lower 10^{-5} g/ml concentration to have similar fluorescence to other evaluated samples. After rinsing for 20 seconds, the fluorescein, fluorescent FITC-dextran and anionic fluorescent StNP control groups displayed no observable levels of fluorescence. In contrast, the cationic fluorescent StNP sample fluorescently illuminated the carious lesions, and rinsing with

DI-water for up to five minutes was unable to remove the fluorescence, suggesting specific adsorption of the nanoparticles to the surface of the carious enamel pores. This provided indirect evidence that the active carious lesions have a negative surface charge, and can be specifically targeted with cationic nanoparticles. Similar rinse studies were repeated with saline solutions, and artificial saliva, yielding consistent results.

To validate the efficacy of the cationic fluorescent StNPs, testing was done on the same teeth, using first the controls, rinsing for 30 seconds, and repeating testing on the same lesion with cationic fluorescent StNPs. Photographs were taken of the teeth, and modified from full-scale lighting to extract the green pixels, as this was found to significantly increase the contrast between lesion and background. The carious lesions are initially slightly darker than the rest of the tooth, and this result is consistent across all controls. The same teeth, treated with the cationic fluorescent StNPs showed fluorescence in the carious lesion region, which was brighter than the background. To quantitatively analyze the images, brightness was measured using ImageJ software. The data are presented with associated pictures in **Figure 3-5** as an intensity difference comparing the carious lesion to the adjacent region of healthy tooth.

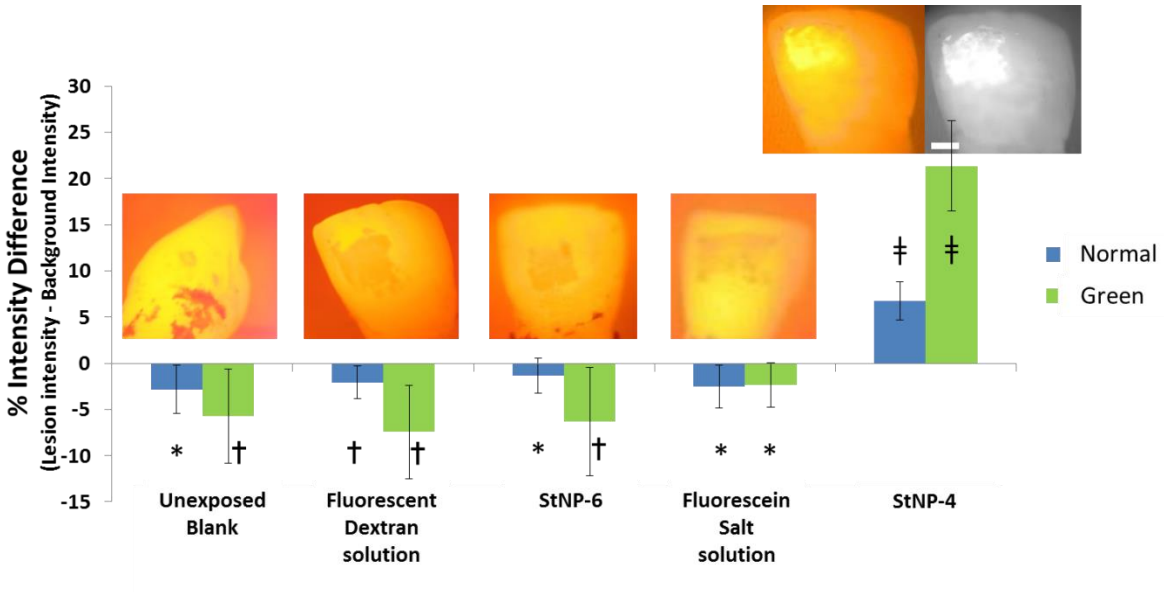

Figure 3-5: Bar graph showing the contrast of carious lesions for various starches as compared to controls, demonstrating positive contrast for the StNP-4 sample. The teeth were illuminated using a standard dental composite curing lamp. "Normal" stands for the percent intensity difference obtained for unmodified images, and "Green" stands for the extracted green pixel images. Orange inserts show the normal light image, and an example of an extracted green pixel image is shown for the StNP-4 sample. Statistical marks as follows: * Negative contrast ($0.05 < p < 0.20$); † Significant negative contrast ($p < 0.05$); ǂ Significant positive contrast ($p < 10^{-5}$).[81]

Positive values indicate that the carious lesion is brighter than the background tooth, and negative values indicate that the carious lesion is darker than the background tooth. Statistical analysis confirms that untreated teeth are indistinguishable from fluorescein, fluorescent FITC-dextran, and anionic fluorescent StNP controls, meaning that these controls did not illuminate carious lesions. The analysis further suggests that untreated carious lesions are slightly distinguishable against the background tooth; however, this is not always statistically significant. In stark contrast, the teeth treated with cationic fluorescent StNPs yielded highly significant positive intensity differences ($p<10^{-5}$), indicating that these particles improved the contrast of carious lesions relative to the background, even to the naked eye. Additionally, analyzing extracted green-pixel images instead of standard Red Green Blue (RGB) pixel images further improved the

contrast. It is interesting to note that comparing the non-illuminated images to the illuminated images highlights differences between the delineated shape of the lesion depending on the optical method used (e.g., image of carious lesions treated with anionic fluorescent particles and corresponding image of lesions treated with cationic fluorescent particles). Conceivably, this variation occurs, because the fluorescent particles will only illuminate an active carious lesion with open porosity, while the closed pores of inactive lesions cannot be detected by the starch nanoparticles. In contrast, the non-illuminated lesion images are darker if there is sub-surface porosity. This approach thus fails to identify inactive caries due to their closed surface porosity. The ability to distinguish between active and inactive lesions is a significant dental advantage of targeted nanoparticles compared to other diagnostic methods. As a further validation of these results, images of the same teeth were taken using a fluorescent scanner with a green 542 nm bandpass filter and blue light illumination. This method was not chosen as the primary method of analysis, because of its limited translatability, though it significantly increased the contrast compared to the optical method and images obtained by camera using a dental curing light ($p<10^{-5}$), with results and images shown in **Figure 3-6**.

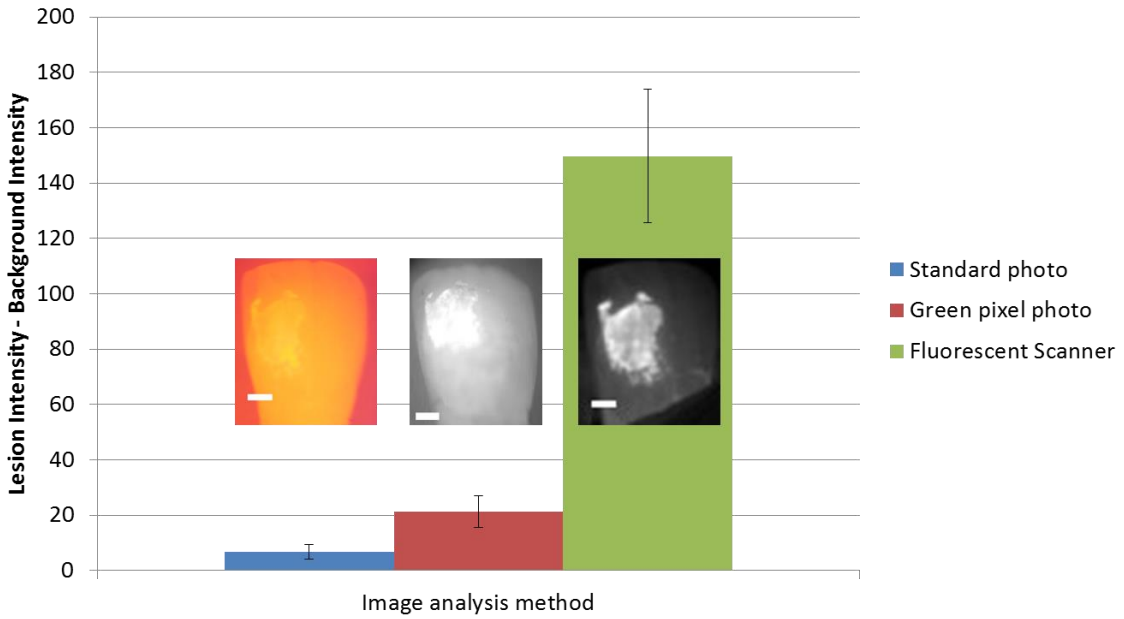

Figure 3-6: Comparison of image analysis techniques for carious lesions illuminated by cationic fluorescent starch nanoparticles, with sample images shown for each method. Scale bar = 2mm.[81]

These results provide further confirmation that the fluorescence seen in the carious lesions is due to the cationic fluorescent starch nanoparticles. Consequently, the prepared cationic fluorescent starch nanoparticles can specifically highlight active caries lesions when illuminated with a standard dental curing lamp *in vitro*, and offer a simple method to assist dentists in diagnosis of white spot carious lesions.

Analysis of Nanoparticle Distribution using Two-Photon Microscopy

To dissect the microscopic distribution of nanoparticles in microcavities, two-photon microscopy images of the different conditions were obtained as shown in **Figure 3-7**. Images show regions of teeth that are 256x256 microns across, with depths ranging from 40-80 microns gated to capture all detectable fluorescence signals.

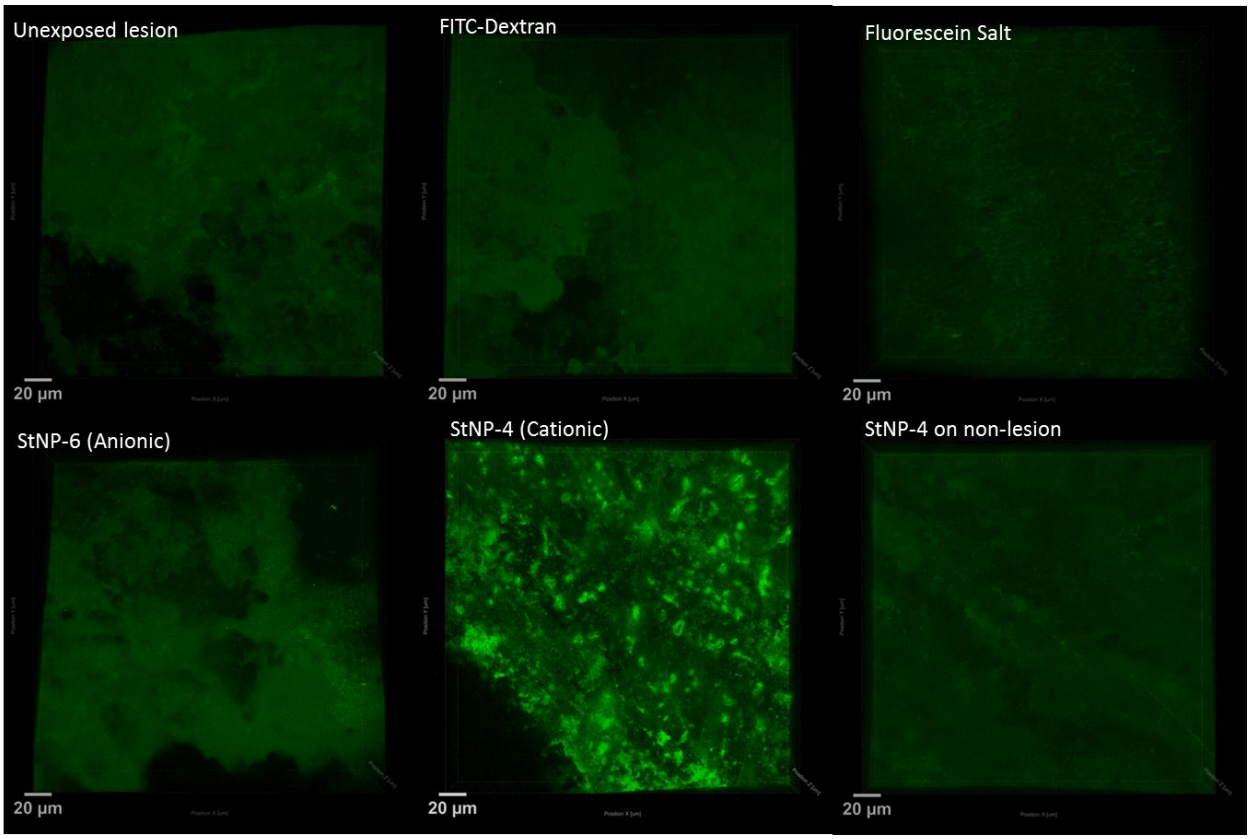

Figure 3-7: Representative top-view two-photon z-stack images of the surface of carious lesions with respective dyes. The lesion unexposed to fluorescent materials has a low fluorescence intensity, similar to the fluorescent FITC-dextran, fluorescein, anionic fluorescent StNP, and cationic non-lesion controls. The sample treated with cationic fluorescent StNPs had a speckled appearance, with bright spots identifying carious lesions on the order of 5-10 microns in diameter and with depths of 5-20 microns.[81]

The various control samples (untreated lesion, or lesion treated with fluorescent FITC-dextran, anionic fluorescent StNPs, or fluorescein sodium salt, or non-lesion treated with cationic fluorescent StNPs) display only low levels of signal due to the autofluorescence of enamel. Darker regions in the control images of carious lesions can be attributed to the porosity of the lesion and may explain their darker macroscopic appearance compared to non-lesion regions of the same tooth. In comparison, the two-photon micrograph of lesions exposed to cationic fluorescent StNPs shows illuminated small pores in the tooth surface of the early carious lesions, resulting in an overall speckled appearance. These results demonstrate, on a microscopic level, the ability of

cationic fluorescent starch particles to penetrate and adsorb specifically to the sub-surface pores of active carious lesions. An important control is the cationic fluorescent starch nanoparticles on a non-carious surface which showed low brightness typical of enamel autofluorescence similar to the negative controls on caries lesions, validating the selectivity of the cationic starch particles on a microscopic scale. Ring-shaped illumination patterns such as the one shown in the inset in **Figure 3-8** suggest that particles are arranged on the surface of carious pores penetrating into the enamel. Furthermore, the architecture of the pores indicates a larger sub-surface porosity covered by a more limited surface porosity, consistent with previously reported studies.[109,111]

These results demonstrate that two-photon microscopy can be used to obtain information about the size and shape of illuminated carious lesions, and provide an interesting experimental method in support of carious lesion development and remineralization studies. For example, the carious lesions shown in **Figure 3-7** have an average sub-surface diameter of 8.5 ± 6.6 microns, an average depth of 10.3 ± 2.9 microns, and an overall porosity of 14 ± 2%. Monitoring porosity in this manner for different tooth conditions could provide a valuable research tool.

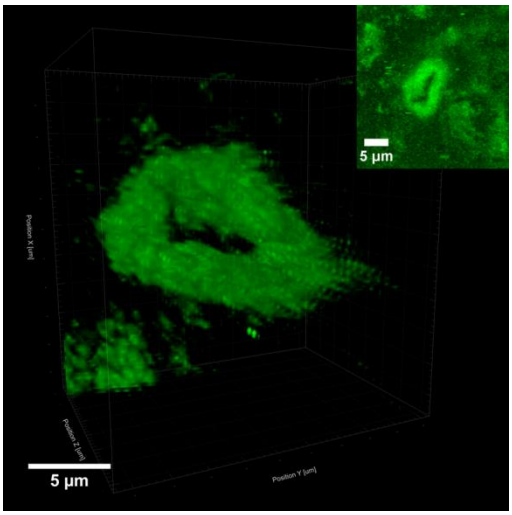

Figure 3-8: Example of carious lesion pore architecture illuminated by cationic fluorescent StNPs. Particles adsorb to the lumen surface of the pore leaving a central gap. Carious lesion is approximately 10 microns wide, by 8 microns deep.[81]

Nanoparticle Targeting to Remineralized Lesions

Teeth with microcavities were remineralized using a fluoride solution to "heal" the surface porosity of the carious lesions, yielding inactive lesions with subsurface porosity (n=8).[121] These lesions were analyzed using the same illumination and image analysis protocol before and after remineralization. The results obtained with a fluorescent scanner are shown in **Figure 3-9**.

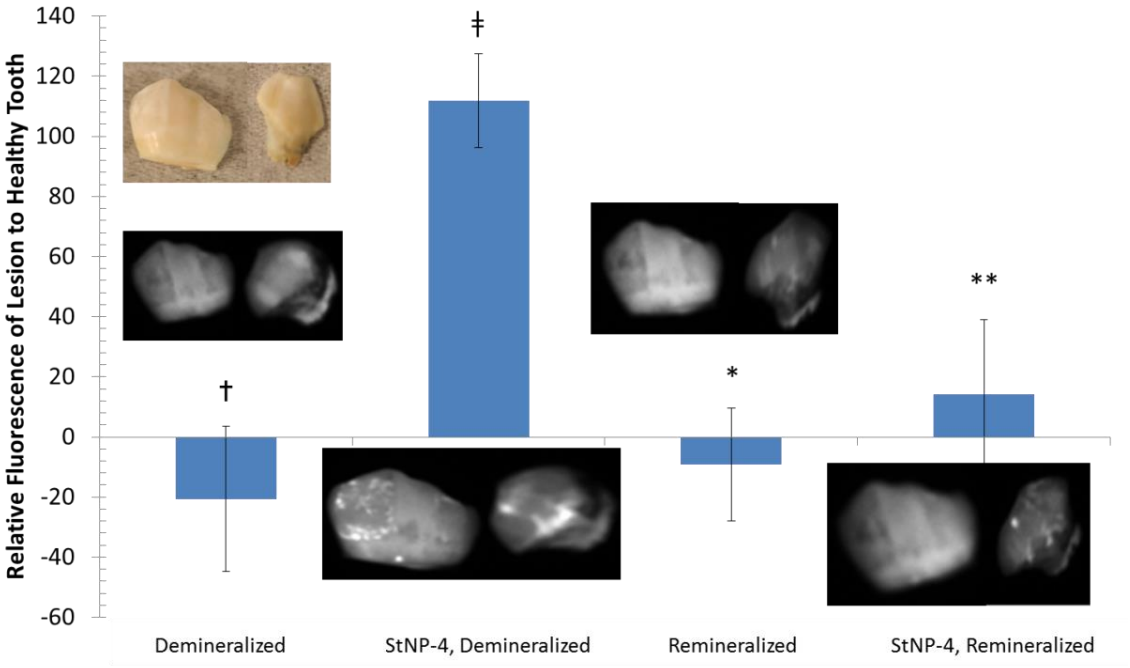

Figure 3-9: Remineralized (inactive) carious lesions do not illuminate after exposure to cationic fluorescent StNPs, in contrast to demineralized (active) carious lesions. * Negative contrast ($0.05 < p < 0.20$), ** Positive contrast ($0.05 < p < 0.30$), † Significant negative contrast ($p < 0.05$), ǂ Significant positive contrast ($p < 10^{-5}$).[81]

By appearance, the remineralized (inactive) lesions were visually indistinguishable from demineralized (active) lesions (inset image in **Figure 3-9**). Furthermore, without illumination by cationic fluorescent StNPs, the active and inactive carious lesions are indistinguishable ($p=0.44$). In contrast, after exposure to cationic fluorescent StNPs, the inactive lesions show only minimal illumination ($p=0.38$), when compared to active lesions ($p<10^{-5}$). Though a low level of fluorescence was detected for the remineralized lesions, this is most likely because the teeth were not fully remineralized during the remineralization protocol. However, in all cases the illumination was lower for the remineralized lesions. Fundamentally, these results validate the high degree of specificity of cationic fluorescent StNPs to diagnose and

differentiate between active and inactive carious lesions. Use of a specific fluorescent nanoparticle probe can identify the activity of dental caries by virtue of surface porosity, which, in active carious lesions allows for diffusion to the subsurface pores, but prevents access to the fluorescent probe in the case of inactive lesions. Clinically, a dentist does not need to treat inactive lesions, and treatments such as fluoride varnishes, gels, washes, or sealants, will have no beneficial effect. In contrast, active lesions are progressing, and appropriate treatment can halt and reverse demineralization. Two-photon micrographs of the remineralized lesions, both before and after exposure to cationic fluorescent StNPs, further support these results (**Figure 3-10**). Contrast in these images has been enhanced to improve the visibility of these samples, as the fluorescent cationic starch nanoparticles did not bind to any sample and measured signal is auto-fluorescence from the enamel.

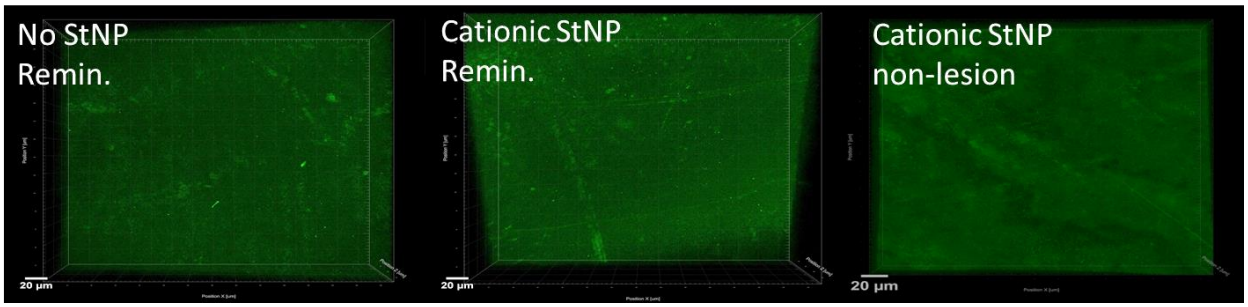

Figure 3-10: Two-photon micrographs of remineralized carious lesions with and without exposure to cationic fluorescent StNPs (left, center). Images most closely resemble the two-photon micrograph of a non-lesion surface (right), highlighting that remineralized lesions are "inactive" and from a surface perspective, healed.[81]

These images show a smooth surface with no observable fluorescent pores, which most closely resemble a non-lesion surface after exposure to cationic fluorescent StNPs. These results highlight that the remineralized lesion, from a surface perspective, has been

healed. Furthermore, dentists and clinical researchers could use the cationic fluorescent StNPs to validate and monitor effective remineralization of carious lesions after treatment, or as a compelling means of quantifying the efficacy of various treatments.

3.4 Summary

We report a novel type of starch-based cationic fluorescent nanoparticles which target and illuminate early forming active carious lesions *in vitro*. The nanoparticles are made from food grade starch, are biodegradable, biocompatible, and are enzymatically degraded in saliva after use. Our ultimate goal is to develop a new clinically valid methodology to diagnose early and active carious lesions that also enables effective monitoring of conservative treatment. With further research and clinical studies, these particles could be used by a dentist or dental hygienist as a local application, mouth wash or rinse which can then be illuminated using a standard dental curing light used in dental practices, and thus improve the detection of microcavities while they are still reversible by improved dental hygiene and targeted fluoride treatments. Using image analysis, and in particular by analyzing the green colors in images, these particles significantly improve the contrast of carious lesions. Furthermore, two-photon microscopy of teeth treated with these nanoparticles allows for analysis of the microscopic architecture of these lesions. Cationic fluorescent starch nanoparticles have the potential to be used for diagnosis of early caries in dental clinics, for point-of-care use, or to monitor tooth remineralization therapies.

CHAPTER 4

Targeting Bacterial Metabolism with Copper-Starch Nanoparticles

The material in this chapter has been adapted with minor modifications from the following article:

(1) N. Jones, U. Kadiyala, B. Serratos, S. van Epps, J. Lahann, "Amylase-Responsive Antibacterial Nanoparticles", *In preparation.*

4.1 Motivation and Background

Though preventable, bacterial infections are a significant medical issue in hospital settings and the developing world. In the US, approximately 7-10% of patients will acquire an infection while being treated for a different condition, and this incidence increases to nearly 50% for high risk patients including newborns, immune-compromised patients, and patients in the ICU.[125] Despite the success of antibiotics, there are more than 2 million infections annually in the US with antibiotic resistant bacteria, which account for approximately 23,000 annual deaths.[126] Consequently, there is a need for new options to prevent infection and limit bacterial resistance, which has resulted in the development of antibacterial polymers[127] and metal oxide nanoparticles, such as those

made of silver,[128,129] copper,[129] or zinc oxide.[130] Metal oxide particles have shown to be a more effective antibacterial agent than antibiotics, with less potential for resistance due to operating on an alternative mechanism of action, which may include oxidative stress, membrane disruption, or ionic oxidation.[128,131] There remain challenges in preparing these antibacterial products, particularly in aqueous solubility, preparation, and stability. With ongoing research in nanotechnology applications in medicine, there have been advances in targeting and treating bacterial infections.[132]

Targeted antibacterial approaches involve passive and active targeting schemes. It has been found that bacterial infection, similar to cancer, increases vascular permeability, allowing the Enhanced Permeation and Retention (EPR) effect of appropriately sized nanoparticles delivered intravenously.[29] Electrostatic interactions are another method of targeting pathogenic bacteria. Bacteria generally exhibit a negative surface charge under physiological conditions, and thus cationic nanoparticles and polymers are capable of binding with bacterial via electrostatic interactions.[124,127] This has advantages due to multivalency and the ability to target polymicrobial infections.[133] Active targeting methods use specific targeting molecules such as vancomycin,[134] lectins,[135] antibodies,[136] or aptamers[137] conjugated to drugs or drug-loaded nanoparticles as a targeted delivery mechanism for a variety of pathogenic bacteria.[138] Secondary targeting methods involve targeting the macrophages which will be recruited to fight the infection, using an assortment of active targeting molecules.[36,139]

Beyond targeting schemes, particles have been prepared to be environmentally responsive, triggered to release by cues found in the microenvironment of infection sites. The acidity of the infection microenvironment is a stimulus which can be harnessed in a

variety of ways. Acid-degradable polymers, such as poly(lactic-co-glycolic acid) (PLGA),[140] poly(caprolactone) (PCL),[141] or chitosan,[28] can be used to limit release of antibacterial drugs until in the presence of an acidic infection. Some polymers are capable of becoming cationic in acidic environments, acting as a trigger for bacterial targeting.[127] More recently, a novel enzyme-sensitive nanoparticle has been prepared which decomposes in the presence of bacterial phosphatase of phospholipase.[142] Following this motivation, we have developed an amylase-responsive cationic starch-based nanoparticle which electrostatically binds to bacteria, and releases antibacterial copper nanoparticles rapidly in the presence of amylase, an enzyme released by certain strains of bacteria.[143] This is a novel method of bacterial targeting, which could be modified with alternative drug loadings for a variety of medical indications.

4.2 Experimental Methods

4.2.1 Materials

All chemicals were lab grade and purchased from Sigma Aldrich unless otherwise noted. These include Tryptic Soy Broth (TSB) media, and glucose. Copper nanoparticles sized 5-7 nm were purchased from Sky Spring Nanomaterials (Texas, USA). Research grade starch nanoparticles were provided by EcoSynthetix Inc. (Burlington, ON, Canada).

4.2.2 Bacterial Strains, Media, & Growth Conditions

The bacterial strains used in this research were methicillin-resistant *Staphylococcus aureus* COL, *Bacillus subtilis* PC 194 CMR, *Staphylococcus epidermidis* RPI 1420, *Escherichia coli* UTI-89, and *Klebsiella pneumoniae* LM 21. Glycerol stocks of all strains maintained at - 80 ^{o}C were plated on tryptic soy agar, cultured overnight at 37 ^{o}C and stored at 4 ^{o}C. Single colony inoculates were grown in tryptic soy broth with or without + 1% glucose w/v (TSBG or TSB, respectively) under shaking conditions until optical density at 600 nm (OD_{600}) reached approximately mid-log (0.4-0.6), prior to dilution to OD600 of 0.01 for planktonic growth curves and quantitative culture studies.

4.2.3 Preparation & Characterization of Copper-Starch Nanoparticles

Electrohydrodynamic Jetting of Copper Starch Nanoparticles

Particles were prepared using EHD jetting as previously described in Chapter 2, according to the schematic in **Figure 4-1**. The jetting recipe was modified to contain 10% mass/volume cationic starch nanoparticles as prepared and reported previously,[81] 3% mass/volume PEGDGE cross-linker, and ~0.5% volume/volume 5-7 nm copper nanoparticle solution, dispersed in 80:20 deionized water : ethanol. The sample was vortexed to fully disperse the hydrophobic copper nanoparticles and created an emulsion of oil in water that remained stable over 24 hours. EHD jetting was performed immediately after preparation of the jetting solution, with a voltage of ~12 kV, a pump speed of 0.05 ml/hr, and a jetting needle to collection plate distance of approximately 30

cm. Collected plates were cured in a 50 ^{o}C oven for 72 hours following jetting of the particles, and the final particles were then collected as a dry aggregate powder.

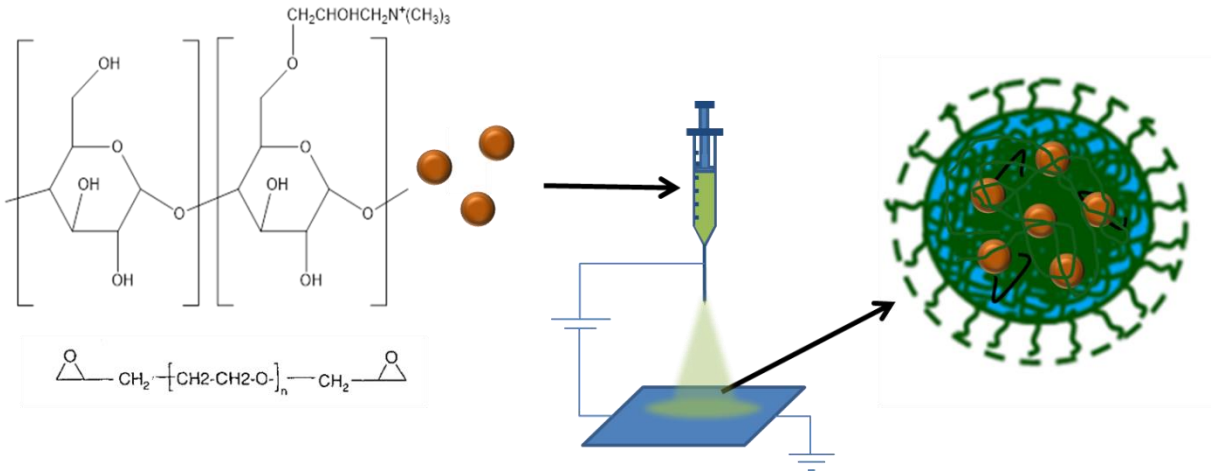

Figure 4-1: Schematic for the preparation of Copper-Starch Nanoparticles (CuStNPs) by reactive EHD jetting. In the final particle schematic, green indicates the starch, black the PEG cross-linker, along with the copper nanoparticles.

Electron Microscopy

Scanning Electron Microscopy was performed using a Quanta SEM with beam voltage of 3 kV and a magnification of 10000x, and a NOVA SEM with beam voltage of 5 kV, 0.4nA, and a magnification of 10000x. Transmission Electron Microscopy was performed using a JEOL 2100 probe-corrected analytical microscope with an accelerating voltage of 100 kV, a zirconated tungsten (100) thermal field emission tip filament, gun vacuum ~1.0e-9 torr and column vacuum ~1.0e-7 torr (Michigan Center for Materials Characterization).

Inductively Coupled Plasma – Orbital Emission Spectroscopy (ICP-OES) Evaluation of Copper Loading

ICP-OES measurements were performed using a Perkin-Elmer Optima 2000 DV with Winlab software. Samples were doped with 1ppm Yttrium as a standard, and degraded by addition of 5% Nitric Acid. All CuStNP samples were prepared at mass concentration of 2 mg/ml in TSB media, and calibrated against a copper ICP standard (Sigma Aldrich).

4.2.4 Bacterial Culture Studies

Bacterial Growth Curves

CuSt-NP suspensions were prepared by vortexing CuSt-NPs into TSB or TSBG for 15 min. The final CuSt-NP concentrations were serial dilutions of the original stock solution. To compare to previously reported data on copper nanoparticles, concentrations are shown in terms of the Cu-NP concentration, as determined by the ICP loading study. The maximum concentration used in this study (25 µg/ml Cu NPs, equivalent to ~ 4.0 mg/ml CuStNP, based off of calculated loading of approximately 0.37% Cu NPs) was in a similar range as previously reported data on Cu NPs.[129,144] Bacterial growth was assessed by measuring optical density at 600 nm (OD_{600}) hourly over 10 h in the presence of CuSt-NPs.

Quantitative Culture

Bacterial cultures were exposed to CuSt-NPs for 7.5 hours, wherein the cultures were serially diluted in DI-H_2O and plated on TSBG agar and allowed to grow for

approximately 8-12 hours for *B. subtilis* and 18-20 hours for *S. aureus* prior to colony enumeration.

pH Analysis

Bacterial cultures were qualitatively monitored for pH changes using litmus paper over the course of 8 hours as a function of exposure to CuStNPs.

4.3 Results and Discussion

Particle Preparation and Characterization

Electrohydrodynamic jetting of particles has been well studied in the Lahann Lab,[89,92,145] and has used compositions of polymers such as poly(lactic-co-glycolic) acid,[106] acetal dextran,[24,95] and others.[92,100] Starch has found little use in the preparation of nanoparticles because the natural crystalline structure of amylose starch, which if unchecked results in uncontrolled aggregation of prepared nanostructures. Success has been found by modifying and cross-linking the starch as shown in recent literature,[60,64,70,72,73] and used commercially by EcoSynthetix Inc. (Burlington, ON, Canada) for their EcoSphere® product.[64,65] In this work, we use research grade starch nanoparticles from EcoSynthetix which have been modified to be cationic as previously reported.[81] We found that the cationic starch nanoparticles can be cross-linked after EHD jetting by incorporation of poly(ethylene glycol) diglycidyl ether and subsequent curing at 50 ^{o}C for approximately 72 hours. Incorporation of other components into the jetting solution allows for loading of material within the starch particle matrix. We added a

small amount of copper nanoparticles (6-7 nm) to the jetting solution, which ordinarily would not be stable in water, but upon vortexing, was able to form a semi-stable Pickering emulsion. This solution remained stable over the course of hours and was jetted onto metal plates, prior to curing and ensuing collection. The particles, as jetted, are shown in **Figure 4-2** by scanning electron microscopy to give a representative view of the particle size distribution and morphology, and by transmission electron microscopy to demonstrate the even distribution of the copper nanoparticles throughout the larger starch nanoparticle matrix.

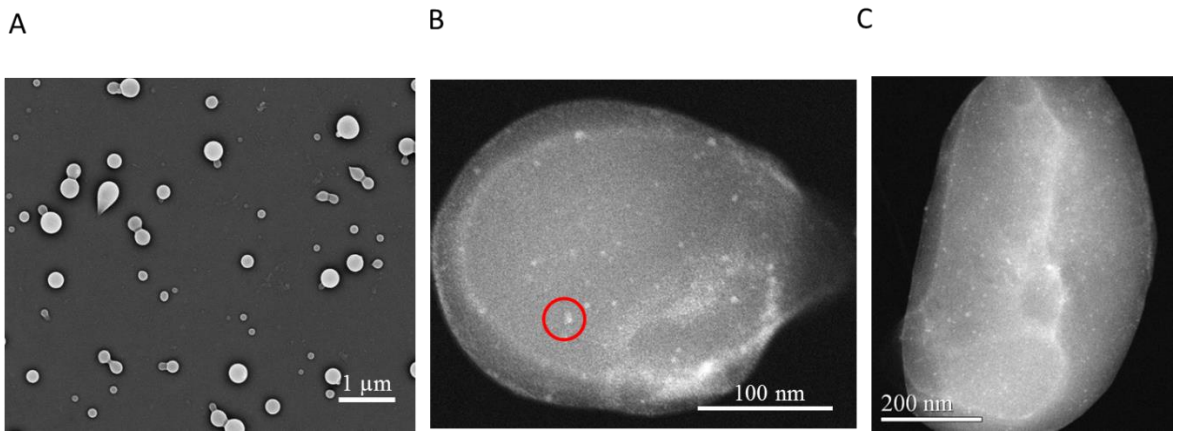

Figure 4-2: (A) Scanning Electron Micrograph of copper-starch nanoparticles as collected following electrohydrodynamic co-jetting and (B-C) Transmission Electron Micrographs of copper-starch nanoparticles, showing high contrast 6-7 nm copper nanoparticles (example circled) distributed throughout the larger starch nanoparticle.

Particle size was measured using dynamic light scattering and the average particle size was determined to be 440 ± 58 nm. This suggests a swell ratio of the particles of approximately 2.3 ± 0.5, as size analysis from the SEM images shows the dry particle size to be approximately 193 ± 91 nm.

ICP Evaluation of Copper Loading

ICP-OES of CuStNP samples were compared to a calibration curve made with copper ICP standards, shown in **Figure 4-3**. The CuStNP samples were prepared at 1, 2, and 4 mg/ml, and the measured copper concentration was calculated from the linear equation fitted to the calibration data (R^2 = 0.99991). The CuNP loading was determined to be 0.34 ± 0.05 % by mass within the CuStNPs, with a loading efficiency of 89.8 ± 13.6 %.

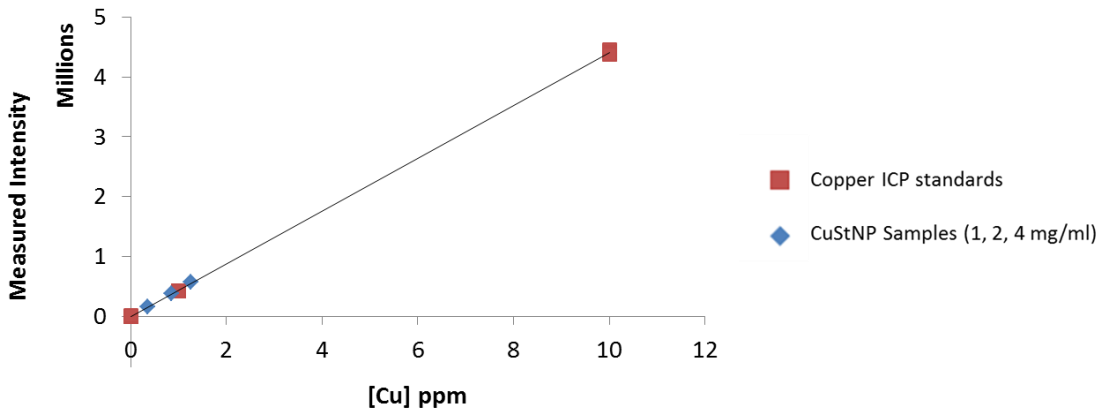

ICP Sample / mL DI water	ICP Measured [Cu] (ppm)
10 µl CuNP solution	1016 ± 64
1 mg CuStNP	3.5 ± 0.3
2 mg CuStNP	8.5 ± 2.4
4 mg CuStNP	12.7 ± 0.2

Figure 4-3: Evaluation of copper loading by ICP-OES. Samples prepared at 1, 2, and 4 mg/ml were compared to ICP standards to determine a loading of approximately 0.34%. Measured values tabulated below graph, show concentration of CuNPs in purchased solution and loading for different concentrations of CuStNPs

Bacterial Culture Assays

These particles were collected and 10 hour bacterial growth curves were evaluated for the Gram-positive *Staphylococcus aureus* COL, *Bacillus subtilis* pC194 CMR, and the Gram-negative *Escherichia coli* UTI-89, and *Klebsiella pneumoniae* LM21 at doses of 2.1 up to 34 µg/ml Cu, equivalent to concentrations from 0.5 to 8 mg/ml CuStNP. Controls using prepared starch nanoparticles without adding copper nanoparticles were considered for *S. aureus* and *E. coli*. Unloaded starch nanoparticles showed minimal effect on bacterial growth, even at high concentrations, as shown in **Figure 4-4**.

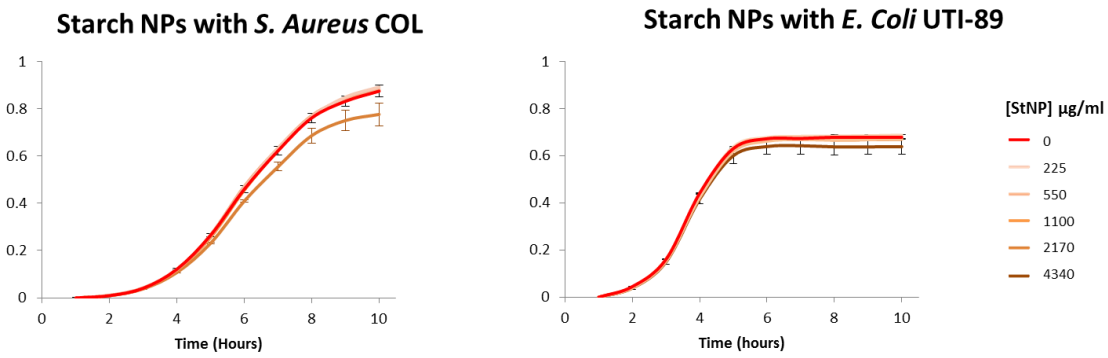

Figure 4-4: Growth curves evaluated for *S. aureus* COL and *E. coli* UTI-89 over the course of ten hours for incremental doses of unloaded starch nanoparticles. Mild toxic effect was only seen at the highest measured doses (~2 mg/ml and ~4 mg/ml for *S. aureus* and *E. coli*, respectively).

Copper-starch nanoparticles were not as effective at killing Gram negative bacteria, shown in **Figure 4-5,** as has been reported for copper nanoparticles previously.[129]

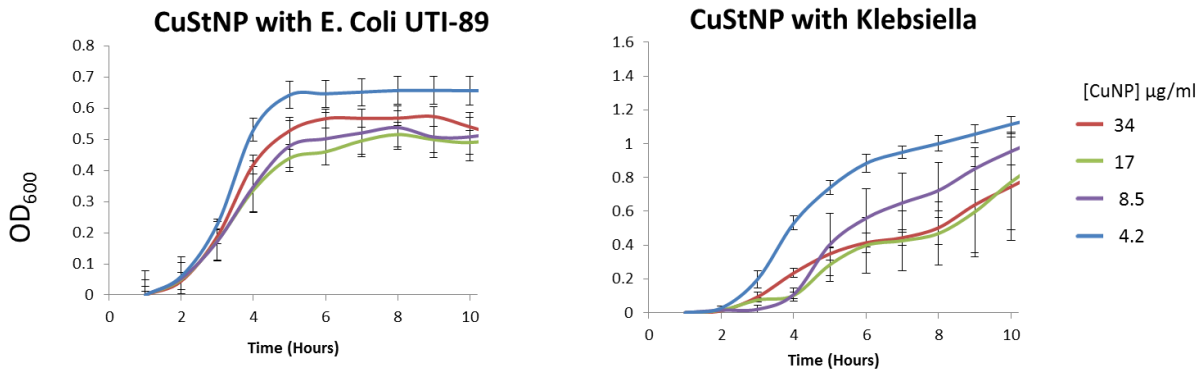

Figure 4-5: Growth curves for various doses of CuStNP with Gram-negative bacteria *E. Coli* UTI-89 and *Klebsiella.*

However, for Gram-positive bacteria, the copper starch nanoparticles showed clear antibacterial efficacy even at effective copper doses of 4.2 µg/ml, demonstrated in **Figure 4-6**, which is an order of magnitude lower dose than previously reported data in the literature.[129,144]

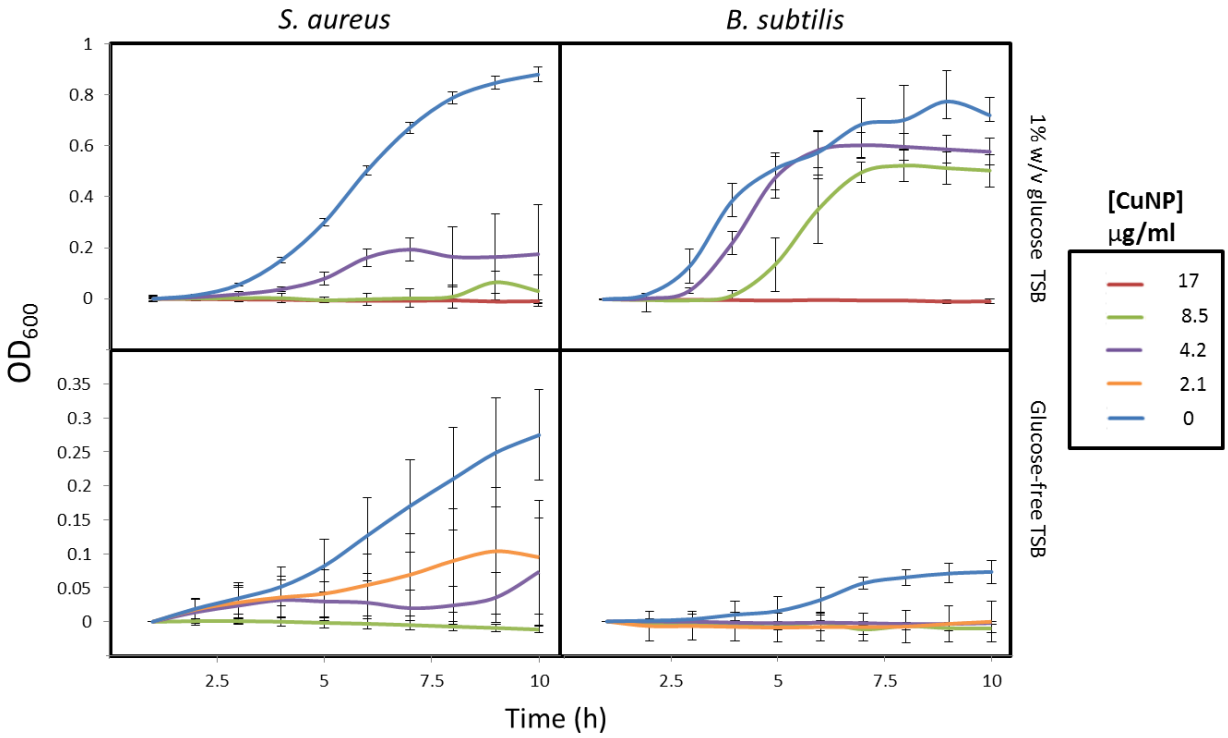

Figure 4-6: Growth curves for *S. aureus* and *B. subtilis* in the presence of increasing concentration of CuStNPs in glucose-containing and glucose-free media.

We hypothesized that the copper starch nanoparticle formulation would be more toxic to *B. subtilis* than *S. aureus* because of the documented ability of *B. subtilis* to produce amylase and digest starch,[143,146] which would result in faster degradation of the particles, releasing copper nanoparticles which are toxic to the bacterial cells. However, in TSB with added glucose (TSBG), this was not observed, and there appeared to be a more significant reduction of growth for *S. aureus* compared to *B. subtilis*, particularly when comparing the 4.2 µg/ml CuStNP dose. When we tested in TSB without additional glucose, we observed the opposite trend, with *B. subtilis* suffering more significant reduction of growth compared to *S. aureus*. This suggests that the bacterial metabolism is affected by the presence of glucose in the media, and that starch-digesting bacteria are

more motivated to digest starch in conditions where there are more limited energy resources, a mechanism which might be conceptually similar to the function of the lac-operon.[143] This is also consistent with the expected result that without additional glucose added to the media, the bacterial growth is reduced. These results were validated by quantitative culture studies with the results shown in **Figure 4-7**.

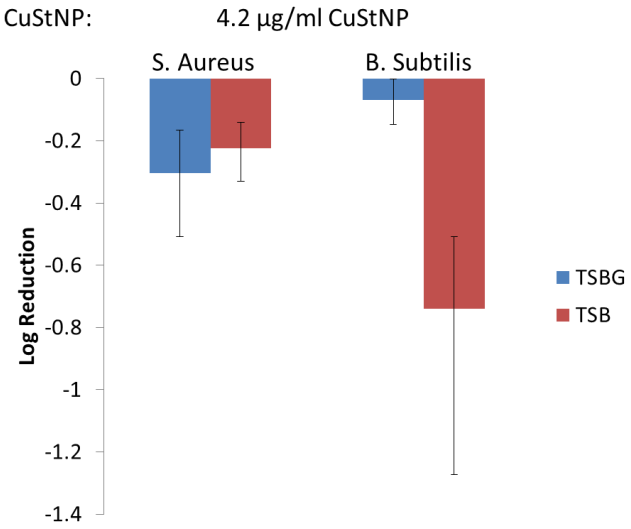

Figure 4-7: Quantitative culture results for bacterial log reduction of *S. aureus* and *B. subtilis* in TSB and TSBG at low (4.2 µg/ml) dose of CuStNP.

At the low dosage of 4.2 µg/ml CuStNP, the particles showed only minimal toxicity with less than a single log reduction, but the trend remains consistent with bacterial log reduction ordered as follows: *B. subtilis* in TSB > *S. aureus* in TSBG ≥ *S. aureus* in TSB > *B. subtilis* in TSBG ($p<0.001$ for all samples, except for the low dose CuStNP for *S. Aureus* in both media conditions).

Evaluation of Bacterial Culture pH

We hypothesized that the pH of the bacterial culture might trigger increased degradation of the starch nanoparticles by hydrolysis of the starch, creating additional acidic functionalities which would accelerate the release of copper ions from the CuNPs. We measured the pH of a variety of bacterial cultures over the course of 24-hours incubating with CuStNPs in TSB and TSBG. Results are plotted in **Figure 4-8**, and show that there was no appreciable change in pH for the samples incubated with CuStNPs, because the bacteria failed to thrive and were killed by the CuStNPs. Controls without the CuStNP and unloaded StNPs showed a slight drop in pH, from 7 to approximately 5 after 24 hours. We infer from these results that pH was likely not a significant factor in the mechanism of CuNP release from the CuStNPs, unless local pH drops were buffered by the degradation of the CuNPs.

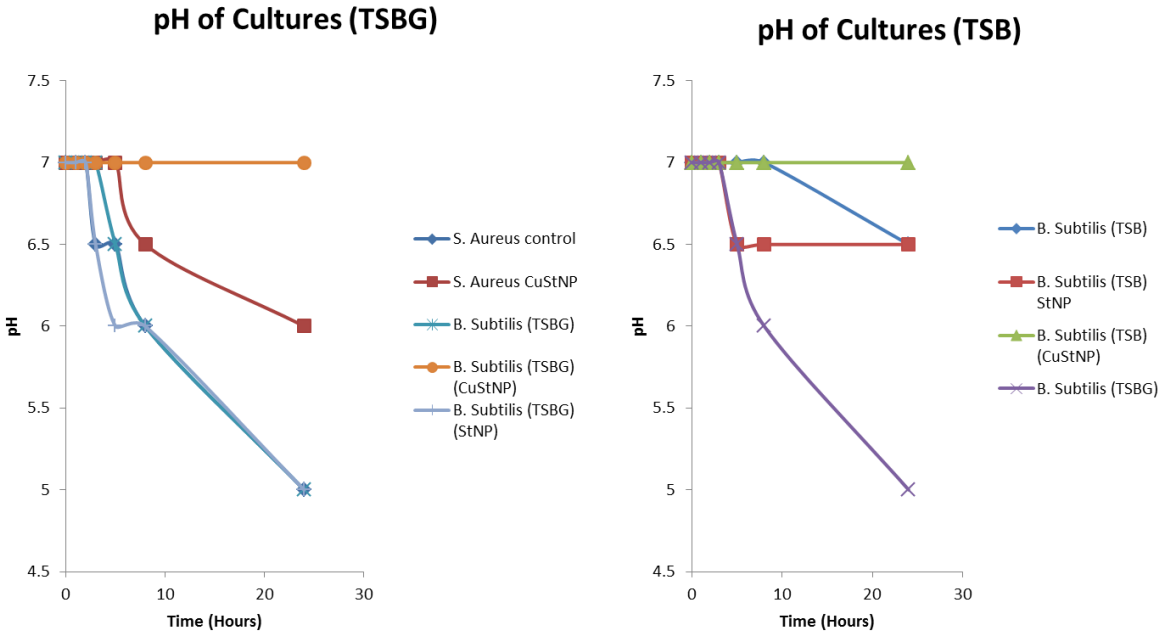

Figure 4-8: pH of bacterial cultures in TSBG (A) and TSB (B), dosed with CuStNP or StNP.

Microscopy Evaluation of CuStNP Interactions with Bacteria

Bacteria were mixed with 4.2 µg/ml CuStNP and after an 8 hour incubation, were prepared for imaging by Scanning Electron Microscopy (SEM). A sample micrograph is shown in **Figure 4-9**, which shows a gold sputter-coated (60s, 18mA) view of the *S. aureus* bacteria (round spheres) interacting with a mesh of the CuStNP particles.

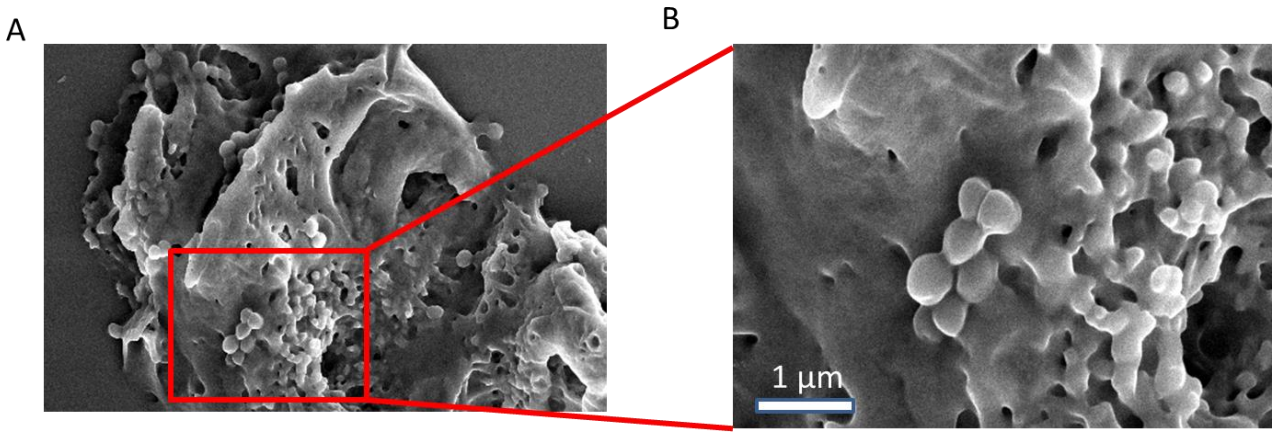

Figure 4-9: SEM showing an aggregate of *S. aureus* coated in a mesh of collapsed hydrogel starch nanoparticles, A) large aggregate B) Bacterial cells coated in starch hydrogel.

Because these particles are hydrogels, after immersion in water they swell to more than twice their size. We suspect that the cationic charge of the particles facilitates strong interactions with the negatively charged bacteria, which results in agglomeration of the bacteria and hydrogel starch particles, which was observed during the longer bacterial culture studies. When imaged with SEM, the hydrogel particles are dried and collapse, giving the appearance of a smooth coating surrounding the bacteria. This is a possible mechanism for the high efficacy of the antibacterial effect of the copper nanoparticles. Even though the dose is ~10 times lower than reported in other studies, the copper

nanoparticles are brought directly in contact with the bacteria by the cationic starch hydrogel nanoparticles. Consequently, the effective local concentration of the copper nanoparticles is seen by the bacteria as being much higher and therefore more effective than a free-floating copper nanoparticle solution. These strong interactions, when coupled with the active digestion of the starch by *B. subtilis*, creates a system which demonstrates very high antibacterial efficacy for the dosage of copper nanoparticles.

4.4 Summary

In this study, we present a novel starch nanoparticle prepared by reactive EHD jetting. The particles are loaded with copper nanoparticles and show efficacy at killing Gram-positive bacteria such as *S. aureus* and *B. subtilis*. The antibacterial efficacy is improved against starch-digesting bacteria in a media without the addition of excess glucose, and demonstrated how the nanoparticle composition can. Furthermore, the cationic nature of these particles facilitates strong electrostatic interactions with bacteria, thereby bringing copper nanoparticles in close proximity to the bacteria, and increasing the therapeutic efficacy up to a seven-log reduction for a copper NP dose of 17 ppm. Co-culture studies showed the potential of targeting bacteria in the presence of other starch-digesting bacteria, as occurs naturally in the lower digestive tract. Future work will evaluate the mechanism of action for this system, and explore loading other therapeutics into the particles, potentially as a method of targeted drug release in the intestine.

CHAPTER 5

Alpha-Mannose Functionalized Polymer Brushes for the Targeting of M2-Polarized Tumor Associated Macrophages

The material in this chapter has been adapted with modifications from the following article:

1) R. Kumar, N.A. Jones, N. Habibi, J. Zarif, D. Kratzer, K. Pienta, J. Lahann. "Alpha-Mannose Functionalized Polymer Brushes for the Isolation of M2-Polarized Tumor Associated Macrophages", *In preparation.*

5.1 Motivation

In the USA, the annual incidence of cancer surpasses 1.5 million cases. Even though total economic costs for care exceed $100 billion, cancer accounts for one in four deaths.[147] A majority of cancers are diagnosed in patients older than 60 years, and with an aging population the incidence of cancer will significantly increase over the next 20 years.[148] Worldwide, continued population growth, aging and life-style changes in developing countries will contribute to greater global incidence.[148] Thus there is significant need for more effective and cost-efficient cancer therapies.

Research into targeted drug delivery promises to improve the efficacy of therapy and reduce side-effects. The current research paradigm is a direct approach that targets the cancer cells, using chemotherapy or ligands, such as antibodies or small molecules (e.g., folic acid and other targeting molecules); however, this has had limited success, with few formulations reaching clinical use.[149,150]

The alternative paradigm recognizes that cancer cells reside within a micro-environment, offering another targeting avenue. It should be possible to indirectly target the cancer by targeting non-cancer cells that associate with the tumor and facilitate cancer growth and aggressivity. For example, angiogenesis inhibitors, such as those which inhibit vascular endothelial growth factor, like Bevacizumab (Genentech/Roche) slow the growth of blood vessels that support the tumor. The tumor is starved of essential nutrients and waste removal is curtailed, such that cancer growth is slowed down or stopped.[151]

The tumor micro-environment is complex and contains many interacting cancer and non-cancer cells. Many of the non-cancer cells support the growth of the tumor and inhibit the effects of anti-cancer treatments. Tumor-associated macrophages (TAMs) are the predominant inflammatory non-cancer cells that reside within solid tumors. They have significant roles in tumor cell proliferation, survival, invasion and metastasis.[36] Presence of TAMs is associated with poor prognosis in a variety of human cancers including lymphoma, lung, breast and prostate cancer. TAMs have also been associated with a lower susceptibility of cancer cells to chemotherapy and radiation treatment.[36] Notably, knock-down of chemokines that are associated with TAM recruitment has been shown to cause tumor regression, particularly in combination with standard

chemotherapy.[152-154] Interestingly, TAMs can reach non-vascularized regions of solid tumors otherwise inaccessible to standard chemotherapy or imaging agents.[155,156]

For these reasons, we hypothesize that TAMs, in addition to actual cancer cells, can be an effective target for cancer therapy and imaging, as well as a prognostic marker for tumor resilience and potential efficacy of TAM-targeted therapies. This project explores the pre-clinical development of a glycocalyx-mimetic synthetic mannose-brush polymer as a novel targeting scheme for TAMs. We hypothesize that the glycocalyx-mimetic mannose brush polymer prevents non-specific adsorption,[43] while facilitating multivalent binding to the mannose receptor overexpressed on TAMs.[8]

5.2 Background

5.2.1 TAMs as a Relevant Target

The cancer microenvironment is complex and contains many different populations of cancerous and non-cancerous cells. For decades it has been known that solid tumors are infiltrated by inflammatory leukocytes in various human and mouse malignancies, including breast, prostate, lung, and lymphoma. Further, the number and density of macrophages has been associated with a poor prognosis in human tumors.[157] The number of tumor macrophages has been correlated with tumor growth, where mouse models which are genetically modified to have excessive presence of inflammatory macrophages showed more rapid tumor growth. Conversely, genetic knockdown of

macrophages has shown delayed tumor growth, less angiogenesis, and fewer metastases.[158]

Though macrophages are associated with cancer growth and metastasis, simultaneously macrophages have a capacity to prevent the spread of tumor cells. This paradox can be explained by the plasticity of macrophages between M1 (non-inflammatory) and M2 (inflammatory) states. M1 macrophages have high microbicidal activity, immune-stimulatory functions, and tumor-cytotoxicity. In contrast, M2 macrophages have high scavenging ability, promote tissue repair and angiogenesis, and favor tumor progression.[159,160] In cancer treatment M2 macrophages have been associated with chemotherapy and radiation resistance, diminishing their therapeutic effect. These different polarizations of macrophages also express different surface markers that allow for macrophage-specific targeting. Because of the association with tumor growth, M2 macrophages have been dubbed as "Tumor Associated Macrophages" (TAMs), and they have emerged as a novel clinical target.

5.2.2 Targeting TAMs

Preliminary research into the targeting of TAMs has identified several active targeting molecules with high specificity. The mannose receptor (MR) has specificity for M2 macrophages as many bacteria express mannose on their bacterial cell walls. The MR has been shown to cause receptor-mediated endocytosis of bound mannose and conjugates, and specificity to the receptor has been improved with use of polyvalent binding with poly-mannose (mannan) or higher density of mannose molecules.[161] To

improve the specificity to TAMs located in the tumor microenvironment, a pH-sensitive labile-PEG coating was added to nanoparticles to allow for passive accumulation of particles in the tumor region, with subsequent shedding of the PEG coating in the acidic tumor microenvironment revealing surface-bound mannose molecules to facilitate active uptake by TAMs.[162] Although TAMs express high levels of the folate-receptor beta, which binds to folate, folate is not a specific targeting molecule and will also be taken up by cancer and other non-cancer cells.[163] Phage-display studies have developed a peptide sequence that shows high specificity for TAMs. This peptide, denoted M2pep (YEQDPWGVKWWY), showed specific binding and uptake with TAMs, and was attached to a proapoptotic peptide $(KLAK)_2$ to specifically reduce TAM populations; in murine models this resulted in delayed mortality and reduced tumor growth rate.[164] In summary, though mechanisms for targeting TAMs have been uncovered, these have not been applied to clinically relevant delivery of drugs or imaging contrast agents.

5.2.3 Applications of Targeting TAMs

TAMs are present in many types of cancer and so they are a very relevant target for a large population of patients. An advantage of an indirect strategy to treating cancer is that the therapy can be tested as a monotherapy, or as an adjunct to existing therapies with possible synergistic interactions. TAMs are unaffected by most chemotherapy drugs as macrophages do not undergo mitosis, and most chemotherapy agents are mitotic disruptors that take advantage of the rapid growth and division of cancer cells. Consequently, targeted therapy of TAMs requires drugs which can kill macrophages

using a different mechanism, or delivery of chemokines such as nucleic acids which can genetically reprogram TAMs to change their polarization.[165] Both of these strategies have been explored experimentally.

First, bisphosphonate drugs have proven to be effective at killing macrophages, but are untargeted when administered intravenously and will collect in bone tissue. Depletion of macrophages by bisphosphonate-encapsulated liposomes[36] or amino-bisphosphonates[166] have shown superiority over non-encapsulated drugs, but would stand to benefit from a TAM-targeted nanoparticle with active and passive targeting. As previously noted, proapoptotic peptides show efficacy at killing TAMs, or any other cell, for that matter, and require a targeting mechanism. A targeted particle would be able to deliver a higher dose of proapoptotic peptide compared to the peptide sequences discussed in Cielsewicz *et al.*, and possibly reduce the nonspecific delivery they had noted to liver and kidneys.[164]

The second therapeutic approach is to alter the polarization of TAMs. This carries the additional benefit of M1 macrophages possessing anticancer properties. While many chemokine-related studies have shown the premise of this method, one study[165] suggested that a DNA vaccine against the M2-associated legumain also induced a $CD8^+$ T cell response against TAMs. Furthermore, a liposomal based delivery system has been used to deliver siRNA to TAMs and knockdown expression of CCR2, a chemokine receptor for pro-inflammatory response. It was found that knockdown of CCR2 in macrophages not only was beneficial for treatment of TAMs, but it was relevant in the reduction of inflammation in the treatment of atherosclerosis, reducing the size of myocardial infarction, and improvement in the acceptance of pancreatic islet transplantation for the

treatment of type 1 diabetes.[167] Last, delivery of DNA or RNA to cell targets is greatly enhanced by the use of targeted nanoparticles. Systemic delivery of nucleic acids is susceptible to nucleases and immunostimulation, and without cellular uptake the therapeutic efficacy is low. Intelligently designed nanoparticles can facilitate endocytosis and endosomolysis, allowing release of the payload to the cell cytoplasm.

An additional approach involves the use of TAMs as a "Trojan horse" to deliver therapy to the necrotic tumor core. The solid tumor environment is crowded with cells and develops a pressure gradient extending from the tumor center, or several centers. Therefore, chemotherapy agents have difficulty reaching the tumor core and fully killing all of the cancer cells, and radiation therapy to hypoxic regions of tumors is less effective because of reduced radiation sensitivity, since radiation damage is strongly associated with oxygen fixation and adduct formation. Notably, TAMs are capable of moving against this pressure gradient and reach all parts of the tumor. One study[155] used mannose-coated gold nanorods which were taken into the tumor core by the TAMs, and upon exposure to near infrared light were able to exhibit a photothermal response and thermally ablate the TAMs and local tumor cells. Thus, TAM-targeting is an effective way of targeting all regions of the tumor, useful for imaging or delivery of drugs/agents, and perhaps radiation sensitizers, to TAMs and also cancer cells within a multicomponent particle.

Targeting TAMs can also serve a prognostic purpose for the pathologist's examination of biopsy samples. Since studies have shown a correlation between the number of TAMs in a tumor biopsy to the patient's prognosis,[36] consequently a method that allows specific isolation and quantification of the number of TAMs would provide

prognostic information to the physician. Furthermore, detection of high levels of TAMs could help to tailor the patient's treatment plan to improve therapeutic outcome, with more significant benefit from a TAM-targeted therapeutic.[168]

Specific targeting of TAMs would facilitate imaging of the tumor size, spread, and growth, and would be useful in disease diagnosis, three-dimensional radiation planning, and monitoring patients. The fact that TAMs are able to extend to all parts of the tumor and to metastatic sites make them an ideal target and useful prognostic marker for many different malignancies, including prostate, breast, lung, and lymphoma.[36]

5.3 Experimental Methods

5.3.1 Summary of Coated Surfaces

Coated surfaces were obtained from R. Kumar from the Lahann Lab and are described in **Table 5-1.**[9]

Table 5-1: Overview of prepared sugar coatings used in this study.

Sample Name	Coating Description
Mannose Brush	Poly(2'-acrylamidoethyl-α-d-mannopyranoside)
Glucose Brush	Poly(2'-acrylamidoethyl-β-d-glucopyranoside)
Mannose Monolayer	α-D-Mannopyranosyl azide clicked to PPX-alkyne
Glucose Monolayer	β-D-Glucopyranosyl azide clicked to PPX-alkyne
Glass	Unmodified glass coverslip

5.3.2 Evaluation of Polarized Macrophage Binding to Coated Surfaces

Coated surfaces were prepared on glass coverslips by R. Kumar (Lahann Lab) and exposed to patient-derived M1 and M2 macrophages (Jelani Zarif, Johns Hopkins University). Cell densities were maintained at 50,000 cells/ml and exposure times were limited to 8 hours, prior to washing with phosphate buffered saline and imaging with light microscopy.

5.4 Results and Discussion

Cellular Binding Experiments:

Prepared surfaces were exposed to patient-derived polarized macrophages (M1 and M2 polarization) by Jelani Zarif at Johns Hopkins University. Light microscopy images were collected following washing and are shown for glass substrates (**Figure 5-1**), and glucose (**Figure 5-2**) or mannose (**Figure 5-3**) coated substrates. Cell numbers were quantified and a comparison of M1 *vs*. M2 binding for each substrate is shown in **Figure 5-4**.

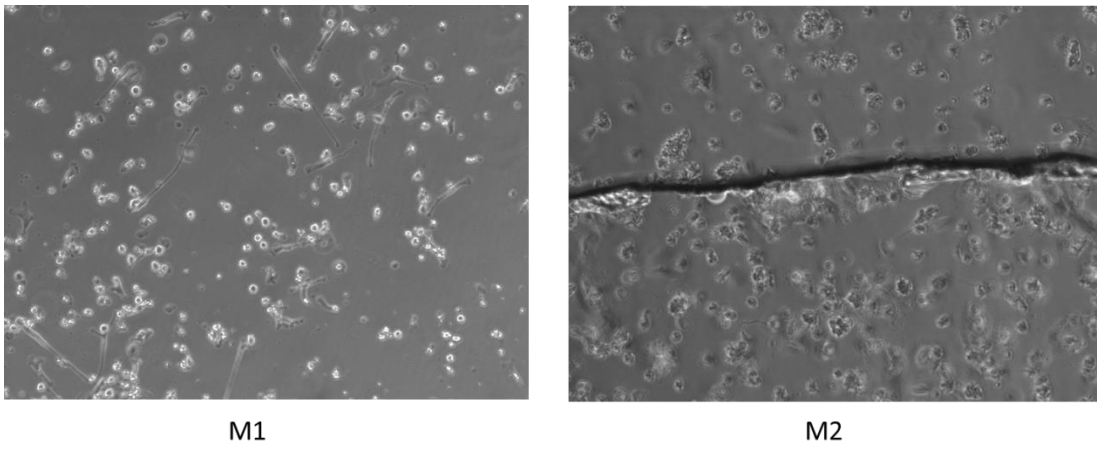

Figure 5-1: Both M1 and M2 macrophages adsorb non-specifically to glass substrates. For the M2 image, the upper half of the image is on polystyrene, which shows similar non-specific adsorption. Images collected by Jelani Zarif (JHU).

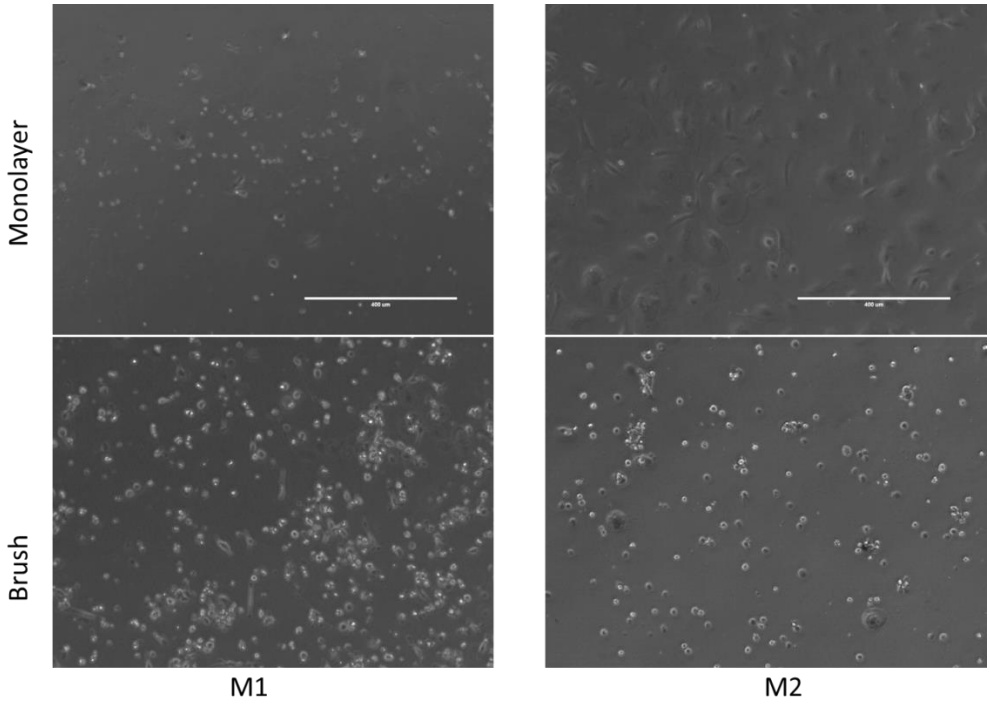

Figure 5-2: Comparison of M1 and M2 binding to glucose-coated surfaces (either brush or monolayer). Cell morphology was unusual for M2 macrophages on glucose monolayer surfaces, but the numbers of bound cells is similar for each condition. Images collected by Jelani Zarif (JHU).

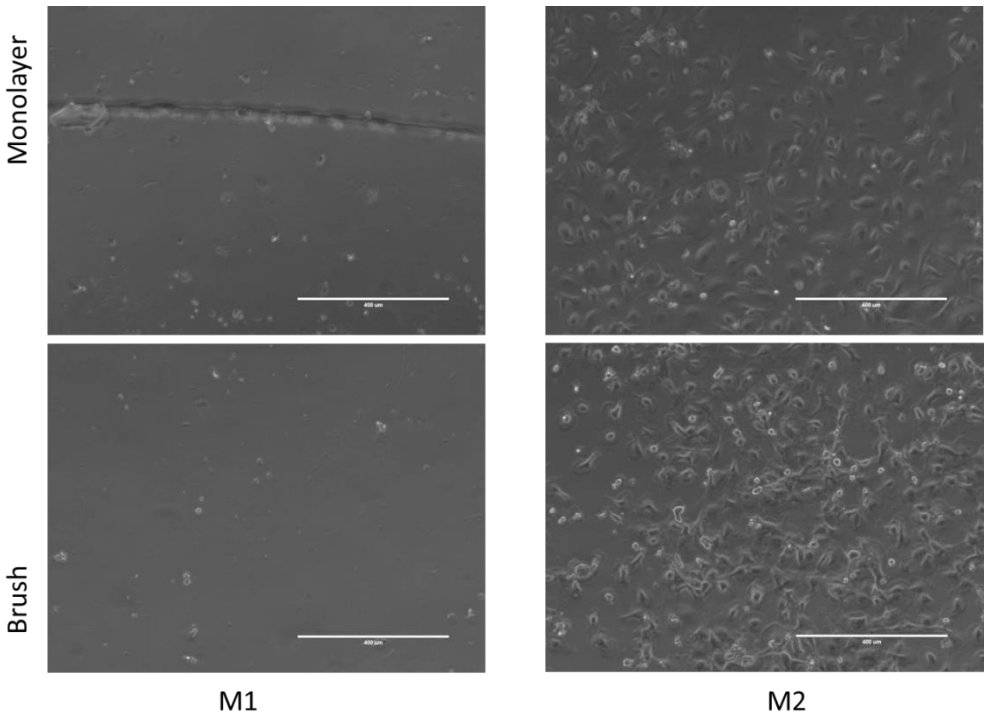

Figure 5-3: Comparison of M1 and M2 macrophage binding to mannose coated surfaces. There is strong preference for the M2 macrophages to bind to the surfaces, while minimal binding was observed for M1 macrophages. Images collected by Jelani Zarif (JHU).

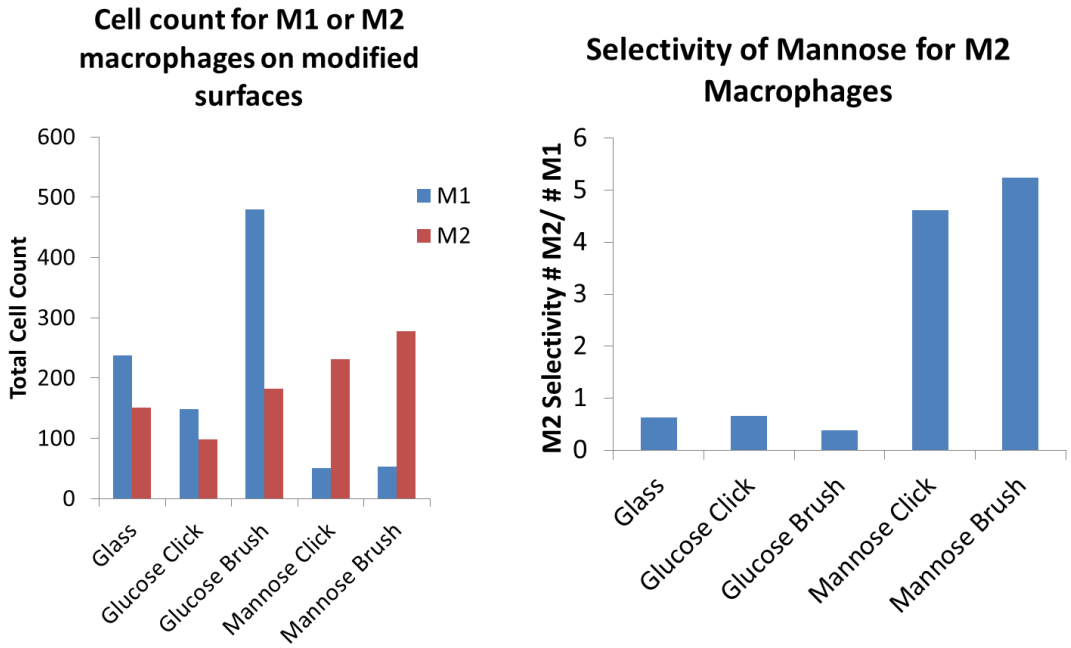

Figure 5-4: Quantification of macrophage binding to various surfaces by: A) number of cells; and B) Selectivity for M2 over M1 macrophages.

The mannose monolayer and brush surfaces showed high positive predictive value towards M2 polarized TAMs (0.822 and 0.840, respectively), while the other surfaces showed slight positive predictive values towards M1 macrophages (glass: 0.61; glucose coating: 0.60; glucose brush: 0.73). These results highlight the potential of mannose brush polymers and monolayers as a highly selective targeting molecule for TAMs.

5.5 Summary

We present a novel targeting molecule for M2 polarized Tumor Associated Macrophages. The brush architecture of the sugar polymers mimics the structure and function of the cellular glycocalyx. These polymer interfaces facilitate multivalent binding,[8] while curtailing non-specific adsorption of proteins,[43] which makes them an exciting molecule for targeting specific cells. There are many potential applications for this type of targeting which will be explored in future studies.

CHAPTER 6

Conclusions and Future Directions

6.1 Conclusions

This thesis has discussed methods to harness the unique properties of polysaccharides, with discussion on chemical and materials modifications and the functionalization of polysaccharides, and specific use in diagnosing dental caries, providing targeted bactericidal delivery, and targeting cancer cells. These examples highlight key lessons about the use of these macromolecules. First, polysaccharides are well-suited for various modifications and processing techniques that allow them to be prepared and functionalized for medical and dental applications, shown in the functionalization of starch nanoparticles and preparation of sugar-brush surface coatings. Next, the natural enzymatic degradation of polysaccharides is a trait which can be harnessed to control the breakdown of the material for diagnostic and therapeutic applications, demonstrated with diagnostic starch nanoparticles for dental caries, and the degradation of copper-nanoparticle containing starch particles for antibacterial applications. And finally, the bio-interactions of polysaccharides can facilitate targeting

of mammalian and prokaryotic cells, highlighted by the specific binding of M2-polarized macrophages to mannose brush coatings. These studies provide proof-of-concept work for a variety of applications, and open the door for continued work, development, and translation of new clinical solutions. Below, specific outlooks for each of the applications are discussed.

6.2 Towards Non-Invasive Nano-Dentistry

A novel diagnostic nanoparticle was presented in Chapter 3 for the early detection of active dental caries. The use of starch in the composition of these nanoparticles benefits from the presence of salivary amylase, which degrades the particles into nontoxic substances. Further optimization of this particle may lead to a clinically useful technique to assist dentists in the detection of active dental caries earlier and more accurately, allowing the application of non-invasive remineralization therapies and a reduction in the need for invasive fillings. Continued development of this system will require the achievement of key milestones: 1) optimization of the particle properties, such as size, charge, and fluorescence intensity; 2) scale-up of production; 3) Proof of concept studies in a clinical setting; 4) rigorous examination of the toxicity and degradation kinetics of the optimized system; and 5) evaluation of the clinical validity of this diagnostic test, with determination of sensitivity and specificity and long term clinical outcomes. Success of these milestones will provide dentists and hygienists with a new technique to aid in the detection of early active lesions and provide remineralization treatment.

While nanomedicine has garnered significant interest,[15,107] there has been limited application of nanotechnology in dentistry,[169] This work provides proof of concept for the potential benefits of nanoparticles, and the particular use of polysaccharides as an easily digestible food-grade material. Similarly designed nanoparticles could be prepared to deliver fluoride, other remineralization aides, or antibacterial therapeutics directly into dental caries. The concept of targeted remineralization of dental caries is novel, as traditional treatments apply remineralization agents diffusely throughout the oral cavity,[170] This approach creates a concentration gradient which leads to complete remineralization of the upper surface of the tooth, while the larger subsurface lesion remains porous, illustrated in **Figure 6-1**.

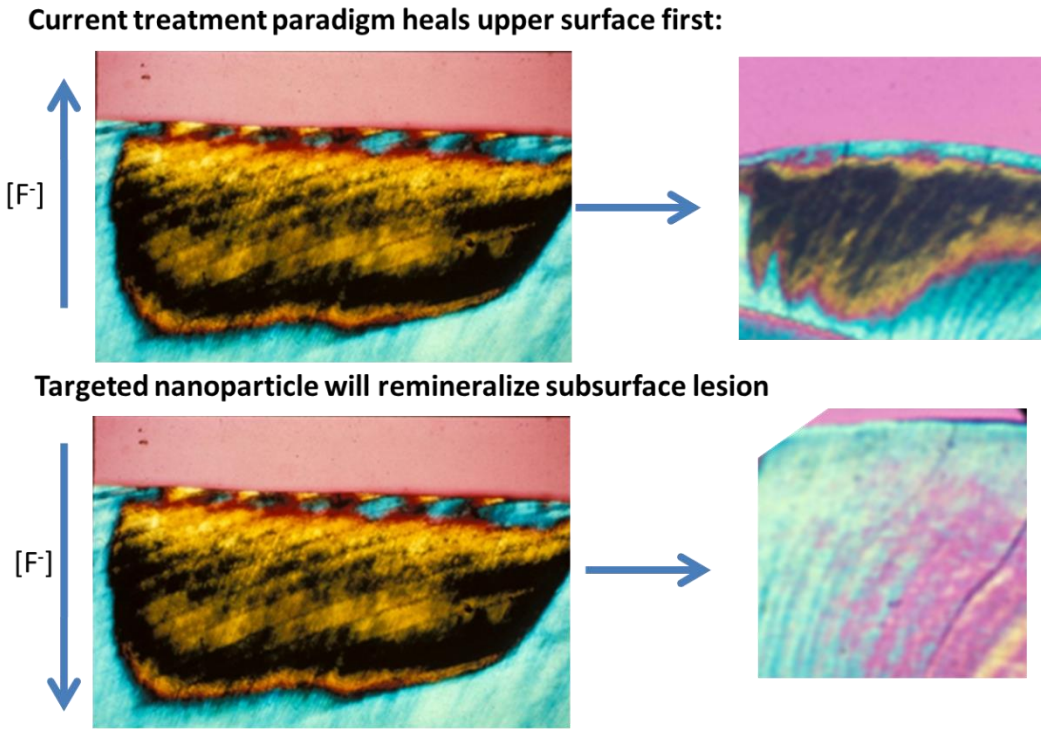

Figure 6-1: Concept behind targeted remineralization of dental caries illustrated with polarized light cross-sectional micrographs of carious enamel lesion, where the sound or remineralized enamel appears blue and the demineralized subsurface appears yellow/brown/black due to greater porosity. The current treatment paradigm (top left) has increased fluoride concentration at the upper surface of the lesion, resulting in

healing of just the upper surface (top right), compared to the targeted treatment paradigm (bottom left), which will facilitate remineralization from within the carious lesion, and possibly better outcomes (bottom right). (Images used with permission from Clarkson Lab, University of Michigan).

The outcome is that the tooth is structurally undermined and is more susceptible to damage, and the subsurface porosity generally leave an unaesthetic appearance.[113] A targeted remineralization treatment will deliver remineralization agents within the subsurface body of the lesion, and reverse the direction of the therapeutic gradient from the base of the lesion to the small surface pores. We hypothesize that this paradigm shift can result in improved remineralization, healing the entirety of the carious lesion, while potentially requiring a lower dose of therapeutic minerals. Some preliminary work explored the utility of the smaller starch nanoparticles towards the loading of sodium fluoride salt; however, the release was rapid and uncontrolled – the rapid degradation of small starch nanoparticles is not a desirable trait for this application. The conclusion was that a different material and/or larger particles are needed to extend the release kinetics for sodium fluoride, which would make a more clinically useful system. Furthermore, starch-based nanoparticles might be well suited for the loading and release of other remineralization therapeutics, such as calcium fluoride,[171] calcium phosphate,[172] hydroxyapatite,[173,174] and phosphate serines.[175] We have tested modifying acetal dextran nanoparticles as an elegant method to release sodium fluoride triggered by the acidic pH within active carious lesions, and preliminary release studies indicate that this is feasible, though continued optimization is needed to validate this system. Success of this work will shift dentistry away from invasive drilling techniques towards non-invasive preventative nano-dentistry, a significant change that promises to improve patient outcomes and reduce dentophobia.[169] Beyond the treatment and diagnosis of dental caries, there are additional opportunities for applying polysaccharide nanoparticles in

dentistry, including in antibacterial treatments[25] and the diagnosis and treatment of oral cancer.[176] Furthermore, similar principals can be applied to the design of other topical diagnostics and therapeutics, including dermal injuries and infections, diseases of the digestive tract, and craniofacial diseases and disorders.[177-179]

6.3 Towards Cellular Metabolism-Targeted Nanomaterials

Chapter 4 identified the utility of starch nanoparticles as a depot for copper nanoparticles as an antibacterial platform. Again, the degradation of starch by amylase, in this case produced by certain strains of bacteria, provides a responsive release of copper nanoparticles which in turn kill the bacterial cells. Furthermore, the modified properties of the starch facilitate strong interactions with the bacteria which assist in targeting the treatment to bacterial cells. Continued work on this project will explore the utility of this strategy for clinical applications, and a furthered understanding of the specific metabolites of different bacteria can guide the design of new particles which can degrade specifically in response to different stimuli. Similar particles can also be prepared with different loadings, including alternative metallic nanoparticles such as zinc oxide[130] or silver,[128] or antibiotics,[180] or combinations therein.[181] Since starch-digesting bacteria are present in the lower gastro-intestinal tract, similar particles can be used to specifically release therapeutics to these regions, useful in targeting bacteria for infections such as *C. difficile* and treatments for inflammatory bowel disease.[132] There is also a potential non-healthcare application in the release of fertilizers in soil, triggered by the presence of starch-digesting bacteria.[182] An additional goal for this project is to

develop a spray-on coating which can slowly release copper, useful for surfaces in the hospital which may not be adequately sterilized on a regular basis.

6.4 Applications of Glycocalyx-Mimetic Interfaces

Chapter 5 identified the utility of mannose-brush polymers for the specific targeting of M2-polarized Tumor Associated Macrophages. While this research demonstrates the use of the polymer brushes on a flat surface, the brushes are equally applicable on nano- and microparticles, and other complex substrates. Using mannosylated surfaces to bind specifically to TAMs has potential, with further engineering and development, to develop new targeted therapeutics and diagnostics, as well as prognostic assays for tumor biopsy samples. These technologies would be useful in the treatment of prostate, lung, breast cancer and lymphomas, and similar targeting of M2 macrophages can also benefit treatments for cardiovascular disease,[37] diabetes,[38] arthritis,[39] and auto-immune diseases.[139] We have prepared poly(lactic-co-glycolic acid) (PLGA) nanoparticles with ATRP initiators and validated the ability to perform SI-ATRP on, and subsequently isolate, these particles. Exploration of the uptake of coated nanoparticles will validate the feasibility of these coatings for therapeutic and diagnostic applications targeting M2 macrophages, as mentioned previously. This pathway will require *in vitro* studies, which if successful can be then be evaluated *in vivo*, prior to pursuing clinical studies. Even without applying these coatings to particles, there are potential opportunities to clinically apply the prepared surfaces. Isolation of M2 cells

from biopsy samples could be useful towards determining a patient's prognosis and tailoring a personalized treatment plan. Furthermore, such coatings could be applied to implantable devices which may be loaded with drugs. Using therapeutics that are capable of polarizing the macrophages to an M1 state would be useful in reducing inflammation,[160] and such coatings could be incorporated in surgical implants and stitches.

6.5 Future Outlook

This dissertation has illustrated some of the utility and potential clinical applications for polysaccharides, highlighting how knowledge of the biological properties and functions of these materials can be harnessed in the design and application of engineered nanomaterials. Engineers are capable of developing exciting novel solutions; however the translation of this research is difficult largely because of unexpected host responses to synthetic materials when moving from *in vitro* to *in vivo*, to clinical use.[150] Potentially the use of biomolecules, such as polysaccharides, can create systems which interface more controllably with biological systems, leading to better outcomes. Novel materials are required that offer specific desirable properties that are beneficial in the diagnosis and treatment of various diseases and disorders, and no singular solution will be applicable to all of these applications. While the research in this dissertation uses well-understood biological interactions, such as the enzymatic degradation of starch, or multivalent specific binding afforded by the glycocalyx, further understanding of biology can help design smart systems for other applications. To this end, collaborative efforts

combining knowledge of materials, chemistry, biology, and clinical experience are critical to the development and optimization of the next generation of medicine.

REFERENCES

1. Daniel-Da-Silva, T.T.a.A.L., *Biofunctional Composites of Polysaccharides Containing Inorganic Nanoparticles,* in *Advances in Nanocomposite Technology*, D.A. Hashim, Editor. 2011, InTech.

2. Magin, C.M., S.P. Cooper, and A.B. Brennan, *Non-toxic antifouling strategies.* Materials Today, 2010. **13**(4): p. 36-44.

3. Mitchell, M.J. and M.R. King, *Physical Biology in Cancer. 3. The role of cell glycocalyx in vascular transport of circulating tumor cells.* American Journal of Physiology - Cell Physiology, 2014. **306**(2): p. C89-C97.

4. Weiner, A., *Bacillus subtilis taken with a Tecnai T-12 TEM*. 2006: Wikipedia.

5. Reitsma, S., et al., *The endothelial glycocalyx: composition, functions, and visualization.* Pflugers Arch, 2007. **454**(3): p. 345-59.

6. Costerton, J.W., R.T. Irvin, and K.J. Cheng, *The bacterial glycocalyx in nature and disease.* Annu Rev Microbiol, 1981. **35**: p. 299-324.

7. Drake-Holland, A.J. and M.I. Noble, *Update on the important new drug target in cardiovascular medicine - the vascular glycocalyx.* Cardiovasc Hematol Disord Drug Targets, 2012. **12**(1): p. 76-81.

8. Park, H., et al., *Glycopolymer Brushes for Specific Lectin Binding by Controlled Multivalent Presentation of N - Acetyllactosamine Glycan Oligomers.* Macromolecular Rapid Communications, 2015. **36**(1): p. 45-54.

9. Kumar, R., et al., *Examining Nanoparticle Adsorption on Electrostatically "Patchy" Glycopolymer Brushes Using Real-Time zeta-Potential Measurements.* Langmuir, 2017. **33**(25): p. 6322-6332.

10. Venugopal, V., *Marine polysaccharides: Food applications*. 2016: CRC Press.

11. Liu, Z., et al., *Polysaccharides-based nanoparticles as drug delivery systems.* Advanced Drug Delivery Reviews, 2008. **60**(15): p. 1650-1662.

12. Stephen, A.M., *Food polysaccharides and their applications*. Vol. 67. 1995: CRC press.

13. Klein, S. *Polysaccharides in oral drug delivery: recent applications and future perspectives*. in *ACS symposium series*. 2009. Oxford University Press.

14. Beneke, C.E., A.M. Viljoen, and J.H. Hamman, *Polymeric plant-derived excipients in drug delivery.* Molecules, 2009. **14**(7): p. 2602-2620.

15. Vasir, J.K. and V. Labhasetwar, *Targeted drug delivery in cancer therapy.* Technol Cancer Res Treat, 2005. **4**(4): p. 363-74.

16. Suarez, S., A. Almutairi, and K.L. Christman, *Micro- and Nanoparticles for Treating Cardiovascular Disease.* Biomater Sci, 2015. **3**(4): p. 564-80.

17. Singh, R. and H.S. Nalwa, *Medical applications of nanoparticles in biological imaging, cell labeling, antimicrobial agents, and anticancer nanodrugs.* Journal of Biomedical Nanotechnology, 2011. **7**(4): p. 489-503.

18. Salata, O.V., *Applications of nanoparticles in biology and medicine.* Journal of Nanobiotechnology, 2004. **2**(1): p. 3.

19. Anselmo, A.C. and S. Mitragotri, *Nanoparticles in the clinic.* Bioengineering & Translational Medicine, 2016. **1**(1): p. 10-29.

20. Agnihotri, S.A., N.N. Mallikarjuna, and T.M. Aminabhavi, *Recent advances on chitosan-based micro-and nanoparticles in drug delivery.* Journal of Controlled Release, 2004. **100**(1): p. 5-28.

21. Tiwari, G., R. Tiwari, and A.K. Rai, *Cyclodextrins in delivery systems: Applications.* J Pharm Bioallied Sci, 2010. **2**(2): p. 72-9.

22. Bachelder, E.M., et al., *Acetal-derivatized dextran: an acid-responsive biodegradable material for therapeutic applications.* J Am Chem Soc, 2008. **130**(32): p. 10494-5.

23. Cohen, J.A., et al., *Acetal-modified dextran microparticles with controlled degradation kinetics and surface functionality for gene delivery in phagocytic and non-phagocytic cells.* Adv Mater, 2010. **22**(32): p. 3593-7.

24. Rahmani, S., et al., *Multimodal delivery of irinotecan from microparticles with two distinct compartments.* J Control Release, 2013. **172**(1): p. 239-45.

25. Chávez de Paz, L.E., et al., *Antimicrobial Effect of Chitosan Nanoparticles on Streptococcus mutans Biofilms.* Applied and Environmental Microbiology, 2011. **77**(11): p. 3892-3895.

26. Raja, M.A., et al., *Synthesis and evaluation of pH-sensitive, self-assembled chitosan-based nanoparticles as efficient doxorubicin carriers.* J Biomater Appl, 2017. **31**(8): p. 1182-1195.

27. Li, J., et al., *Glucose-conjugated chitosan nanoparticles for targeted drug delivery and their specific interaction with tumor cells.* Frontiers of Materials Science, 2014. **8**(4): p. 363-372.

28. Qi, L., et al., *Preparation and antibacterial activity of chitosan nanoparticles.* Carbohydrate Research, 2004. **339**(16): p. 2693-2700.

29. Maeda, H., *Vascular permeability in cancer and infection as related to macromolecular drug delivery, with emphasis on the EPR effect for tumor-selective drug targeting.* Proceedings of the Japan Academy, Series B, 2012. **88**(3): p. 53-71.

30. Maeda, H., et al., *Tumor vascular permeability and the EPR effect in macromolecular therapeutics: a review.* J Control Release, 2000. **65**(1-2): p. 271-84.

31. Weiss, G.J., et al., *First-in-human phase 1/2a trial of CRLX101, a cyclodextrin-containing polymer-camptothecin nanopharmaceutical in patients with advanced solid tumor malignancies.* Invest New Drugs, 2013. **31**(4): p. 986-1000.

32. Zuckerman, J.E., et al., *siRNA delivery to the glomerular mesangium using polycationic cyclodextrin nanoparticles containing siRNA.* Nucleic Acid Ther, 2015. **25**(2): p. 53-64.

33. Bhavani, A.L. and J. Nisha, *Dextran—the polysaccharide with versatile uses.* Int J Pharm Biol Sci, 2010. **1**(4): p. 569-573.

34. Han, S.-o., et al., *Development of Biomaterials for Gene Therapy.* Molecular Therapy. **2**(4): p. 302-317.

35. Edgar, K.J., *Cellulose esters in drug delivery.* Cellulose, 2007. **14**(1): p. 49-64.

36. Cook, J. and T. Hagemann, *Tumour-associated macrophages and cancer.* Curr Opin Pharmacol, 2013. **13**(4): p. 595-601.

37. Frantz, S. and M. Nahrendorf, *Cardiac macrophages and their role in ischaemic heart disease.* Cardiovascular Research, 2014. **102**(2): p. 240-248.

38. Olefsky, J.M. and C.K. Glass, *Macrophages, inflammation, and insulin resistance.* Annu Rev Physiol, 2010. **72**: p. 219-46.

39. Laria, A., et al., *The macrophages in rheumatic diseases.* Journal of Inflammation Research, 2016. **9**: p. 1-11.

40. Salman, H.H., et al., *Bioadhesive mannosylated nanoparticles for oral drug delivery.* Journal of Nanoscience and Nanotechnology, 2006. **6**(9-1): p. 3203-3209.

41. Jain, A., et al., *Mannosylated solid lipid nanoparticles as vectors for site-specific delivery of an anti-cancer drug.* Journal of Controlled Release, 2010. **148**(3): p. 359-367.

42. Jain, S.K., et al., *Mannosylated gelatin nanoparticles bearing an anti-HIV drug didanosine for site-specific delivery.* Nanomedicine: Nanotechnology, Biology and Medicine, 2008. **4**(1): p. 41-48.

43. Wan, S., et al., *The "sweet" side of the protein corona: effects of glycosylation on nanoparticle–cell interactions.* ACS Nano, 2015. **9**(2): p. 2157-2166.

44. Jiang, X., et al., *Nanoparticles of 2-deoxy-D-glucose functionalized poly (ethylene glycol)-co-poly (trimethylene carbonate) for dual-targeted drug delivery in glioma treatment.* Biomaterials, 2014. **35**(1): p. 518-529.

45. Zhang, F., C.-L. Xu, and C.-M. Liu, *Drug delivery strategies to enhance the permeability of the blood–brain barrier for treatment of glioma.* Drug Design, Development and Therapy, 2015. **9**: p. 2089-2100.

46. Kwak, J.Y., *Fucoidan as a marine anticancer agent in preclinical development.* Mar Drugs, 2014. **12**(2): p. 851-70.

47. Lu, K.Y., et al., *Development of a new type of multifunctional fucoidan-based nanoparticles for anticancer drug delivery.* Carbohydr Polym, 2017. **165**: p. 410-420.

48. Senthilkumar, K., et al., *Brown seaweed fucoidan: biological activity and apoptosis, growth signaling mechanism in cancer.* Int J Biol Macromol, 2013. **60**: p. 366-74.

49. Shamay, Y., et al., *P-selectin is a nanotherapeutic delivery target in the tumor microenvironment.* Science Translational Medicine, 2016. **8**(345): p. 345ra87-345ra87.

50. Doh, K.-O. and Y. Yeo, *Application of polysaccharides for surface modification of nanomedicines.* Therapeutic Delivery, 2012. **3**(12): p. 1447-1456.

51. Wolk, A., et al., *Long-term intake of dietary fiber and decreased risk of coronary heart disease among women.* Jama, 1999. **281**(21): p. 1998-2004.

52. Chang, R., *Bioactive polysaccharides from traditional Chinese medicine herbs as anticancer adjuvants.* The Journal of Alternative & Complementary Medicine, 2002. **8**(5): p. 559-565.

53. Barrow, C. and F. Shahidi, *Marine nutraceuticals and functional foods*. 2007: CRC Press.

54. Jiménez-Escrig, A., E. Gomez-Ordonez, and P. Rupérez, *26 Seaweed as a Source of Novel Nutraceuticals: Sulfated Polysaccharides and Peptides.* Advances in Food and Nutrition Research, 2011. **64**(64): p. 325-337.

55. Giavasis, I., *Bioactive fungal polysaccharides as potential functional ingredients in food and nutraceuticals.* Current Opinion in Biotechnology, 2014. **26**: p. 162-173.

56. Suleria, H.A.R., et al., *Marine-Based Nutraceuticals: An Innovative Trend in the Food and Supplement Industries.* Marine Drugs, 2015. **13**(10): p. 6336-6351.

57. Fullerton, S., et al., *Induction of apoptosis in human prostatic cancer cells with beta-glucan (Maitake mushroom polysaccharide).* Molecular Urology, 2000. **4**(1): p. 7-13.

58. Garner, S.T., *Pharmaceutical Preformulation-Osteoarthritis Therapy Via Two Drug Delivery Applications: The Mutual Prodrug and the Transdermal Delivery of a Well-known Nutraceutical, Glucosamine*. 2005, University of Georgia.

59. Salvatore, S., et al., *A pilot study of N - acetyl glucosamine, a nutritional substrate for glycosaminoglycan synthesis, in paediatric chronic inflammatory bowel disease.* Alimentary Pharmacology & Therapeutics, 2000. **14**(12): p. 1567-1579.

60. Le Corre, D., J. Bras, and A. Dufresne, *Starch nanoparticles: a review.* Biomacromolecules, 2010. **11**(5): p. 1139-53.

61. Kim, H.Y., et al., *Characterization of nanoparticles prepared by acid hydrolysis of various starches.* Starch - Stärke, 2012. **64**(5): p. 367-373.

62. Ma, X., et al., *Fabrication and characterization of citric acid-modified starch nanoparticles/plasticized-starch composites.* Biomacromolecules, 2008. **9**(11): p. 3314-3320.

63. Ghaeb, M., H. Tavanai, and M. Kadivar, *Electrosprayed maize starch and its constituents (amylose and amylopectin) nanoparticles.* Polymers for Advanced Technologies, 2015. **26**(8): p. 917-923.

64. Bloembergen, S., et al. *Ongoing developments in biolatex binders with a very low carbon footprint for paper and board manufacturing*. in *64th Appita Annual Conference and Exhibition, Melbourne 18-21 April 2010: Conference Technical Papers*. 2010. Appita Inc.

65. Shin, J.Y., et al. *Rheological properties of starch latex dispersions and starch latex-containing coating colors*. in *Paper Conference and Trade Show 2012: Growing the Future, PaperCon 2012-Co-located with Control Systems 2012*. 2012.

66. Smeets, N.M.B., S. Imbrogno, and S. Bloembergen, *Carbohydrate functionalized hybrid latex particles.* Carbohydr Polym, 2017. **173**: p. 233-252.

67. Huang, Y., et al., *Ultra-small and innocuous cationic starch nanospheres: preparation, characterization and drug delivery study.* Int J Biol Macromol, 2013. **58**: p. 231-9.

68. Bendoraitiene, J., et al., *Peculiarities of Starch Cationization with Glycidyltrimethylammonium Chloride.* Starch - Stärke, 2006. **58**(12): p. 623-631.

69. Santander-Ortega, M., et al., *Nanoparticles made from novel starch derivatives for transdermal drug delivery.* Journal of Controlled Release, 2010. **141**(1): p. 85-92.

70. Chin, S.F., S.C. Pang, and S.H. Tay, *Size controlled synthesis of starch nanoparticles by a simple nanoprecipitation method.* Carbohydrate Polymers, 2011. **86**(4): p. 1817-1819.

71. Likhitkar, S. and A. Bajpai, *Magnetically controlled release of cisplatin from superparamagnetic starch nanoparticles.* Carbohydrate Polymers, 2012. **87**(1): p. 300-308.

72. Shi, A.-m., et al., *Preparation of starch-based nanoparticles through high-pressure homogenization and miniemulsion cross-linking: Influence of various process parameters on particle size and stability.* Carbohydrate Polymers, 2011. **83**(4): p. 1604-1610.

73. Yu, D., et al., *Dialdehyde starch nanoparticles: Preparation and application in drug carrier.* Chinese Science Bulletin, 2007. **52**(21): p. 2913-2918.

74. Carr, M., *Preparation of cationic starch containing quaternary ammonium substituents by reactive twin - screw extrusion processing.* Journal of Applied Polymer Science, 1994. **54**(12): p. 1855-1861.

75. Kulkarni, A.R., et al., *Urea–formaldehyde crosslinked starch and guar gum matrices for encapsulation of natural liquid pesticide [Azadirachta Indica A. Juss.(neem) seed oil]: swelling and release kinetics.* Journal of Applied Polymer Science, 1999. **73**(12): p. 2437-2446.

76. El-Naggar, M.E., et al., *Synthesis, characterization, release kinetics and toxicity profile of drug-loaded starch nanoparticles.* International Journal of Biological Macromolecules, 2015. **81**: p. 718-729.

77. Jain, A.K., et al., *Effective insulin delivery using starch nanoparticles as a potential trans-nasal mucoadhesive carrier.* European Journal of Pharmaceutics and Biopharmaceutics, 2008. **69**(2): p. 426-435.

78. Xiao, S., et al., *Studies of poly-L-lysine-starch nanoparticle preparation and its application as gene carrier.* Science in China Series B: Chemistry, 2005. **48**(2): p. 162-166.

79. Xiao, S., et al., *Preparation of folate-conjugated starch nanoparticles and its application to tumor-targeted drug delivery vector.* Chinese Science Bulletin, 2006. **51**(14): p. 1693-1697.

80. Bloembergen, S., et al., *Aptamer bioconjugate drug delivery device*. 2011, Google Patents.

81. Jones, N.A., et al., *Nanoparticle-Based Targeting and Detection of Microcavities.* Adv Healthc Mater, 2017. **6**(1).

82. Kato, Y., R. Matsuo, and A. Isogai, *Oxidation process of water-soluble starch in TEMPO-mediated system.* Carbohydrate Polymers, 2003. **51**(1): p. 69-75.

83. Fischer, M.J., *Amine coupling through EDC/NHS: a practical approach.* Surface Plasmon Resonance: Methods and Protocols, 2010: p. 55-73.

84. Yu, K. and J.N. Kizhakkedathu, *Synthesis of functional polymer brushes containing carbohydrate residues in the pyranose form and their specific and nonspecific interactions with proteins.* Biomacromolecules, 2010. **11**(11): p. 3073-3085.

85. Heinze, T., V. Haack, and S. Rensing, *Starch derivatives of high degree of functionalization. 7. Preparation of cationic 2 - hydroxypropyltrimethylammonium chloride starches.* Starch - Stärke, 2004. **56**(7): p. 288-296.

86. Pi-xin, W., et al., *Preparation and characterization of cationic corn starch with a high degree of substitution in dioxane-THF-water media.* Carbohydr Res, 2009. **344**(7): p. 851-5.

87. Filipe, V., A. Hawe, and W. Jiskoot, *Critical evaluation of Nanoparticle Tracking Analysis (NTA) by NanoSight for the measurement of nanoparticles and protein aggregates.* Pharm Res, 2010. **27**(5): p. 796-810.

88. Bhaskar, S., et al., *Towards designer microparticles: simultaneous control of anisotropy, shape, and size.* Small, 2010. **6**(3): p. 404-11.

89. Rahmani, S. and J. Lahann, *Recent progress with multicompartmental nanoparticles.* MRS Bulletin, 2014. **39**(3): p. 251-257.

90. Rahmani, S., et al., *Long-circulating Janus nanoparticles made by electrohydrodynamic co-jetting for systemic drug delivery applications.* J Drug Target, 2015. **23**(7-8): p. 750-8.

91. Roh, K.H., D.C. Martin, and J. Lahann, *Biphasic Janus particles with nanoscale anisotropy.* Nat Mater, 2005. **4**(10): p. 759-63.

92. Misra, A.C., et al., *Multicompartmental particles for combined imaging and siRNA delivery.* Adv Mater, 2012. **24**(28): p. 3850-6.

93. Roh, K.H., M. Yoshida, and J. Lahann, *Water-stable biphasic nanocolloids with potential use as anisotropic imaging probes.* Langmuir, 2007. **23**(10): p. 5683-8.

94. Park, T.H., et al., *Photoswitchable particles for on-demand degradation and triggered release.* Small, 2013. **9**(18): p. 3051-7.

95. Rahmani, S., et al., *Dual Release Carriers for Cochlear Delivery.* Adv Healthc Mater, 2016. **5**(1): p. 94-100.

96. Kazemi, A. and J. Lahann, *Environmentally responsive core/shell particles via electrohydrodynamic co-jetting of fully miscible polymer solutions.* Small, 2008. **4**(10): p. 1756-62.

97. Roh, K.H., D.C. Martin, and J. Lahann, *Triphasic nanocolloids.* J Am Chem Soc, 2006. **128**(21): p. 6796-7.

98. Hwang, S., et al., *Anisotropic hybrid particles based on electrohydrodynamic co-jetting of nanoparticle suspensions.* Phys Chem Chem Phys, 2010. **12**(38): p. 11894-9.

99. Rahmani, S., et al., *Chemically orthogonal three-patch microparticles.* Angew Chem Int Ed Engl, 2014. **53**(9): p. 2332-8.

100. Sokolovskaya, E., et al., *Dual-stimuli-responsive microparticles.* ACS Appl Mater Interfaces, 2015. **7**(18): p. 9744-51.

101. Bally, F., et al., *Co-immobilization of biomolecules on ultrathin reactive chemical vapor deposition coatings using multiple click chemistry strategies.* ACS Appl Mater Interfaces, 2013. **5**(19): p. 9262-8.

102. Hwang, S. and J. Lahann, *Differentially degradable janus particles for controlled release applications.* Macromol Rapid Commun, 2012. **33**(14): p. 1178-83.

103. Bhaskar, S., et al., *Multicompartmental microcylinders.* Angew Chem Int Ed Engl, 2009. **48**(25): p. 4589-93.

104. Bhaskar, S. and J. Lahann, *Microstructured materials based on multicompartmental fibers.* J Am Chem Soc, 2009. **131**(19): p. 6650-1.

105. Doshi, N., et al., *Red blood cell-mimicking synthetic biomaterial particles.* Proc Natl Acad Sci U S A, 2009. **106**(51): p. 21495-9.

106. Misra, A.C., et al., *CXCR4-Targeted Nanocarriers for Triple Negative Breast Cancers.* Biomacromolecules, 2015. **16**(8): p. 2412-7.

107. Parveen, S., R. Misra, and S.K. Sahoo, *Nanoparticles: a boon to drug delivery, therapeutics, diagnostics and imaging.* Nanomedicine: Nanotechnology, Biology and Medicine, 2012. **8**(2): p. 147-166.

108. Bader, J.D., et al., *Diagnosis and management of dental caries: summary.* 2001.

109. Featherstone, J.D., *The caries balance: the basis for caries management by risk assessment.* Oral Health Prev Dent, 2004. **2 Suppl 1**: p. 259-64.

110. Marthaler, T., *Changes in dental caries 1953–2003.* Caries Research, 2004. **38**(3): p. 173-181.

111. Clarkson, B.H., J.S. Wefel, and L.M. Silverstone, *Redistribution of enamel fluoride during white spot lesion formation: an in vitro study on human dental enamel.* Caries Res, 1981. **15**(2): p. 158-65.

112. Silverstone, L.M., et al., *Remineralization of natural and artificial lesions in human dental enamel in vitro. Effect of calcium concentration of the calcifying fluid.* Caries Res, 1981. **15**(2): p. 138-57.

113. Ismail, A., et al., *The International Caries Detection and Assessment System (ICDAS): an integrated system for measuring dental caries.* Community Dentistry and Oral Epidemiology, 2007. **35**(3): p. 170-178.

114. Summitt, J.B., et al., *Fundamentals of operative dentistry: a contemporary approach*. 2006: Quintessence Pub.

115. Ward, M.L., *The American Text-book of Operative Dentistry*. Vol. 1. 1920: Lea & Febiger.

116. Ferreira, R.I., et al., *Assessment of enamel demineralization using conventional, digital, and digitized radiography.* Brazilian Oral Research, 2006. **20**(2): p. 114-119.

117. Zeitouny, M., et al., *SOPROLIFE system: an accurate diagnostic enhancer.* The Scientific World Journal, 2014. **2014**.

118. Hara, T., M. Inami, and T. Hara, *Efficacy and safety of fluorescein angiography with orally administered sodium fluorescein.* Am J Ophthalmol, 1998. **126**(4): p. 560-4.

119. Mathews, K.R., J.D. Landmark, and D.F. Stickle, *Quantitative assay for starch by colorimetry using a desktop scanner.* J. Chem. Educ, 2004. **81**(5): p. 702.

120. Nassar, H.M., et al., *Dentifrice fluoride and abrasivity interplay on artificial caries lesions.* Caries Research, 2014. **48**(6): p. 557-565.

121. Maas, J.R., et al., *Differences in loosely bound fluoride formation and anticaries effect of resin-based fluoride varnishes.* Int J Paediatr Dent, 2013. **23**(3): p. 166-72.

122. Fischer, S. and F. Piller, *Neue Erkenntnisse über den Abbau der Stärke mit Hypochlorit. 7. Untersuchung der Wirkung der Hypochloritoxydation auf Amylose mit Hilfe des Abbaues mit β - Amylase und Bestimmung des Jodbindungsvermögens.* Starch - Stärke, 1978. **30**(1): p. 4-7.

123. Young, A., et al., *Zeta potentials of human enamel and hydroxyapatite as measured by the Coulter® DELSA 440.* Advances in Dental Research, 1997. **11**(4): p. 560-565.

124. Weerkamp, A., H. Uyen, and H. Busscher, *Effect of zeta potential and surface energy on bacterial adhesion to uncoated and saliva-coated human enamel and dentin.* Journal of Dental Research, 1988. **67**(12): p. 1483-1487.

125. Culver, D.H., et al., *Surgical wound infection rates by wound class, operative procedure, and patient risk index.* The American Journal of Medicine, 1991. **91**(3): p. S152-S157.

126. Spellberg, B., et al., *The epidemic of antibiotic-resistant infections: a call to action for the medical community from the Infectious Diseases Society of America.* Clinical Infectious Diseases, 2008. **46**(2): p. 155-164.

127. Palermo, E.F. and K. Kuroda, *Structural determinants of antimicrobial activity in polymers which mimic host defense peptides.* Applied Microbiology and Biotechnology, 2010. **87**(5): p. 1605-1615.

128. Marin, S., et al., *Applications and toxicity of silver nanoparticles: a recent review.* Curr Top Med Chem, 2015. **15**(16): p. 1596-604.

129. Ruparelia, J.P., et al., *Strain specificity in antimicrobial activity of silver and copper nanoparticles.* Acta Biomaterialia, 2008. **4**(3): p. 707-716.

130. McGuffie, M.J., et al., *Zinc oxide nanoparticle suspensions and layer-by-layer coatings inhibit staphylococcal growth.* Nanomedicine, 2016. **12**(1): p. 33-42.

131. Pal, S., Y.K. Tak, and J.M. Song, *Does the antibacterial activity of silver nanoparticles depend on the shape of the nanoparticle? A study of the gram-negative bacterium Escherichia coli.* Applied and Environmental Microbiology, 2007. **73**(6): p. 1712-1720.

132. Gao, W., et al., *Nanoparticle Approaches against Bacterial Infections.* Wiley interdisciplinary reviews. Nanomedicine and Nanobiotechnology, 2014. **6**(6): p. 532-547.

133. Radovic-Moreno, A.F., et al., *Surface charge-switching polymeric nanoparticles for bacterial cell wall-targeted delivery of antibiotics.* ACS Nano, 2012. **6**(5): p. 4279-4287.

134. Kell, A.J., et al., *Vancomycin-modified nanoparticles for efficient targeting and preconcentration of Gram-positive and Gram-negative bacteria.* ACS Nano, 2008. **2**(9): p. 1777-1788.

135. Furukawa, H., et al., *Affinity selection of target cells from cell surface displayed libraries: a novel procedure using thermo-responsive magnetic nanoparticles.* Applied Microbiology and Biotechnology, 2003. **62**(5-6): p. 478-483.

136. Zhou, Y., et al., *Impact of single-chain Fv antibody fragment affinity on nanoparticle targeting of epidermal growth factor receptor-expressing tumor cells.* Journal of Molecular Biology, 2007. **371**(4): p. 934-947.

137. Chang, Y.-C., et al., *Rapid single cell detection of Staphylococcus aureus by aptamer-conjugated gold nanoparticles.* Scientific Reports, 2013. **3**.

138. Zhang, L., et al., *Development of nanoparticles for antimicrobial drug delivery.* Current Medicinal Chemistry, 2010. **17**(6): p. 585-594.

139. Leuschner, F., et al., *Therapeutic siRNA silencing in inflammatory monocytes in mice.* Nat Biotechnol, 2011. **29**(11): p. 1005-10.

140. Toti, U.S., et al., *Targeted delivery of antibiotics to intracellular chlamydial infections using PLGA nanoparticles.* Biomaterials, 2011. **32**(27): p. 6606-6613.

141. Misra, R., et al., *Sustained antibacterial activity of doxycycline-loaded poly (D, L-lactide-co-glycolide) and poly (ε-caprolactone) nanoparticles.* Nanomedicine, 2009. **4**(5): p. 519-530.

142. Thamphiwatana, S., et al., *Phospholipase A2-responsive antibiotic delivery via nanoparticle-stabilized liposomes for the treatment of bacterial infection.* Journal of Materials Chemistry B, 2014. **2**(46): p. 8201-8207.

143. Priest, F.G., *Extracellular enzyme synthesis in the genus Bacillus.* Bacteriological Reviews, 1977. **41**(3): p. 711-753.

144. Yoon, K.-Y., et al., *Susceptibility constants of Escherichia coli and Bacillus subtilis to silver and copper nanoparticles.* Science of the Total Environment, 2007. **373**(2): p. 572-575.

145. Jordahl, J.H., et al., *Needleless Electrohydrodynamic Cojetting of Bicompartmental Particles and Fibers from an Extended Fluid Interface.* Macromol Rapid Commun, 2017. **38**(1).

146. Konsula, Z. and M. Liakopoulou-Kyriakides, *Hydrolysis of starches by the action of an α-amylase from Bacillus subtilis.* Process Biochemistry, 2004. **39**(11): p. 1745-1749.

147. Siegel, R., D. Naishadham, and A. Jemal, *Cancer statistics, 2013.* CA Cancer J Clin, 2013. **63**(1): p. 11-30.

148. Smith, B.D., et al., *Future of cancer incidence in the United States: burdens upon an aging, changing nation.* J Clin Oncol, 2009. **27**(17): p. 2758-65.

149. Davis, M.E., Z.G. Chen, and D.M. Shin, *Nanoparticle therapeutics: an emerging treatment modality for cancer.* Nat Rev Drug Discov, 2008. **7**(9): p. 771-82.

150. Yu, D., *Translational research: current status, challenges and future strategies.* American Journal of Translational Research, 2011. **3**(5): p. 422-433.

151. Garcia, A.A., et al., *Phase II clinical trial of bevacizumab and low-dose metronomic oral cyclophosphamide in recurrent ovarian cancer: a trial of the California, Chicago, and Princess Margaret Hospital phase II consortia.* J Clin Oncol, 2008. **26**(1): p. 76-82.

152. Loberg, R.D., et al., *Targeting CCL2 with systemic delivery of neutralizing antibodies induces prostate cancer tumor regression in vivo.* Cancer Res, 2007. **67**(19): p. 9417-24.

153. Roca, H., et al., *CCL2 and interleukin-6 promote survival of human CD11b+ peripheral blood mononuclear cells and induce M2-type macrophage polarization.* J Biol Chem, 2009. **284**(49): p. 34342-54.

154. Zhang, J., L. Patel, and K.J. Pienta, *Targeting chemokine (C-C motif) ligand 2 (CCL2) as an example of translation of cancer molecular biology to the clinic.* Prog Mol Biol Transl Sci, 2010. **95**: p. 31-53.

155. Melancon, M.P., et al., *Targeted imaging of tumor-associated M2 macrophages using a macromolecular contrast agent PG-Gd-NIR813.* Biomaterials, 2010. **31**(25): p. 6567-73.

156. Choi, M.R., et al., *A cellular Trojan Horse for delivery of therapeutic nanoparticles into tumors.* Nano Lett, 2007. **7**(12): p. 3759-65.

157. Lewis, C.E. and J.W. Pollard, *Distinct role of macrophages in different tumor microenvironments.* Cancer Res, 2006. **66**(2): p. 605-12.

158. Lin, E.Y., et al., *Colony-stimulating factor 1 promotes progression of mammary tumors to malignancy.* J Exp Med, 2001. **193**(6): p. 727-40.

159. Sica, A., et al., *Macrophage polarization in tumour progression.* Semin Cancer Biol, 2008. **18**(5): p. 349-55.

160. Sica, A. and A. Mantovani, *Macrophage plasticity and polarization: in vivo veritas.* J Clin Invest, 2012. **122**(3): p. 787-95.

161. Sato, Y. and E. Beutler, *Binding, internalization, and degradation of mannose-terminated glucocerebrosidase by macrophages.* J Clin Invest, 1993. **91**(5): p. 1909-17.

162. Zhu, S., et al., *Targeting of tumor-associated macrophages made possible by PEG-sheddable, mannose-modified nanoparticles.* Mol Pharm, 2013. **10**(9): p. 3525-30.

163. Kurahara, H., et al., *Clinical significance of folate receptor beta-expressing tumor-associated macrophages in pancreatic cancer.* Ann Surg Oncol, 2012. **19**(7): p. 2264-71.

164. Cieslewicz, M., et al., *Targeted delivery of proapoptotic peptides to tumor-associated macrophages improves survival.* Proc Natl Acad Sci U S A, 2013. **110**(40): p. 15919-24.

165. Lewen, S., et al., *A Legumain-based minigene vaccine targets the tumor stroma and suppresses breast cancer growth and angiogenesis.* Cancer Immunol Immunother, 2008. **57**(4): p. 507-15.

166. Giraudo, E., M. Inoue, and D. Hanahan, *An amino-bisphosphonate targets MMP-9–expressing macrophages and angiogenesis to impair cervical carcinogenesis.* Journal of Clinical Investigation, 2004. **114**(5): p. 623.

167. Longmire, M., P.L. Choyke, and H. Kobayashi, *Clearance properties of nano-sized particles and molecules as imaging agents: considerations and caveats.* Nanomedicine (Lond), 2008. **3**(5): p. 703-17.

168. Tang, X., et al., *Anti-tumour strategies aiming to target tumour-associated macrophages.* Immunology, 2013. **138**(2): p. 93-104.

169. Abiodun-Solanke, I.M.F., D.M. Ajayi, and A.O. Arigbede, *Nanotechnology and its Application in Dentistry.* Annals of Medical and Health Sciences Research, 2014. **4**(Suppl 3): p. S171-S177.

170. Amaechi, B.T., *Remineralization Therapies for Initial Caries Lesions.* Current Oral Health Reports, 2015. **2**(2): p. 95-101.

171. Navarro, M., et al., *Calcium fluoride uptake by human enamel after use of fluoridated mouthrinses.* Braz Dent J, 2001. **12**(3): p. 178-82.

172. Reynolds, E.C., *Calcium phosphate-based remineralization systems: scientific evidence?* Aust Dent J, 2008. **53**(3): p. 268-73.

173. Mielczarek, A. and J. Michalik, *The effect of nano-hydroxyapatite toothpaste on enamel surface remineralization. An in vitro study.* Am J Dent, 2014. **27**(6): p. 287-90.

174. Swarup, J.S. and A. Rao, *Enamel surface remineralization: Using synthetic nanohydroxyapatite.* Contemp Clin Dent, 2012. **3**(4): p. 433-6.

175. Niu, L.-n., et al., *Biomimetic remineralization of dentin.* Dental Materials : Official Publication of the Academy of Dental Materials, 2014. **30**(1): p. 10.1016/j.dental.2013.07.013.

176. Virupakshappa, B., *Applications of nanomedicine in oral cancer.* Oral Health Dent Manag, 2012. **11**(2): p. 62-8.

177. Wu, Y., K. Briley, and X. Tao, *Nanoparticle-based imaging of inflammatory bowel disease.* Wiley Interdiscip Rev Nanomed Nanobiotechnol, 2016. **8**(2): p. 300-15.

178. Sundar, S. and V.K. Prajapati, *Drug targeting to infectious diseases by nanoparticles surface functionalized with special biomolecules.* Current Medicinal Chemistry, 2012. **19**(19): p. 3196-3202.

179. Zhang, Z., et al., *Polymeric nanoparticles-based topical delivery systems for the treatment of dermatological diseases.* Wiley Interdisciplinary Reviews. Nanomedicine and Nanobiotechnology, 2013. **5**(3): p. 205-218.

180. Brown, A.N., et al., *Nanoparticles functionalized with ampicillin destroy multiple-antibiotic-resistant isolates of Pseudomonas aeruginosa and Enterobacter aerogenes and methicillin-resistant Staphylococcus aureus.* Appl Environ Microbiol, 2012. **78**(8): p. 2768-74.

181. Allahverdiyev, A.M., et al., *Coping with antibiotic resistance: combining nanoparticles with antibiotics and other antimicrobial agents.* Expert Rev Anti Infect Ther, 2011. **9**(11): p. 1035-52.

182. Dimkpa, C.O. and P.S. Bindraban, *Nanofertilizers: New Products for the Industry?* J Agric Food Chem, 2017.